Industrielle Gemeinschaftsforschung

Schlussbericht

zu IGF-Vorhaben Nr. 161EN

Thema

Oberflächenfunktionalisierte Pulver für 3D-Fertigung (OpP3D)

Berichtszeitraum

01.06.2016 - 31.05.2018

Forschungsvereinigung

Verein für das Forschungsinstitut für Edelmetalle und Metallchemie e.V. - FEM

Forschungseinrichtung(en)

Forschungsstelle 1 : Forschungsinstitut für Edelmetalle und Metallchemie

Katharinenstraße 17 - 73525 Schwäbisch Gmünd

Forschungsstelle 2 : Fraunhofer-Institut für Umwelt-, Sicherheits-

und Energietechnik UMSICHT - Institutsteil Sulzbach-Rosenberg

An der Maxhütte 1 - 92237 Sulzbach-Rosenberg

Schwäbisch Gmünd, 26.11.18 — Ulrich Klotz

Sulzbach-Rosenberg, 23.11.18 — Gerhard Wolf

Ort, Datum

Name und Unterschrift aller Projektleiterinnen und Projektleiter der Forschungseinrichtung(en)

Forschungsnetzwerk Mittelstand

Gefördert durch:

Bundesministerium für Wirtschaft und Energie

aufgrund eines Beschlusses des Deutschen Bundestages

Supported by:

Federal Ministry for Economic Affairs and Energy

on the basis of a decision by the German Bundestag

Wallonie

cornet

Final Report

for the CORNET Project entitled

Optimised powders for 3D printing (OpP3D)

Reporting period

01.06.2016 - 31.05.2018

German Research Partners

Research center 1: Forschungsinstitut für Edelmetalle und Metallchemie

Katharinenstraße 17 - 73525 Schwäbisch Gmünd

Research center 2: Fraunhofer-Institut für Umwelt-, Sicherheits-

und Energietechnik UMSICHT - Institutsteil Sulzbach-Rosenberg

An der Maxhütte 1 - 92237 Sulzbach-Rosenberg

Belgian Research Partners

Research center 1: Sirris – The Collective Center of the Belgian technological industry

Reyerslaan 80 – 1030 Brussels

Research center 2: Materia Nova

Avenue Copernic 1- 7000 Mons

Content

1 Topic of research and summary

There is a recognized problem of reduced capability in additive manufacturing (AM) due to the limited materials palette and the lack of understanding of fundamental principles between process and powder feedstock. It has also been realized that solution to the technical issues in AM – including materials – can boost the sector's expected volume from $11 to $105 billions by 2020. That is why this project has been designed to enlarge the materials choice to allow for the fabrication and marketing of new products (e.g. the complex coil of an electric motor) and increase the share of manufacturing to the GDP (Gross Domestic Product) in Europe from 15 to 20 %.

Currently, the fabrication of components from Cu, Fe and Al powders in AM is hampered by the material's low laser absorption and proneness to oxidation, respectively, resulting in poor sinterability and poor part properties (for e.g. electrical conductivity reduction of Cu by 40-60 %, high porosity for wall thickness < 1mm). As Cu-, Fe- and Al-components find widespread application in the electronics / electrics, transport, aeronautics and aerospace sectors, and as Laser Beam Melting (LBM) and 3D Printing of metallic powders (M3DP) allow the fabrication of complex and lightweight parts, the need for the usage of these materials in the laser beam melting process and the 3D printing process without the above-listed shortcomings has been identified.

The research approach was to develop coating techniques via physical/chemical vapor deposition – PVD/PECVD (Materia Nova), reactive annealing and in-situ reactive melt atomization (Fraunhofer UMSICHT) to Al and Cu powders, respectively, in order to form a thin (in the nm region) layer on each particle. These layers increase the laser absorption (by "darkening" the particle surface) or protect the surface from oxidation (by shielding it from direct contact with air) and/or increase the wettability on preforms and hence allow for their enhanced processability in the LBM and M3DP techniques. Integrity and purity of parts made from these powders should be maintained by desorption of the applied layer into the atmosphere or through dissolution in the bulk material of the part without compromising properties like density, low porosity and electrical conductivity.

During the course of the project, fem investigated the processability of pure Cu powder and its alloys with selective laser melting, also by developing a quick screening methods based on metal sheets instead of powder. Several powders were tested, including: pure Cu, oxidized Cu, Ti coated copper, sulfide coated copper, CuSn and CuNiSi alloys. Process parameters for an optimal processability with a low power laser (100 W) were developed for the CuNiSi alloys and for the Ti-coated Cu powder. A coil for an innovative light-weight electric motor was designed and built in cooperation with the SME Unicorn Engineering, which is planning further cooperation with fem to develop new products based on the results obtained in this research.

Fraunhofer UMSICHT investigated and developed methods for the coating of Cu powders by forming copper sulfides on the particle surfaces via chemical reactions. Three basic routes have been realized and extensively tested with the reactive sulfur in solution (water, toluene), as elemental vapor and as component in gas mixtures (H_2S/N_2). A fluidized bed reactor has been designed and optimized for the application of the vapor/gaseous media. A huge range of parameters has been realized with variations in S concentration, reaction temperatures and times for finding optimum reaction conditions for each method. The results show that it is possible to generate low-oxygen thin and homogeneous Cu sulfide coatings with the vapor and gas mixtures. The solution treatments suffered from forming oxides (aqueous solution) or localized Cu sulfide crystal growth (toluene). The vapor based method has the disadvantage of a less fine adjustment of the sulfur concentration, if

compared to the gaseous phase mixtures. Finally, laser melting and compaction of the CuS coated powders exhibit a considerable improvement against pure Cu powder, however, the “balling” effect could not be completely suppressed so far by the sulfide coatings. Further improvements can be expected, if the powders are processed with a laser energy greater than 300 W.

Materia Nova developed a new rotary stirring system to obtain homogenous coatings on metallic powders. With said equipment, 316L and Cu powders were coated for further processing with LBM and 3D printing techniques (respectively with Ti and Cr). For the 316L (Fe) powder, the study has shown the technical feasibility for the material. The Cr coating improved the flowability of particles but did not improve infiltration. The Ti coating on Cu powder drastically improved the processability of the material by reducing the laser reflectivity. Further improvement should focus on the thickness of the coating and on reducing the oxygen content in the powder to prevent Ti-oxide formation, so that the porosity in the part can be further reduced. The performed life cycle assessment study demonstrated that the plasma process for the treatment of powders entails little additional environmental impact compared to the complete process.

The project objective for Sirris, namely to develop new materials for binder jetting process, which should be more efficient than existing stainless steel-bronze composite, hasn’t been completely reached. For 316L, this study has shown the technical feasibility of infiltration with both tested materials BNi7 and F300 Höganäs brazing alloys. But diffusion of melting depressants P and Si inducing the infiltrant circuit to collapse forced to develop a new procedure of infiltration, different than the one of bronze infiltration. Solutions have been proposed and tested with more or less success. However, mechanical testing and optical microscopy have highlighted the significant presence of uninfiltrated residual porosities, lowering mechanical characteristics. Additional combined solutions should thus be considered to lead to success (thermal treatment under void or clean inert atmosphere) but these solutions can’t be implemented at Sirris on existing equipment’s. Through said solutions, nearly full infiltration should be possible leading to more ductile composite material compare to stainless steel-bronze composite. In the case of aluminum, the study was not brought to completion due to powder surface oxidation problem encountered as soon as printing step. Potential solutions have been suggested, similar to those considered for 316L.

2 Research approach and economic relevance for SMEs

In order to enable the efficient use of the Cu, Fe and Al in LBM and M3DP processes, this project should improve the processability of the mentioned materials (Cu for LBM and Fe/Al for M3DP), using surface modification (application of a “dark” / protective layer), consequently improving the quality of built parts in terms of density, surface roughness, strength, etc.

The processability of the required powder feedstock will be achieved through surface modification of said feedstock. In order to satisfy the addressed needs of the community, this project should:

- develop the coatings needed to achieve the functionalization of the powder particles, e.g. sulfidation or plasma coating (oxide or metal) of Cu in order to increase the laser absorption, protection and polymer like coating of Fe- and Al-powder particles to prevent their oxidation and improve their wettability

- deliver a process for the surface treatment of powder materials using a new combination of existing techniques that allows to provide surface modified Cu-, Fe- and Al-materials at a market-oriented (competitive) prize for application in the manufacturing process
- allow for the production of Cu, Fe and Al parts that meet the requirements for electrical conductivity and high density and allow for the realization of thin walls in the component
- determine the parameters for the processing of these materials in LBM and M3DP to produce the parts that meet the requirements in terms of mechanical strength, surface roughness, porosity and functional properties (e.g. electrical conductivity)

The treatment of the powder particle surface should provide the solution to the problems of low laser absorption (Cu) and proneness to oxidation (Al/Fe), i.e. either its optical "darkening" by coating with a sulfur or an oxide layer (Cu), or by application of a thin protective polymer layer (Al/Fe), respectively. The underlying working hypothesis is as follows:

- a thin surface layer on the powder particles improves the powder properties (increased laser absorption for Cu, oxidation prevention for Al and higher wettability) in terms of processability (higher production speed, lower energy consumption) and resulting part properties (higher density, fewer pores, lower surface roughness)
- the deposited layer either desorbs / decomposes during the building process (e.g. through evaporation) or at least does not negatively influence the final parts when dissolved in the material. Any evolving gases are transported away via the gas in the machine's chamber or sintering furnace
- the resulting parts have better of at least the same properties as conventionally manufactured ones, i.e. electrical conductivity, hardness, mechanical strength
- the building process using LBM / M3DP is faster / easier / possible thanks to the powder's modified surface properties and hence more economical (higher throughput, higher productivity, lower costs)

Core of the project is therefore the surface modification of the powder materials which will combine several techniques (PVD/PECVD, reactive annealing, reactive hot gas atomization). This step is preceded by the pretreatment of the powder, e.g. the oxide removal from Al-powder, and is followed by the making of test parts (complex electrical coil / space antenna supports) and their testing for functionality to show the proof of the concept.

The innovative character of the chosen methodology lies in the novel combination of existing techniques and expertise (powder metallurgy, powder surface treatment, test part fabrication, part testing) available at the project partners and the accompanying industries (users committee). Furthermore, coating techniques (among them plasma deposition or plasma polymerization), that are commonly used on flat surfaces as state of the art, will be adapted for the coating of powder materials which require special equipment.

There is a recognized problem of curtailed capability of additive manufacturing (AM) caused by a limited choice of materials [1] that hampers its firm anchorage in high value production on a European scale. That is why this project has been designed to obtain new and efficient materials (Cu, Fe and Al being the benchmarks) to broaden the available materials palette in order to promote this technique's further rise from prototyping to production and to fulfill the European Union's growth expectations [1] in manufacturing.

Using these improved powder materials, manufacturers will be able to widen their product range and to focus on new, customized design and innovative geometries, which shall give European manufacturers a decisive market advantage in a field of strong competition from US and Asian markets [1].

A rise from currently 15 to 20 % of the contribution of manufacturing to the gross domestic product (GDP) is demanded by the EU [1]. Based on the observation of a trend towards regionalization of production and serving specific, customized regional and societal needs, AM will significantly contribute to this development by fostering regional production close to the market (as e.g. blueprints can easily be sent from one location to another, meaning that production is not bound to one location) and by bringing back jobs that had previously been outsourced to other countries.

However, AM in Europe faces the threat from heavy investment and intense research into this technology in the US and Asia (predominantly China) [1]. In order not to fall behind these markets there is a clear need for increased research in Europe, in particular in the field of metal powder materials for AM, where the platform “New Materials for Additive Manufacturing” concluded that in comparison to plastics, there are still weaknesses concerning metallic materials in AM: specifically, there is a need for the understanding of the basic science, of microstructures, a property database and testing methods [1].

Therefore, and because materials are a basic parameter in AM, this project has been designed to allow for the manufacture of new products (e.g. coils for electric motors, complex wiring geometries, lightweight design in the transport sector) for new or expanding markets through increasing the materials palette, where Cu, Fe and Al will be the chosen benchmark materials. Electronics / electrics, automotive, consumer goods and aeronautics will be the primary industries served by this project.

The whole value chain from powder production to the final part will benefit from the results of this project (i.e. surface modified Cu-, Fe- and Al-powders for (easier) processability and higher productivity), because powder suppliers (of which there are many SMEs) can increase their product portfolio with the new powder materials, service providers in manufacturing can offer to make new products from these powders and end users have a greater choice of materials and hence a greater choice of components to design and make through AM. The project is therefore fully in line with European initiatives to strengthen high value manufacturing, to bring back outsourced jobs and to maintain (or even increase) the quality of life in Europe.

2.1 State of the art

2.1.1 Processing of Cu and its alloys with the LBM process

Due to its high electrical conductivity, Cu is the primary material choice for complex electrical components. In contrast to Ag and Au that can be alloyed to limit (although only partially) the negative influence of their physical properties, this approach cannot be used in the case of Cu, where alloying would compromise its electric conductivity. In order to enable the production of electrical components such as the complex coil of an electric motor via AM (which will be done during the course of this project), Cu powder with high laser energy absorption is needed that allows for the fabrication of dense parts while maintaining its electrical properties. At the moment, this is not possible using the existing technology for the materials mentioned above.

The processing of pure copper with selective laser melting is very challenging. The material possesses a very high electrical conductivity which is for metals directly proportional to the thermal conductivity, according to the Wiedemann-Franz-law. Commonly used Nd-YAG Laser operating at a

wavelength of 1.070 nm, show practically a total reflection of the laser energy [13,14]. The challenges encountered during the processing of Cu and its alloys are widely discussed in the literature [2, 3, 4], which currently focuses on 99.9% copper and bronze [5]. Concerning pure copper, Becker et al. describe the difficulties in melting the material due to its physical properties (light reflection, conductivity, surface tension) and to the consequent “balling effect”. The balling effect is related to the high surface tension, which causes the formation of melt beads instead of a continuous melting track. Because of the uneven melting tracks, the produced parts present a high porosity. This behavior can be observed also for gold and silver [6,7].

Ikeshoij [3] shows that the laser power required to produce parts with 99.6 - 99.9% density (see Figure 2b) is very high (800-1000W), which is also stated by Becker et al. [4], who showed examples of tool insert in copper alloys produced with 1000 W laser power. On the contrary, for a CuSn11 bronze alloy, Poltz et al. obtained a 94 % part density by using only 100 W laser power (see Figure 2c). The use of EBM (electron beam melting), as described by Guschlbauer [8], allows to produce dense parts, since the coupling of electrons with copper succeeds substantially better than the one of laser light. However, EBM parts show higher surface roughness because of the larger powder particle size employed in said process (see Figure 2a). Alloying of Cu with Sn significantly reduces porosity in LBM parts [9], but their electrical conductivity drops as well (from 100 % IACS of pure copper down to 12 % IACS of CuSn10).

The best combination of mechanical strength and electrical conductivity in the Cu-based alloys group can be obtained with copper-beryllium alloys. For example in case of the CuBe2 alloy, by strain hardening a tensile strength of 1.520 MPa and an electrical conductivity of 21% IACS can be obtained [10]. Although the CuBe alloys possess the mentioned favorable properties, they also have the disadvantage of the toxicity and the limited availability of beryllium. The CuNiSi alloys have established themselves as substitution materials. These alloys offer a good compromise between mechanical strength and conductivity and, therefore, are widely used in electric connectors. By solution annealing and aging treatment, it is possible to strongly increase the mechanical and physical properties of these alloys. A tensile strength of about 900 MPa and an electrical conductivity of about 50% IACS [11] can be reached. The correlated age-hardening mechanisms (with formations of Ni_2Si precipitations) are described in the literature by Zhao et al. for a CuNiSi alloy with weight % compositions of 3.2 % Ni and 0.75 % Si [12].

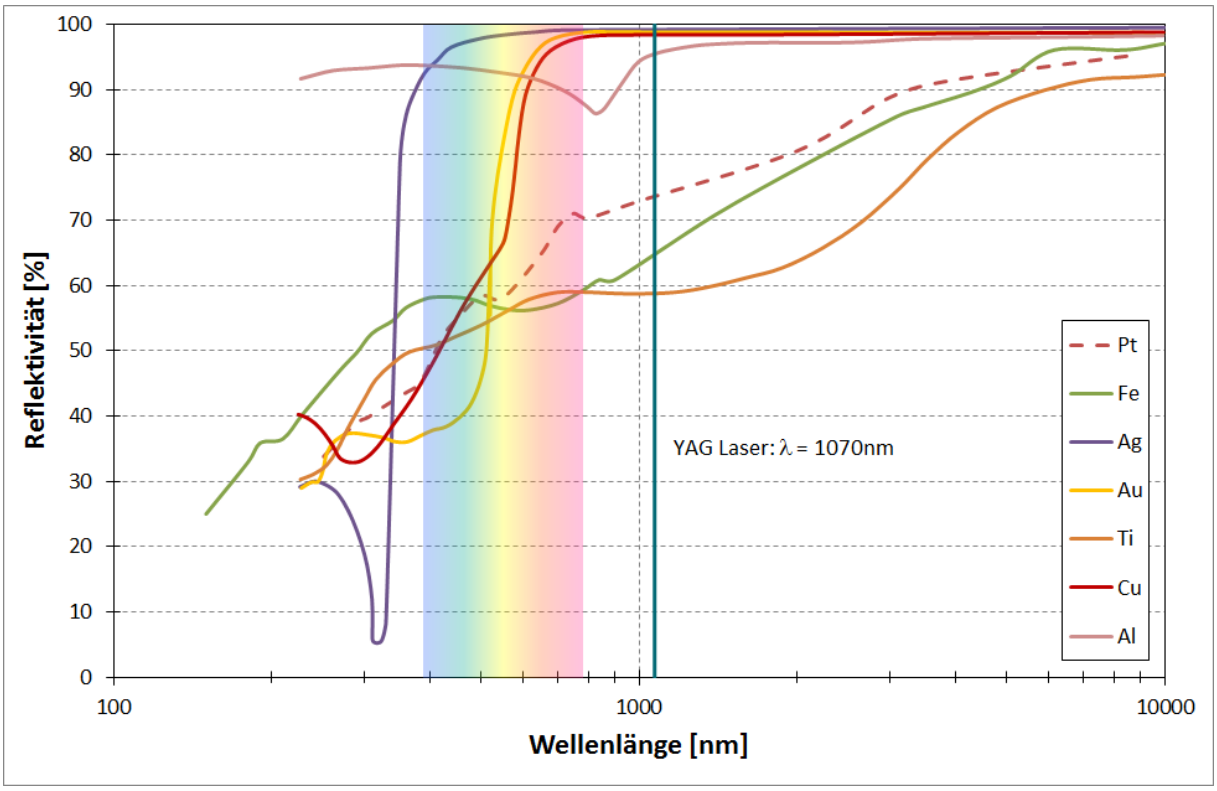

Figure 1: Reflectivity of several pure metals [13, 14]

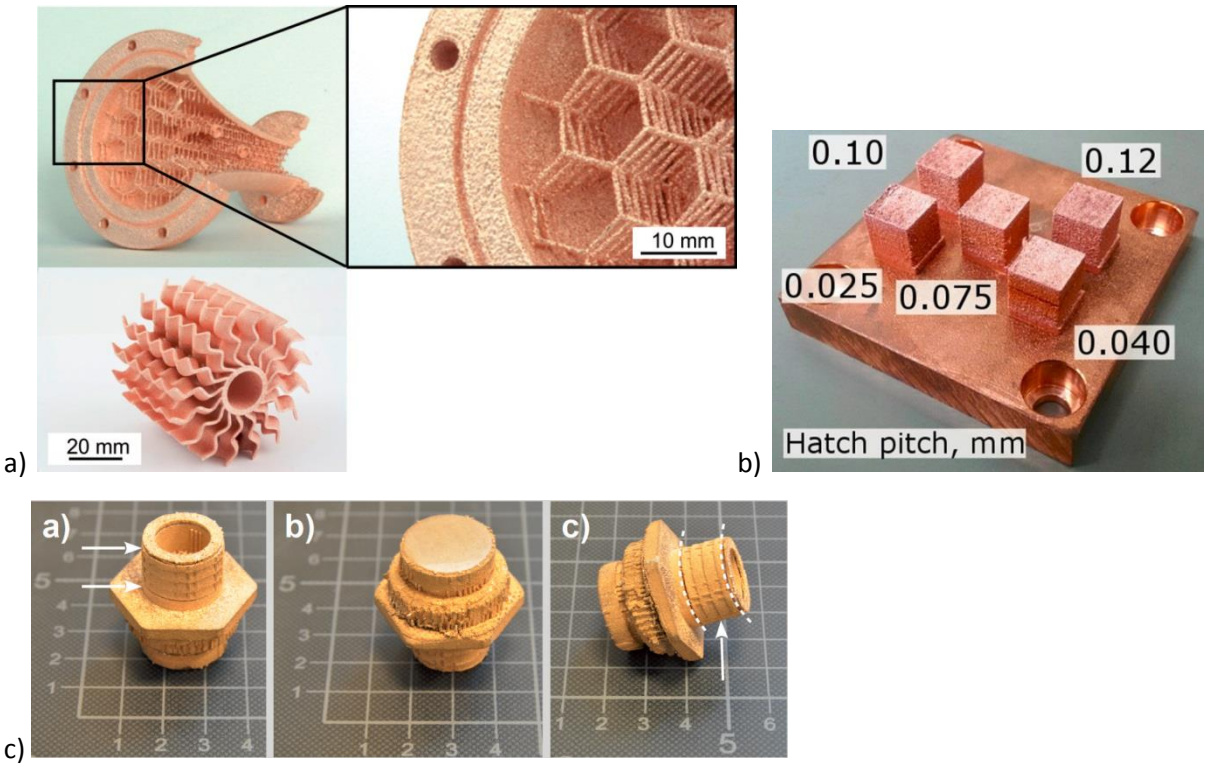

Figure 2: a) EBM-parts in pure copper [8] b) Test part in pure copper built with LBM [3] c) Bronze parts built with LBM [5]

2.1.2 Processing of Fe/Al in the 3D Printing process

Iron and aluminum are two of the most commonly used metals worldwide, e.g. in the transport and construction sectors. Their application in 3D printing (3DP) is particularly interesting for functional prototypes in short series and metal parts with internal complex geometry (like lattice structure) but also as mould inserts for thermoplastic injection. However, the technique suffers from limitations in terms of the length of infiltration, which is linked to the wettability of the matrix. It is hence necessary to improve the wettability of the powder to allow the production of larger parts. On the other hand, although there is high demand for high quality aluminum (alloys), until now, this technique is not applicable for Al-based parts. The thin passivation layer of aluminum oxide on the surface of the powders prevents the pre-sintering and makes the infiltration step almost impossible.

In the 3D printing process, parts are built up by deposition of a liquid binder through inkjet nozzles on a powder bed. The binder links powder grains according to CAD-data and “prints” the cross section of a part layer by layer from bottom to top. Then, the green part is heat-treated in a furnace to sinter the grains and to remove the binder. The density obtained at this stage is close to 60%. This density is too low to allow sintering of pre-forms without too high deformations (except for very small parts). The solution to solve this problem and to increase the final density of parts is to add a step of infiltration by a low-melting point metal using capillarity phenomenon [15]. The advantages of this M3DP process are its high speed, the ability to produce a large number of parts simultaneously and its flexibility using a broad range of different powders and functional inks.

The technique is particularly interesting because it allows the production of massive parts without contraction cavities (unlike in foundry process). Another main advantage of the technique is that support structures are not needed during the build-up of the parts. Additional supports may be used for backing during thermal treatment after printing of the part (mostly of ceramic materials, not directly connected).

Unfortunately, this technique suffers from some limitations. The depth of infiltration is linked to the wettability of the matrix. It is then necessary to improve the wettability of the powder to allow the manufacture of bigger/longer parts. It is a crucial parameter to process a reliable infiltration. This concept has already been studied but still needs to be improved and adapted to Al and Fe alloys [16].

Furthermore, an important limitation of the M3DP is that, so far, the technique is not directly applicable to aluminum while the request of high quality alloys is high. It is well known that Al alloy powders are difficult to sinter because of the stable aluminum oxide film covering the powder particles and thus reducing sinterability. Investigations of the effect of Mg on the sintering of Al-powders showed that densification is enhanced by adding of Mg [16]. This is attributed to a reduction of oxide films on the Al alloy particle surfaces. Significant improvements in the sinterability of aluminium alloys were reported to be achieved by liquid phase sintering leading to improved densification of the alloys, where the formation of the liquid phase assists densification. The effect of trace additions of selected elements such as Pb, Sn, Se, Bi, and Sb on the sinterability of aluminium alloys was investigated. Therefore, it is necessary to study the infiltration step of the Al preforms by low melting Al [17], the removal of the oxide layer on the powder’s surface which (based on experiments) improves the characteristics before adding selected elements [18, 19], and the grafting of chemical organic function present in the binder on the particle surface in order to increase the efficiency of the binder (e.g. for increased wettability) [20].

3 Description of the project results

3.1 Results of the single workpackages

Based on the working hypothesis (surface treated powders allow for improved production) and the derived four-step process (powder procurement, powder surface treatment, fabrication of test parts, characterization of test parts), the project's overall work is divided into seven work packages (WPs). WP0 is devoted to project management, while WP1 to WP4 cover the technical aspects according to the four-step process, WP5 deals with the technical and economic assessment of the applied methods for powder production and surface treatment, and WP6 covers all aspects of dissemination. The results achieved by each research performer are presented separately.

3.1.1 WP0: Management

3.1.1.1 Performed activities – fem / UMSICHT

The project partners met regularly during the course of the project. A kick-off meeting and four further steering committee meetings were coordinated and held every six months. In coordination with all research partners, also four SME committee meetings took place (on a respective national level), and a public final workshop with all the industry partners was organized at the end of the project (see Table 1 for a detailed list). The project meetings served essentially to present and discuss the research results, as well as to discuss further steps. The project coordinator at fem kept contact via phone with the other partners during the course of the whole project.

The final meeting has been organized to include a public 1-day workshop in order to present the project results to the industry and the research community in a fast and effective manner.

Table 1: List of the conducted project meetings

Steering committee meetings		**SME committee meetings**	
Date	*Place*	*Date*	*Place*
9.6.2016	Fraunhofer UMSICHT, Sulzbach-Rosenberg (Kick-Off)	21.07.2016	Indutherm, Walzbachtal
		28.09.2016	Materia Nova, Mons, BE
8.12.2016	Materia Nova, Mons, BE	02.12.2016	fem, Schwäbisch-Gmünd
		14.06.2017	Sirris, Liège, BE
31.5.-01.06.2017	fem, Schwäbisch Gmünd	29.09.2017	Fraunhofer UMSICHT, Sulzbach-Rosenberg
6.12.-7.12.2017	Sirris, Liège, BE	20.12.2017	Unicorn Engineering, Schwäbisch Gmünd
7.05.2018	fem, Schwäbisch Gmünd	24.01.2018	Materia Nova, Mons, BE
		08.05.2018	fem, Schwäbisch Gmünd (Final Workshop)
		27.06.2018	Materia Nova, Mons, BE (Final Belgian SME committee Meeting)

3.1.2 WP1: Synthesis of Base Powder Materials and in-situ surface treatment

3.1.2.1 Performed activities – fem

- Commercially available powders were purchased and characterized: OFHC 99,95 Cu-powder (particle size 15-45µm), CuSn10 (particle size 5-45µm) and CuNiSiCr (particle size 20-45µm)
- CuSn6 and two CuNiSi variants (CuNi1,5Si and CuNi3Si) were gas atomized from industry partner Indutherm and characterized at fem (after a classification performed by UMSICHT)

All the powders were gas atomised with nitrogen gas and obtained from different suppliers:

- pure Cu (TLS Technik GmbH & Co. Spezialpulver KG)
- CuSn6, CuNi1.5Si and CuNi3Si (Indutherm Gießtechnologie GmbH)
- CuSn10 (Concept Laser GmbH)
- CuNiSiCr (M4P – Metals for printing GmbH).

Details on the process parameters for atomisation were not disclosed. The CuNiSi were additionally classified in three batches with different powder sizes (5-20µm, 10-25µm and 10-45µm - see below the performed activities of UMSICHT for details).

The composition of the powders and of the starting material used for the atomization of the CuNiSi alloys was investigated via ICP-optical emission spectrometry (equipment: Varian Vista-Pro). The chemical analysis confirmed the purity of the Cu powder (99,99%); an oxygen content of 0,04% could be measured through carrier gas hot extraction. The particle size distribution was measured with laser diffraction and can be seen in Figure 3a: the characteristic diameters are D10=15,12 µm, D50=31,75 µm and D90=48,31 µm. A round powder shape and a slight satellite formation could be seen through the SEM investigation (Figure 3b). The latter was caused by a low fine fraction (particle size < 10 µm) in the powder. Said fraction did not however compromise the flowability of the powder, whose processability in the LBM machine was sufficient. No Cu-oxide was visible during the SEM investigation, neither on the surface, nor in the metallographic sample.

As for the Cu powder, the CuSn powders showed in the SEM investigation a spherical shape with single spattered and elongated particles (see Figure 4) The particle size was in the 5-45µm range. Although a slight satellite formation was noticeable also in case of the CuSn6 powder, both bronze powders showed a sufficient flowability during the building process (see WP3).

The results of the chemical analysis (ICP) on the used powders are listed in Table 2. For the composition of the CuNiSi alloys a slight decrease of the Zn content and a significant increase of the oxygen content are noticeable after the atomization process of the sheet material. The CuNiSiCr alloy shows a very low Si content (0.02%), which is considerably higher in the CuNi1.5Si and CuNi3Si alloys (0.29% and 0.49%, respectively).

Table 2: Results of the ICP Analysis on the used materials and powders

Mass [%]	Cu Powder	CuSn6 powder	CuSn10 powder	CuNiSiCr Powder	CuNi1.5Si Metal sheet	CuNi1.5Si Powder	CuNi3Si Metal sheet	CuNi3Si Powder
Cu	Bal.	Bal.	Bal.	Bal.	Bal.	Bal.	Bal.	Bal.
Ni	0.007	0,016	0,051	1.95	1.43	1.43	2.46	2.48
Si	<0.02	-		0.02	0.29	0.29	0.48	0.49
Mg	<0.001	-		<0.001	<0.001	<0.001	0.087	0.078
Zn	<0.005	0,079	<0,005	<0.005	0.14	0.096	0.058	0.046
Cr	<0.001	-	-	0.074	<0.001	<0.001	0.019	0.019
Fe	<0,001	0,012	0,009	0,067	0,010	0,010	0,012	0,012
O	0.051	0,11	0,045	0.63	0.002	0.038	<0.001	0.028
Sn	-	5,4	10,4	-	-	-	-	-

The SEM investigations on the particle morphologies after sieving and sifting have shown for all CuNiSi powder materials (CuNiSiCr, CuNi1,5Si and CuNi3Si) a predominantly spherical form with only a few spattered or elongated particle shapes (see Figure 5). Although a slight satellite formation could be observed within the 10-45 µm and 10-25 µm size fractions (as was the case for Cu and CuSn), all powders have been proved to possess a sufficient flowability during the building process.

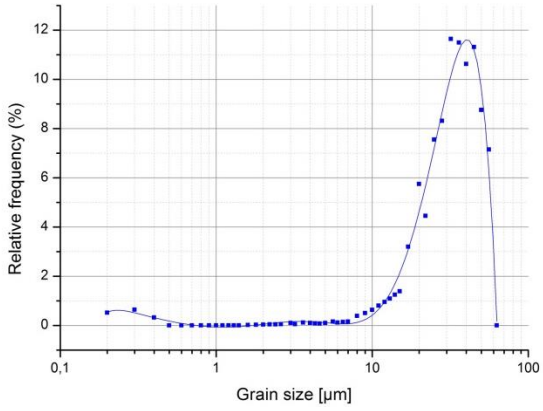

a)

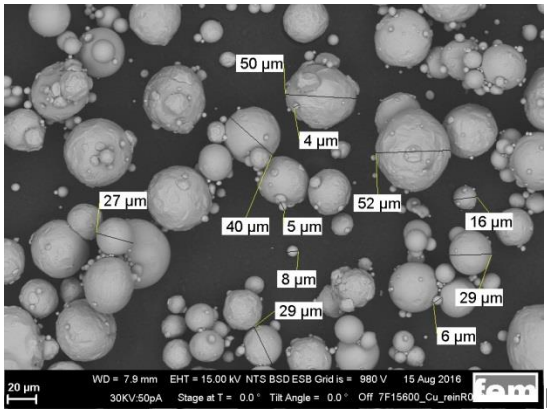

b)

Figure 3: a) Grain size distribution of the commercially available Cu-power b) SEM investigation of the powder (visible satellite formation) – measurement of the grain size

a)

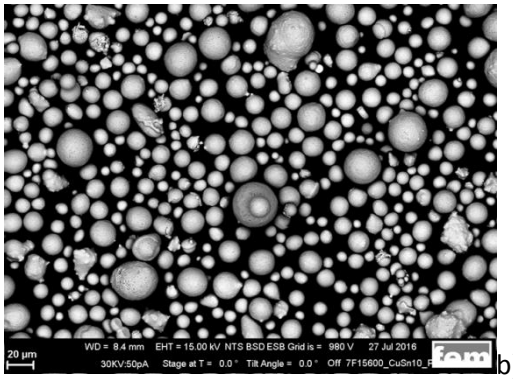

b)

Figure 4: SEM investigation of the employed CuSn powders- a) CuSn6-powder (slight satellite formation is noticeable) b) CuSn10-powder

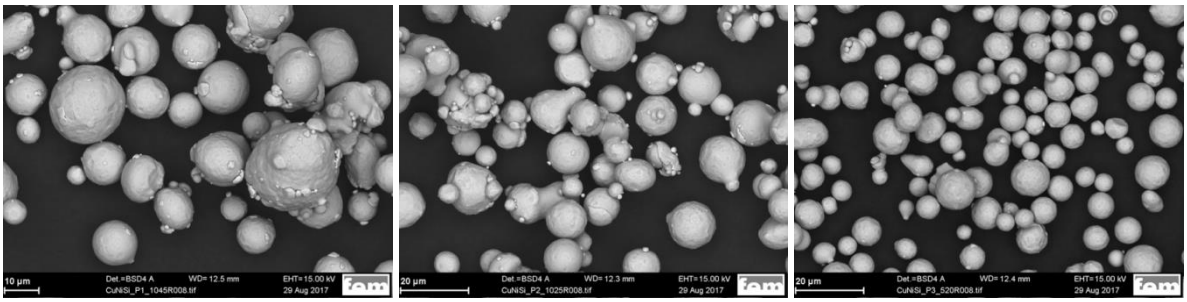

Figure 5: SEM images of CuNi1.5Si powders in size fractions 10-45µm / 10-25µm / 5-20µm

3.1.2.2 Performed activities – UMSICHT

- Preparation of powders

The aim of this work package at Fraunhofer UMSICHT was the preparation of powders in order to provide Cu and Cu alloy powder qualities which are specifically suitable to be further processed via the powder bed fusion process (LBM). Conventional inert gas atomization (IGV) and a special hot gas atomization process (HGV), potentially performed with reactive gas components (R-HGV), and sizing equipment have been planned to be involved in this work.

Since spherical, inertly gas atomized (N_2) pure copper powders are available as standard powders on the commercial markets, these powders have been purchased from industrial suppliers (ECKA Granules Germany GmbH, Schlenk Metallic Pigments GmbH) and further processed by classifying and coatings operations. Two CuNiSi alloy powders (CuNi1.5Si, CuNi3Si) have been purchased from the cooperating SME Indutherm Gießtechnologie GmbH whereby the company took over a considerable part of the manufacturing costs. These alloy powders have been delivered in a standard size fraction from 10 µm to 63 µm with some remaining fines < 10 µm. In order to investigate the basic influence of the particle sizes and size ranges on the LBM parts qualities, these powders have been subsequently further classified at Fraunhofer UMSICHT in several size fractions (see the following section).

The manufacturing of further alloy compositions such as the possible candidates CuAg and CuB has not been realized in the course of the project. Preliminary tests at fem with laser experiments on respective metal sheets showed that (micro-) alloying of the Cu with these elements will not support the LBM process remarkably in the interesting range of compositions (low losses in electrical conductivity).

In agreement with the project consortium, the (reactive) hot gas atomization process has also not been involved in the project work for two reasons:

1) The purchased powders had enough fine powder particle content in order to provide finer classified powder qualities.
2) Preliminary results at fem by applying LBM on oxidized metal sheets showed that CuO will not effectively support the process. Thus, the in-situ oxide coating via a reactive hot gas atomization was no more required.
3) The atomizer at UMSICHT was not available for several months due to service.

Consequently, the work at UMSICHT concentrated on the adjustment of powder size ranges (see following chapter) and the development of sulfide coatings on Cu powders. The latter point has been

investigated thoroughly and not performed work from WP1 is balanced by the extended work for the coating development (section WP2). The hot gas atomization technique is discussed in section WP5 under technological and economic aspects for its enhanced capability to produce fine powders.

- Classification of the the CuNiSi powders (CuNi1,5Si and CuNi3Si) into three different fractions

The CuNiSi powders were classified via sieving and sifting operations in order to achieve specific particle size ranges between 10 µm and 45 µm (related results during processing are detailed in WP3). The particle size distributions have been measured with a Sympatec HELOS laser granulometer. The classification processes for the different powders, namely the sieve size and the sifting parameters, have been adjusted to generate three different size classes from the as-atomized powders: a 10-45 µm fraction corresponding to a commonly used size dstribution and two finer powder size ranges, i.e. 5-20 µm and 10-25 µm. The size distributions of the achieved powder qualities for alloy CuNi1.5Si are shown in Figure 6. As can be seen, the powder in size fraction 10-25 µm contains still a considerable portion of particles less than 10 µm (approx. 12 % 6-10 µm) whereas the both other size fractions are very well inside the specified range. This result is also true for the classified CuNi3Si powders which are not displayed in the diagram.

Furthermore, powder mixtures from the fine fraction less than 15 µm with the size fraction 20 -45 µm in a mixing ratio of 80/20 (mass-%) have been prepared in order to evaluate the possible influence of a higher apparent density (see dotted curve in Figure 6).

At this point it can be stated that the particle sizes clearly play an important role in the LBM process with Cu (alloys) by allowing to form denser parts with increasing fineness of the size fractions (see fem work in section WP3). This can be attributed to the higher laser energy absorption with decreasing particle size [2]. However, the flowability of the powders is reduced with increasing fineness and, the mixed powder which contains a high portion of particles less than 10 µm, was no more practical to be processed via LBM at fem. Flowability measurements on the different powder qualities have been made by using a so-called Hall apparatus according to ISO 4490:2018: a certain amount of powder flows out from a funnel with defined opening and the time is measured. Only the powders in size fraction 10-45 µm were able to be measured reliably with this instrument. All other powders with finer size distributions started to block the funnel outlet and data acquisition was not possible.

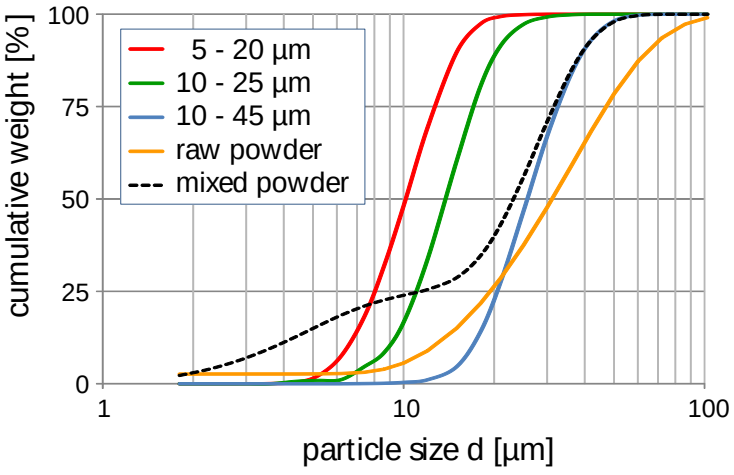

Figure 6: Particle size distributions of the raw CuNi1.5Si powder and its classified fractions.

Figure 7 displays the corresponding SEM images from the different particle size fractions of the prepared CuNi3Si powders. The powders exhibit a low amount of satellite formation (adherent fine particles on larger ones).

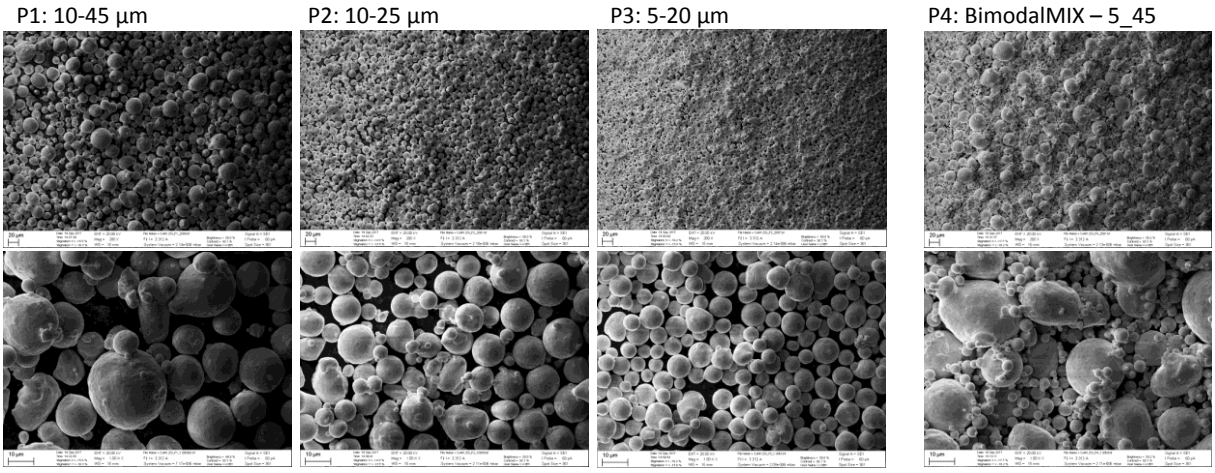

Figure 7: SEM images of the different prepared particle size fractions from CuNi1.5Si alloy

3.1.2.3 Performed activities – Sirris

- Base stainless steel and aluminum powder provision and characterization

Two kinds of powders had to be selected for this study:

- A powder to be printed, with a higher melting point, that will be used to shape the parts by 3DP
- A powder to be used as an infiltrant, with a lower melting point, that will melt during thermal treatment, be sucked by capillarity and fill the porosity of pre-sintered body coming from 3DP

Important parameters for selection are the melting points of printed and infiltrant materials, and the wettability of the infiltrated material by the molten infiltrant. Printed powder has also to have a suitable particle size range, compatible with the 3DP process. Infiltrated material powder can be coated with specific elements in surface to improve wettability.

For stainless steel, 316L powders (melting point: 1430°C) of three particle size ranges have been provided by Höganäs (member of the Belgian SME UC): 45-60µm, alloys 5220 and 5520. Cumulative distributions of these three powders are shown in Figure 8. Packing density and Hall flowability have been measured and compared to values of certificate of analysis (Table 3).

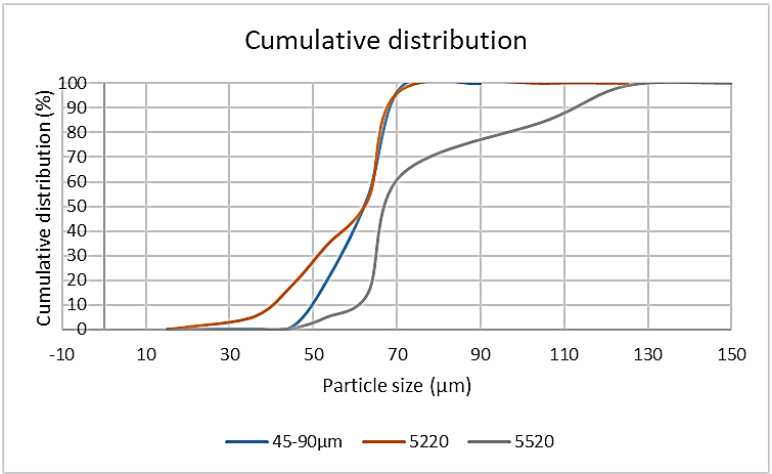

Figure 8: Cumulative particle size distribution of the 316L powders

Table 3: Packing density and Hall flowability of 316L powders. * powder sieved at 120µm.

	45-90µm	5220	5520
Packing density - Hoganas (g/cm³)	4,09	4,08	4,11
Packing density - Sirris (g/cm³)	4,23	4,29	4,39*
Flowability Hall-Hoganas (s/50g)	17,1	17,2	17,5
Flowability Hall - Sirris (s/50g)	18,5	17,6	15,7*

Alloys selected for 316L infiltration were brazing steel, also from Höganäs:

- Brazelet BNi7: Ni-alloy with a melting point of 890°C, with a recommended brazing temperature range of 980-1095°C.
- Brazelet F300: highly alloyed steel with a melting range of 1020-1050°C, with a recommended brazing temperature range of 1100-1150°C.

These alloys are provided in powder form, and the most important characteristic for infiltrants is their composition, which is given in Table 4. Elements highlighted in red will be discussed in the following WP.

Table 4: Composition of the two brazing alloys

BNi7	
Ni (balance)	75,9%
Cr	14,0%
P	**10,0%**
Fe	0,1%

F300	
Fe (balance)	39,0%
Ni	20,0%
Cr	20,0%
Cu	10,0%
P	**7,0%**
Si	**4,0%**

For aluminum, 3004 aluminum alloy has been selected to be printed because of its high melting range (630-650 °C) close to its of pure aluminum (660 °C). Unfortunately, this alloy is not available as a powder. A special batch with specific particle size range (50-100 µm, centered on 60 µm) has been made on demand by Nanoval. This size distribution is most suitable for the 3DP process.
Al-alloys have been selected as potential infiltrant material for their low melting range:

- AlSi10Mg, with a melting range of 560-600 °C,
- AlSi12Cu, with a melting range of 570-580 °C,
- AlMg20, with a melting range of 450-550 °C.

All these three materials are available at Sirris in ingot or powder state. Composition of all aluminum alloys are gathered in Table 5. Figure 9 shows the Al-Si and Al-Mg phase diagrams.

Table 5: Weight composition of aluminum alloys (3004 + infiltrants)

Alu 3004	w%
Al	97,8
Mn	1,2
Mg	1

AlSi10Mg	w%
Al	89,5
Si	10
Mg	0,5

AlSi12Cu	w%
Al	87
Si	12
Cu	max 1

AlMg20	w%
Al	80
Mg	20

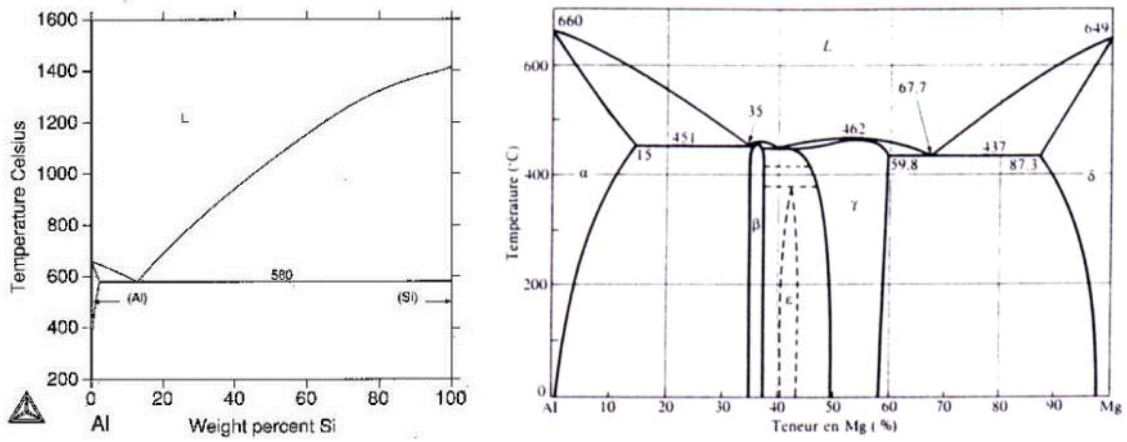

Figure 9: Al-Si (left) and Al-Mg (right) phase diagrams.

3.1.3 WP2: Surface modification of powder materials

3.1.3.1 Performed activities – UMSICHT

The aim of this working package at UMSICHT has been the development of methods and coatings from copper sulfide on copper powder particles. Copper sulfides and sulfur have some interesting properties in respect to the project aims:

- A high absorption coefficient and, as a thin coating, a certain transmissivity at the LBM wavelength [21]
- Nearly no solid solubility of S in Cu and, thus, potentially a low influence on the electrical conductivity
- A melting point close to Cu (for Cu_2S)
- Reactivity with Cu oxides

The methods for generating copper sulfide have been selected to be based on the reaction of the particles in a sulfur containing atmosphere at elevated temperatures, either in gaseous or vapor phase. For the vapor phase reaction a so-called isopiestic reactor has been proposed, i.e. the reaction under a specified constant partial pressure of the S vapor. According to these aims, a reactor has been designed and coating processes have been investigated.

Furthermore, methods for coating manufacturing in liquid phases have been investigated due to the fact that the particle surfaces might be contacted more uniformly by liquid mixtures than it might be the case for bulk powders in contact with the gaseous phases.

The reaction of sulfur with copper is slightly exothermic and could be realized by only mixing these two components in powder form. However, this reaction has to be initiated by a slight temperature increase in order to get the reaction started with remarkable conversion rates. During the reaction different stoichiometric compositions form which may be expressed by the common chemical formula

$$(2-x)\,Cu + \frac{1}{8}\,S_8 \rightarrow Cu_{2-x}S$$

Aside the most stable reaction product Cu_2S (chalcocite) numerous other crystalline compositions can form such as covellite (CuS), digenite ($Cu_{1.8}S$) or djurleite ($Cu_{1.95}S$). All generated powder products have been investigated via optical methods (light and electron microscopy), X-ray diffraction (XRD), elemental (EDX) and thermal analysis (DTA/TG). High resolution SEM/FIB investigations have been performed by fem for getting more information about the achieved coatings thickness (see section "Performed activities – fem" in this chapter).

The work performed at UMSICHT can be summarized as follows:

- Lay-out and manufacturing of reactor chambers suitable to generate a fluidized powder bed with reactive gas and vapor components
- Coating experiments with Cu powder and Ar/H_2S gas mixtures and S vapor at different temperatures, coating times and sulfur concentrations
- Optimization of reactor chambers and parameter sets
- Manufacturing of a simple reactor for wet chemical reaction of Cu powder with sulfur diluted in water and in toluene
- Investigation of the generated coatings
- Laser melting tests with a simple test stand and application of a 300 W NdYAG laser
- Test powders for further investigations by fem in its LBM unit

Wet chemical methods

Coating investigations have been performed in a simple reactor (glass bulb) with a resistance heating mantle. Powder and liquid are stirred continuously during the reaction process by a rotation of the bulb and a stirring element inside the bulb. For the achievement of a specified coating thickness, the concentration of the solutions has been adjusted according to the estimated free powder particle surface (from laser granulometry measurements) and the assumption that the reaction of solved S with the available Cu surfaces will be 100 %. Two forms of liquid solvents have been investigated by modifying S concentration, temperatures and reaction times. The considered temperature range has been between room temperature and maximal 80 °C for these experiments.

a) Potassium poly-sulfide in water (+ NaOH)

The main sulfide reaction product has been identified via XRD to be the $Cu_{1.92}S$ modification. In all tested experiments Cu sulfide formation was accompanied by the formation of Cu oxide species on the powder surfaces at. Therefore, these experiments have been stopped in an early project state.

b) Sulfur in toluene

The solubility of S in toluene is approx. 2 % at room temperature and increases to about 3 % at 60°C. No reaction of the dissolved S with the Cu powders could be observed at room temperature. A minimum temperature of 40°C has been identified in order to start the reaction. However, despite the investigation of a huge range of parameters with different solution concentrations (atomic-% range of the ratio $S/Cu_{surface}$ = 1 - 3 by assuming 250 nm Cu_2S layer thickness) and reaction temperatures (20°C - 50°C), it was not possible to generate suitable thin and homogeneous coatings. The most probable explanation for this phenomenon is that the exothermic reaction leads to

localized “hot spots” on the particle surfaces which accelerate the reaction at these points. As a consequence, it then propagates locally to form large crystals instead of closed coatings and/or a huge amount of particles with thick coatings and uncoated ones are the result.

Figure 10 depicts SEM, EDX and XRD results from both coating modifications showing the differences in CuS coating morphologies and phases for clearly “overreacted” powders. The SEM images demonstrate the “localized” character of sulfide formation and the differences in the crystallite structure. In general, the sulfides are brittle and obviously do not have a chemical bonding to the base material Cu. The XRD measurements (Figure 10c) reveal a $Cu_{1.92}S$ phase (djurleite) and Cu_2O for the potassium poly-sulfide whereas no oxide is detected for the toluene solution and the two (similar) sulfide modifications $Cu_{7.2}S_4$ and $Cu_{1.8}S$ (digenite) can be identified.

At this stage it shall be noted that the CuS layers can no more be identified via the used XRD equipment, if they are below approx. 200 nm thickness. Thermal analysis (DTA with simultaneous TG) has been used for getting supplemental information. Figure 11 displays a measurement on Cu coated with Cu sulfide with a toluene process. The presence of Cu sulfides can clearly be detected by the weight loss at 740°C and 970°C which can be ascribed to the formation of stable Cu_2S according to the formula $Cu_{2-x}S \rightarrow Cu_2S + S_{x\ vapor}$ and the measureable melting point of Cu_2S at 1100°C.

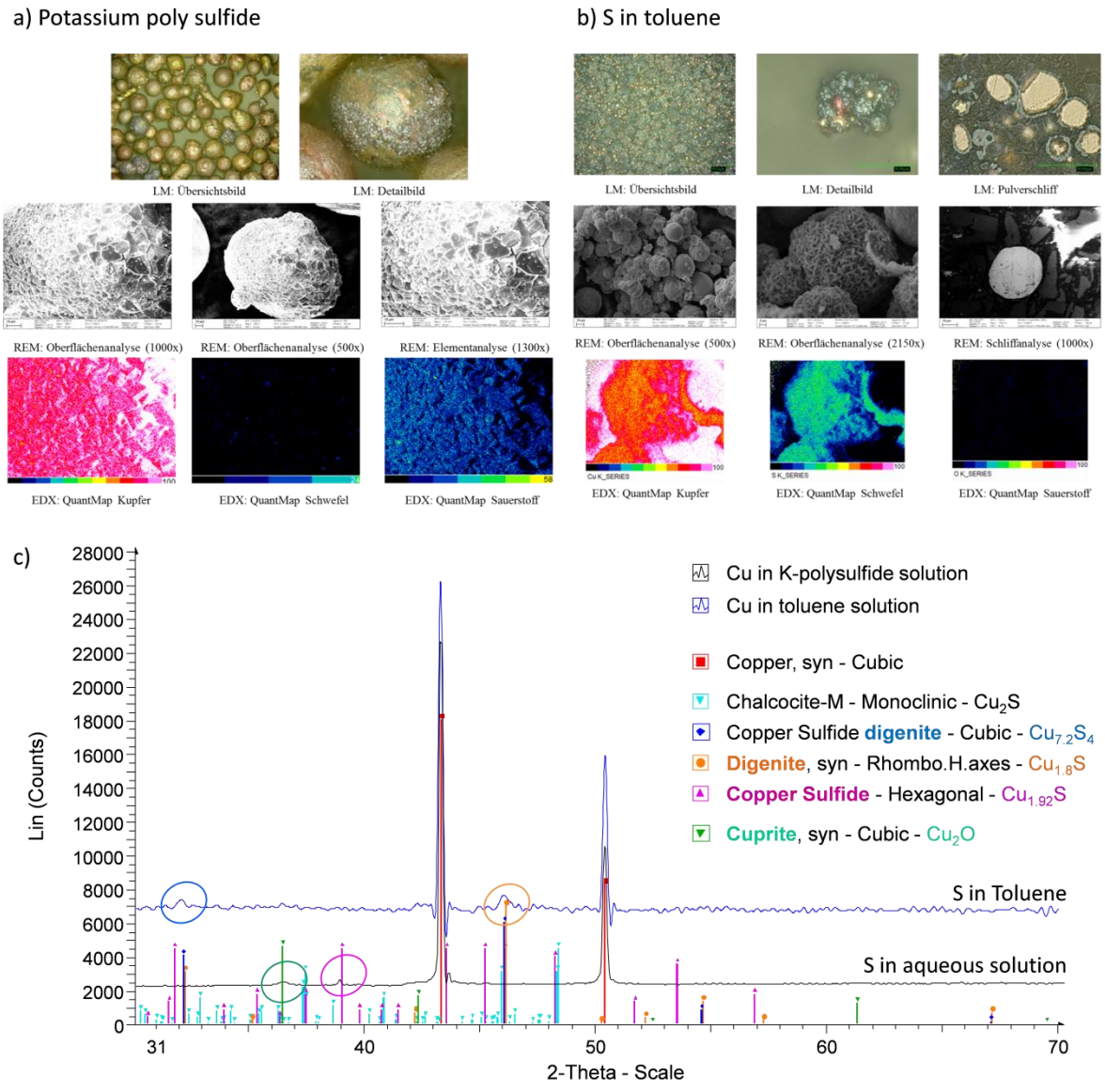

Figure 10: Light microscopic, SEM and EDX images from reacted Cu powder in a) potassium polysulfide and in b) S-toluene solution together with c) the corresponding XRD pattern

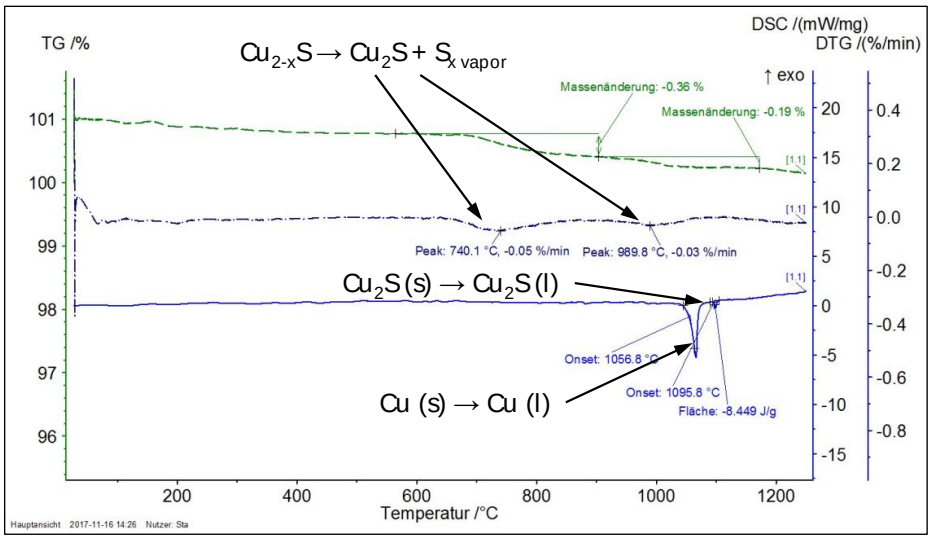

Figure 11: DTA measurement from a Cu powder coated by a toluene solution process (dashed lines = TG measurement curve and its derivative)

Conclusions:

The use of aqueous solutions is inappropriate for forming Cu sulfide coatings due to the accompanied formation of oxides. In contrast, oxide formation can be completely avoided during the Cu sulfide coating process in toluene solutions. However, despite the continuous stirring of the solvent and powder, the sulfide formation on the individual particles and the powder did not form homogeneous coatings under the realized experimental conditions. It is assumed that the exothermic reaction (simplified Cu + S → CuS - 53 kJ/mol) leads to a preferred crystal formation and growth at localized points on the particle surfaces after its initiation. This problem may be successfully solved, if sulfur concentration in the solution is further reduced and the movement of powders in the solution is accelerated. Then it can be expected that (local) excess heat on the particle surfaces can be efficiently dissipated through the solvent. In this case, it would be an attractive and economic production route to produce sulfide coated copper powders, since the sulfur concentration can be adjusted very precisely and the solvent can be re-used many times without remarkable losses.

Vapor and gas phase methods

The basic reactor design which has been realized and optimized during the project work is depicted in Figure 12. The powder containment chamber can be adopted for the use of different powder bed configurations and is able to treat up to 6 kg per batch. It is equipped with gas supports and gas flow controllers which provide the main gas (fluidizing gas F) and gas mixtures (K2 and K8). Gas mixtures can be realized by premixed gases or by mixing gas components with separate gas flow controllers. The reactor, the gases and the vapor source can be heated independently (T1, T2).

The fluidization characteristics have been estimated by the deposition of a bulk copper powder layer on a steel powder bed. Due to the color difference and a similar density of the materials, the powder bed movement can be simulated and visualized. Figure 13a) shows an example where the copper powder is placed as a layer on top of the steel powder. After a short fluidizing period the powder is removed from the container layer by layer (photo sequence from left to right) giving a view on the mixing of both components at different height levels. The schematic drawing in Figure 13b) shows the resulting powder movement and mixing behavior after a 1-minute period of fluidizing. These

experiments supported the optimization of the powder containment and gas diffusor design as well as the adjustment of the gas flow rates.

For the coating processes, the chamber is filled with pure Cu powder and is then slightly purged with an inert gas stream. The oxygen content in the exiting gas has been measured to adjust the time for reaching an oxygen level < 100 ppm inside the reactor before starting the heating sequence. After reaching the demanded reaction temperature, the inert gas flow (argon 4.6) is increased to reach fluidizing conditions and the reactive component flow (Ar/H_2S) is started. Both gases reach the chamber in a preheated stage (=chamber or pre-heating temperature). In the case of the sulfur vapor arrangement, the sulfur is heated separately for vapor generation which then enters the chamber together with the preheated purging gas (Ar).

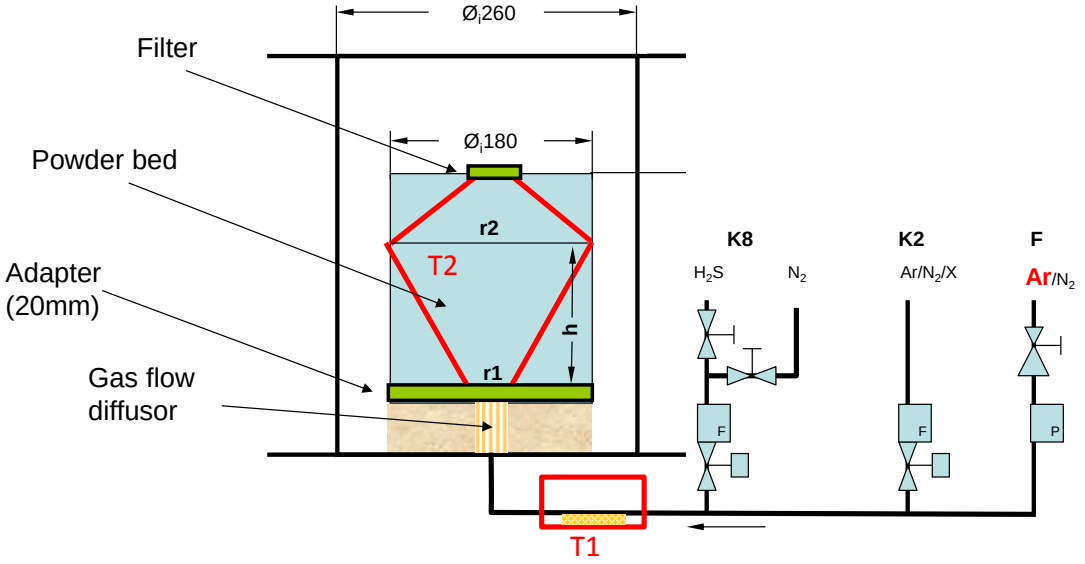

Figure 12: Sketch of the basic reactor design with different gas supplies (N_2, Ar, H_2S) and sulfur vapor generation.

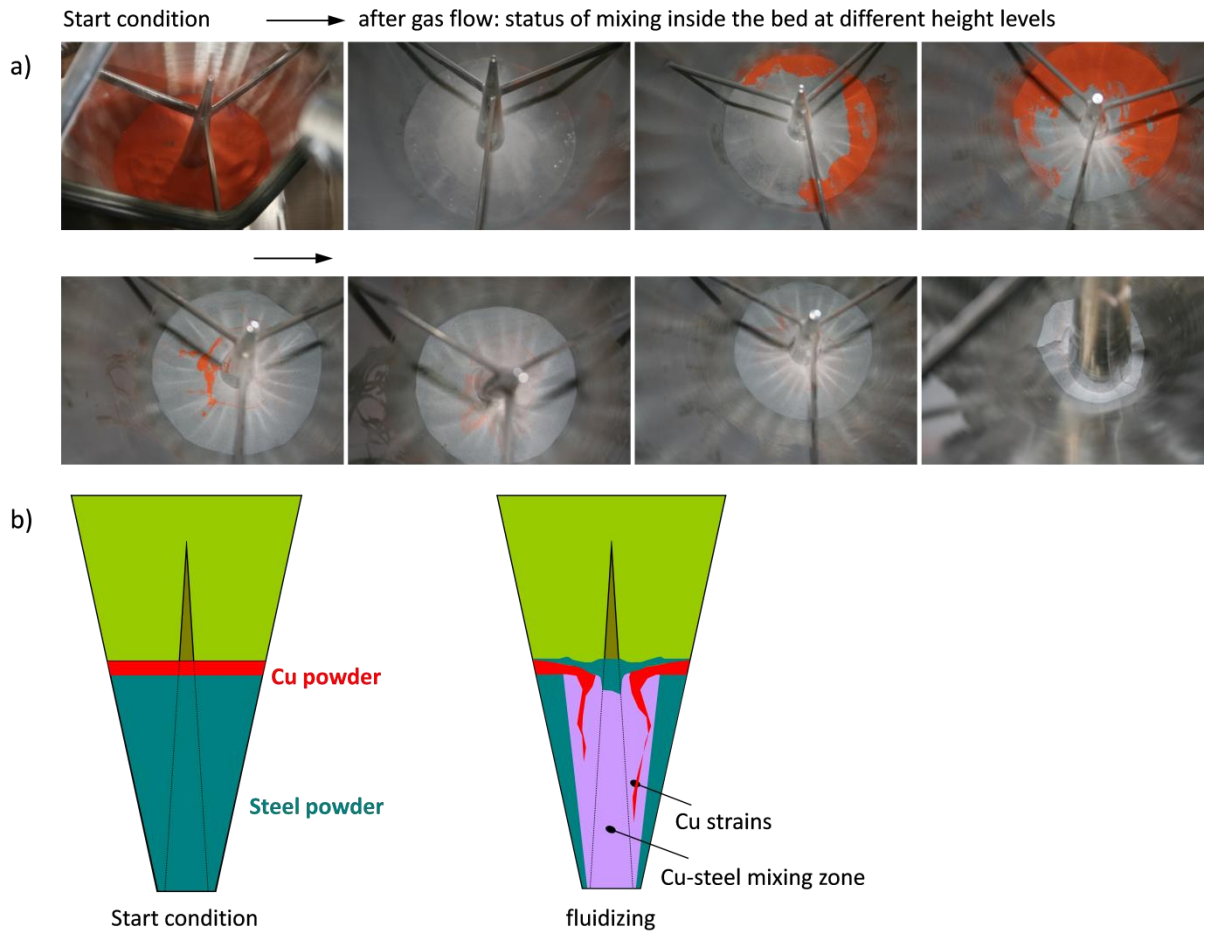

Figure 13: a) View into the powder containment filled with steel powder (grey) and copper powder on top before (upper left) and after a fluidizing action (from left to the right at different height levels) and b) schematic drawing describing the start and end situation of the 1 minute fluidizing action.

The isopiestic process route requires that the temperatures within the complete transportation and reaction paths (container) are adjusted very precisely at the same temperature. This could not be realized in a satisfying manner. Therefore, the S vapor experiments have been performed by weighing in balanced amounts of sulfur (in relation to the amount of Cu powder surface) which are then heated up at specified heating rates (1 to 3.5 K/min) up to 450 °C for a complete evaporation the S source ($T_{evap.}$ = 444 °C). The powder containment has been held at specific (lower) temperatures.

For the H_2S experiments the reaction temperatures have been kept low (up to 50 °C). In both modifications, the main task was to find the optimum working point for a good mixing of the powder and to adjust temperatures properly. Similar coating results have been generated as described before for the wet chemical routes with inhomogeneous and too thick coatings. With further refinement of the processes, coating homogeneity could successfully be enhanced and coatings thickness reduced, mainly by adjusting the temperature and the provided sulfur concentration. This is demonstrated in Figure 14a, which depicts the results from S vapor experiments performed at different temperatures and heating rates. Similar results have been achieved with the coating experiments in H_2S gas.

The resulting surface sulfur concentrations which are given in the following descriptions in wt.-% are estimated as mean values from several EDX measurements on the powders. This method is only a rough specification, however, the values are in good agreement with the optical observations.

Coatings with thickness of approx. 400 nm still tend to form cracks and to delaminate from the copper particle surfaces (Figure 14b). This is no more the case, if the coatings thickness is reduced to approx. 100 nm (Figure 14c). Therefore, the generation of such thin coatings is a twofold need in view of i) providing a reliable powder quality and ii) in order to reduce the introduced amount of foreign elements in the LBM process and built copper parts. The question was: are these coatings effective during LBM.

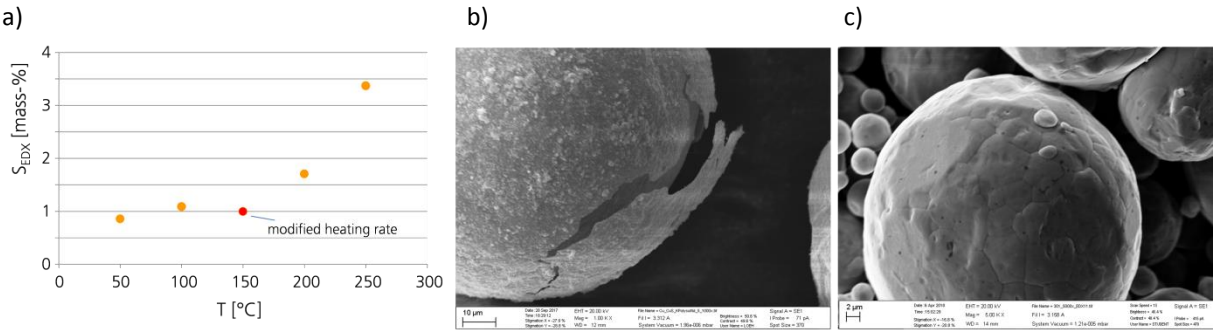

Figure 14: Variation of sulfur concentration from surface sulfide (EDX) as a function of coating temperature (powder containment) and heating rate (S vapor generation) and SEM images from b) approx. 400 nm generated in S vapor and c) approx. 100 nm coating from an H_2S experiment.

For a first impression of the influence of the sulfide coatings on the processing of the Cu selected powder qualities have been checked in respect of their laser melting behavior by using a simple experimental set-up: Powder layers have been deposited manually on a height adjustable steel substrate and up to 5 laser melting procedures (layers) have been performed by using a scanning module with a 300 W laser at the OTH Amberg. The experiments have been performed under argon with different laser powers at 200 m/s scanning speed and a hatch distance of 0.036 mm. The scanning direction has been altered by 90° from layer to layer. The argon purging of the process chamber allowed oxygen levels less than 1.8 %.

Figure 15 shows examples from these experiments: Pure copper powder neither does adhere to the substrate nor does it form a closed layer due to heavy balling effects. The results are considerably improved, if powders with Cu sulfide coatings are used. Already at a surface sulfide as low as 0.03 wt.-% sulfur a positive effect can be observed. With increasing surface sulfide concentration the process is further enhanced. Above a surface sulfide concentration of approx. 1 wt.-% S the positive effect is reduced again.

EDX measurements made from the generated coatings reveal no remaining sulfur (Figure 15c). Therefore, the sulfur might be completely vanished by evaporation and/or reaction with the present oxygen. Optically, no evaporation events have been observed during laser melting so that the latter one may be the predominant phenomenon.

Despite the clearly enhanced processability, the balling effect cannot be suppressed efficiently. Large pores and a poor interlayer connectivity are clearly visible. These results are in agreement with the findings at fem in their LBM unit (see chapter WP3).

Conclusions:

A fluidized bed reactor has been realized where thin and homogeneous CuS coatings can be generated successfully via the introduction of sulfur vapor or H_2S gas which is added as reactive component to the fluidizing gas. Coating thickness can now be adjusted by choosing the appropriate parameter settings such as S concentration, reaction temperature and time.

The surface sulfides enhance the processability of the Cu powders remarkably, however, the balling effect cannot be suppressed effectively. According to the investigations of D. Becker [2], the adaptation of LBM process conditions, mainly in terms of an increased laser powder, seems to be the only solution. Therefore, the present results are promising by helping to lower the necessary laser power. Further investigations by using higher laser energies and by adopting the LBM process conditions accordingly are still necessary in order to prove the present development and concept.

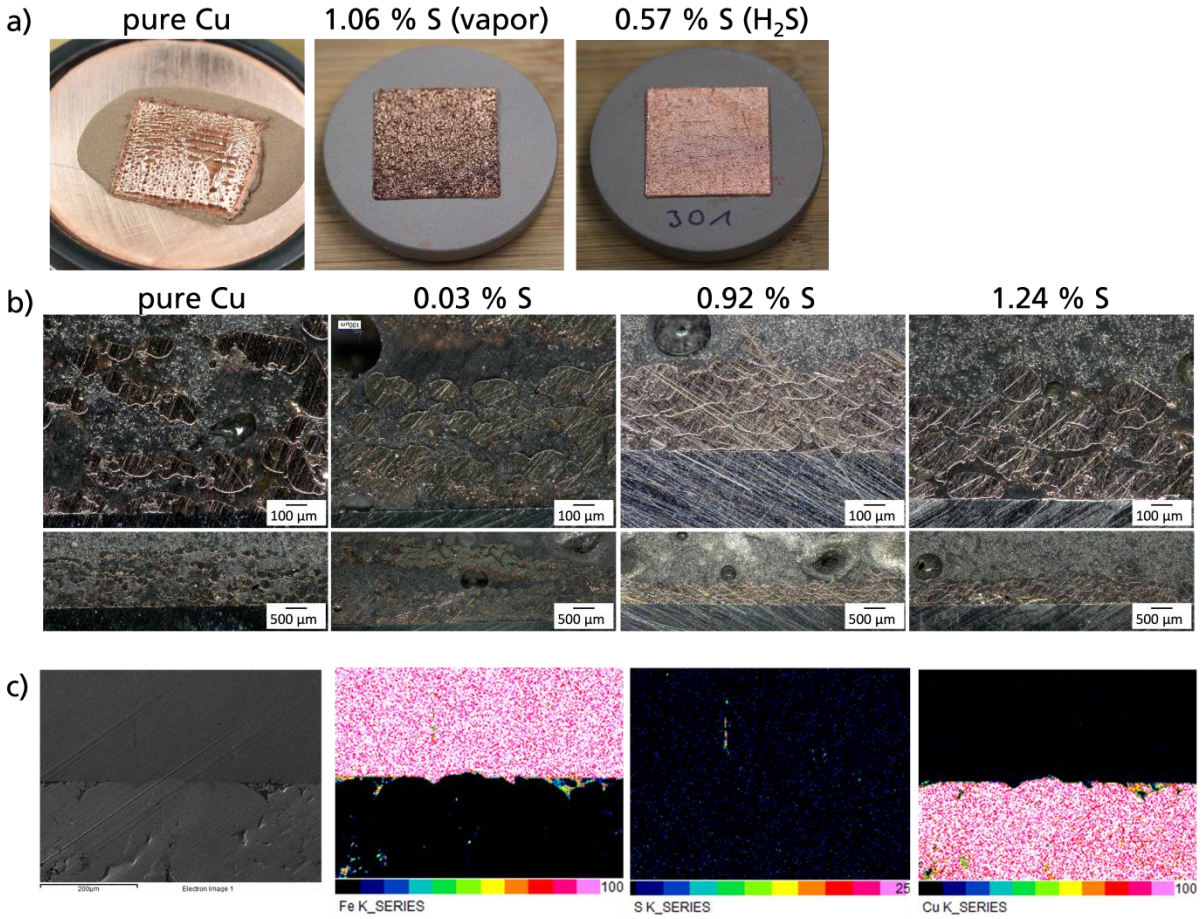

Figure 15: Laser molten Cu powders without and with Cu sulfide coatings with different surface sulfide concentrations (S in wt.-%): a) generated layers on the steel substrate, b) microsections from generated layers and c) EDX measurement from the layers with 0.92 wt.-% S in the surface sulfide

3.1.3.2 Performed activities – fem

- Cu-powder was thermally treated in a furnace with different hold times and investigated with SEM and FIB
- Two batches of sulfur-coated powders (both solution coated and vapor deposition coated) were investigated with SEM and FIB
- Two batches of Ti-coated powders (both solution coated and vapor deposition coated) were investigated with SEM and FIB

The thermal treatment of the pure Cu-powder had the goal of increasing its processability through the formation of an oxide layer. Different holding times and temperatures were tested, in order to optimize the oxide layer thickness and its regularity. A temperature of 200°C (hold time 1 h) led to a strong oxidation and almost sintering of the material, which compromised the flowability too much. Therefore the temperature was reduced at first to 150°C, and then to 125°C. At 150°C an irregular oxide layer formed (20-60 nm) on the particles surface, whereas the temperature of 125°C, combined with a holding time of 2-4 h, generated a regular layer thickness (20-25 nm – see Figure 16)

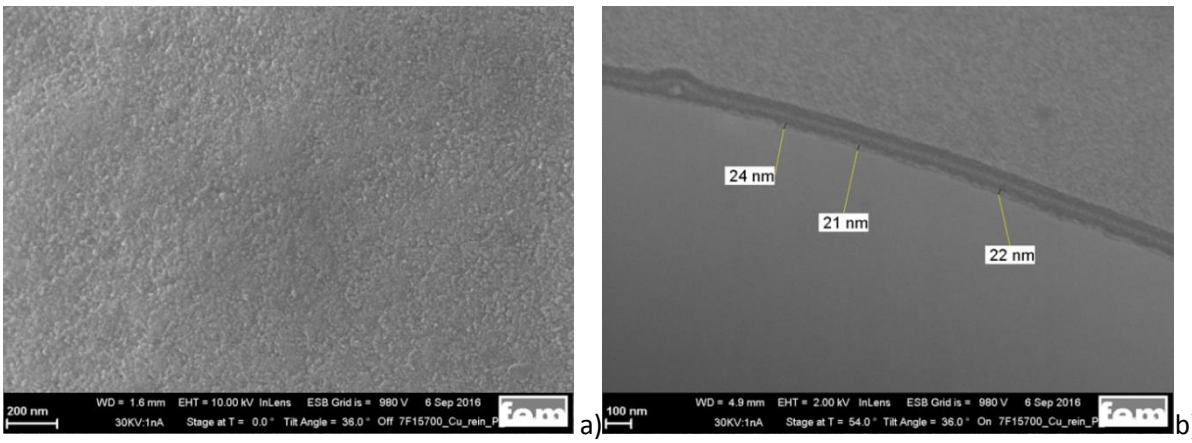

Figure 16: Thermal treatment of the Cu powder in furnace at 125°C (2 h) a) oxidized surface of a powder particle b) FIB-cut to measure the oxide layer thickness

The SEM investigation of the solution coated powder (SL-P115) showed a non-homogeneous copper sulfide layer on the particles. The coating was irregular (depending on the particle), and through the FIB-cut thicknesses from 30-1000 nm could be measured (see Figure 17). The SEM investigation on the powder coated through vapor deposition revealed a more regular coating on the particles surface, and thickness was established to be around 70 nm (Figure 18). Given the irregularity of its coating, it was decided not to use the solution coated powder for selective laser melting trials, opting instead for the batch coated through vapor deposition (results obtained are shown in WP3).

The pure Cu-powders were coated from the research partner Materia Nova in Belgium: a first batch produced with a non-optimized trial, and a second batch coated by using improved equipment. Both batches were investigated at fem and employed for laser melting trials. The composition of the powder was investigated with ICP Analysis, and the results can be found in Table 6. The titanium content of the second powder batch was significantly higher, but a remarkable increase of the oxygen content was also registered.

Table 6: Results of the chemical analysis performed on the two batches of Ti-coated pure copper powder

Ti-coated powder	Ti [m%]	O [m%]
First batch	0,17	0,003
Second batch	1,10	0,25

The SEM investigation of the powder particles revealed that the coating on the first batch was not homogeneous, and while singular particles showed a very thick Ti deposition on their surface, others were still in the original blank state (Figure 50a-b). The investigation of the second batch showed on the other hand a regular Ti-coating on the particles surface (Figure 50c-d).

The FIB investigation confirmed the irregularity of the coating on the first powder batch: the measured thickness varies between 0 nm and 850 nm on the same particle (Figure 51a-b). The FIB cuts of powder particles belonging to the second batch show on the contrary a more regular thickness (85-130 nm, depending on the particle – see Figure 51c-d). The results obtained with two powder batches are shown in WP3.

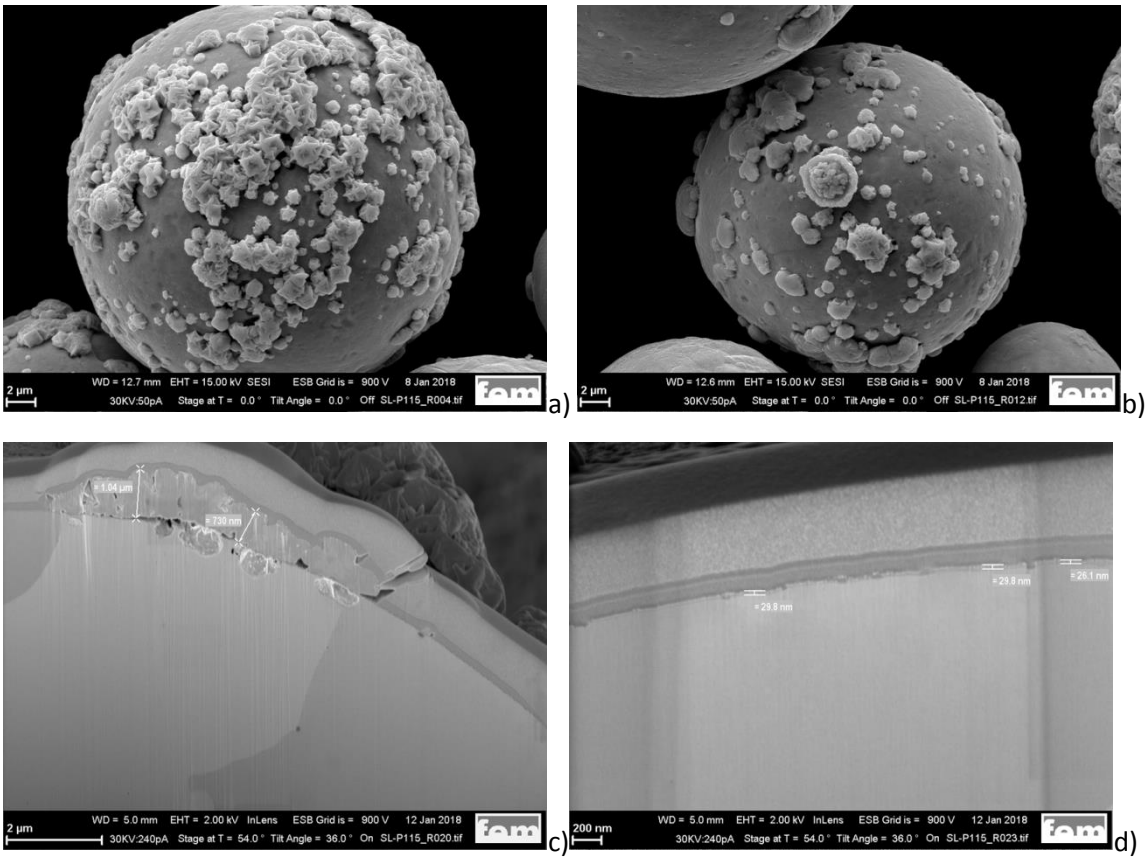

Figure 17: Sulphur solution coated powder - a) / b): SEM investigation of the particles surface with irregular copper sulphide coating c) / d) FIB-cut with coating thickness measurements c) 700-1000 nm d) 30 nm

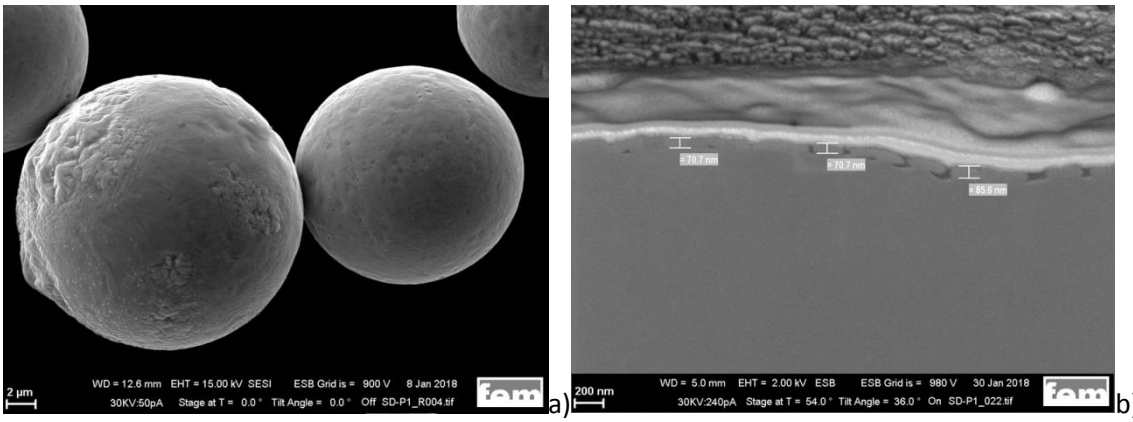

Figure 18: Sulphur vapor coated powder – a) SEM investigation of the particles surface b) FIB-cut with coating thickness measurement (~70 nm)

3.1.3.3 Performed activities – Sirris

- Base powder provision and feedback for optimization

Sirris chose chromium as element for coating of the 316L powder from Materia Nova, to counteract the effect of the melting depressants (Si and P) contained in the two infiltrants. Enough treated powder was provided to make the required tests (see WP3 for results).

3.1.3.4 Performed activities – Materia Nova

- Coating of 316L and pure Cu powders (respectively with chromium and titanium) through the magnetron sputtering technique

Magnetron sputtering is one of the most widely used methods for thin film deposition. It can be utilized to manufacture nearly every metal coating or metal composite as well as nitride or oxide layers, thus making magnetron sputtering a most versatile coating method. The possibility to coat large area substrates, and the easy to handle process parameters of magnetron sputtering allow a wide range of industrially important applications. Although coating plane substrates is state of the art, coating powder-substrates, granulates and particles of approximately 2–600 µm diameter by magnetron sputtering is a more difficult task. This is due to:

- Each side of every single particle has to be exposed to the sputter beam in order to get coated uniformly; therefore a particle mixing or rotating mechanism is necessary
- Small particles of different sizes and shapes become wedged together during the mixing process, which prohibits most of the particles from being coated (since they are not exposed to the sputtering beam)
- In vacuum the particles tend to stick together as coating proceeds, especially when the powder is coated with pure metal, because of the lack of any separation layer between the coating of two particles in contact (i.e. air, water film or an oxide layer). Rotary plasma reactor is presented below

To overcome these issues there are several approaches, such as:

- Adapted rotating drum, where the axis of rotation is horizontal and the barrel can be shaped in different ways (e.g. circular with inlets, hexagonal or conical), and the targets are positioned within the drum or perpendicular to the drum
- Vibration, where the sample stage is connected to an ultrasonic or electromagnetic vibration generator which keeps the particles tumbling

- Tilted rotating vessels, which can also have different shapes
- To vibrate the powder, a mechanical shock was applied to the rotating drum during the deposition. For this application, Home Concrete Vibrators were used.

Figure 19 shows the main part of the barrel-sputtering system. A barrel was placed in the vacuum chamber to hold powdery materials. The barrel could be rotated using a motor drive at different speed during sputtering, thus making it possible for the powdery particles to be agitated.

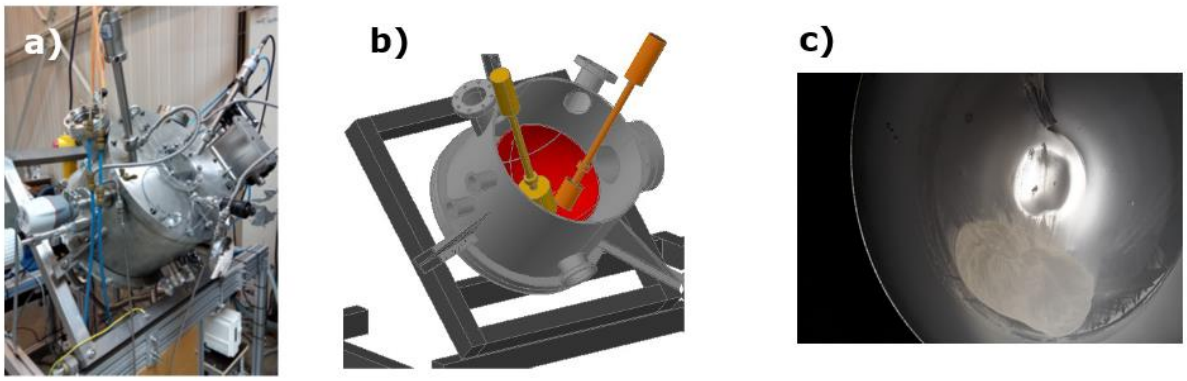

Figure 19: a) Rotary plasma reactor b) Reactor schematic view and c) Powder in the "bowl"

For this work, the powder stirring system was adapted several times. A metal rod turns very fast in a tube and induces a vibration with a drilling machine (the result is presented in Figure 20)

Figure 20: Reactor with Home Concrete Vibrators.

Powder morphology

Figure 21 shows the powder morphology and the cross section of a coated particle of the copper powder with titanium.

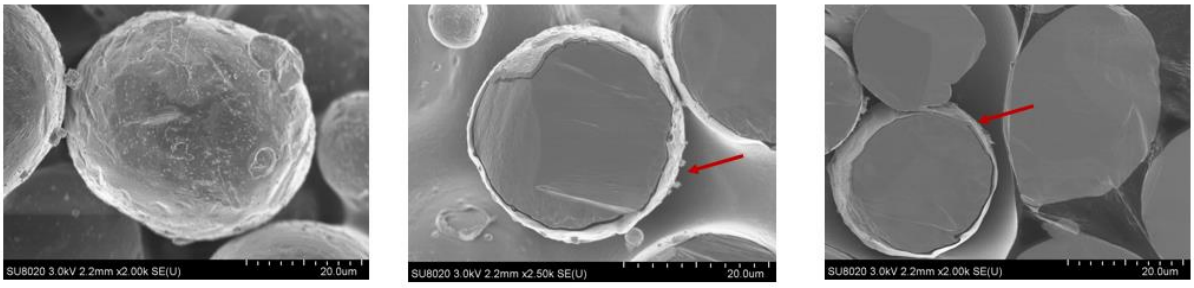

Figure 21: Copper powder Plasma Magnetron Sputter coated with Cr: SEM image

Powder flowability

The flowability is another important powder property for the LBM process. The Dynamic Angle of Repose is a generally accepted characterisation technique to measure the flowability of powders. The Cr coating improved the flowability of particles as compared to the virgin Cu or Fe powders. It is believed that the Cr coating efficiently reduced the tendency of agglomeration.

Powder laser absorption

In addition to the flow properties, the laser absorption of the alloy is an important property for the LBM process efficiency. The lower the laser absorption of the alloy, the more difficult it is to process it by means of LBM. Copper is known to have a high reflectivity and as such a low laser absorption. Therefore, the purpose of coating the copper powder with a metal that has better optical properties (i.e. high laser absorption) could drastically increase the laser absorption efficiency of the powder bed based LBM process. As such, the copper-based powders were assessed to a range of wavelengths using an absorption spectroscopy device at room temperature.

Figure 22 gives an overview of the laser absorption curves of the Cu-Ti powders as a function of the laser wavelength. The fiber laser is used as optical source in the LBM process to melt the powder locally. In addition, the laser absorption values of the coated Cu based powders for the fiber laser are shown in Table 7. Based on this data, the effect of the Ti coating is beneficial for the processing with LBM, since the energy absorption is increased.

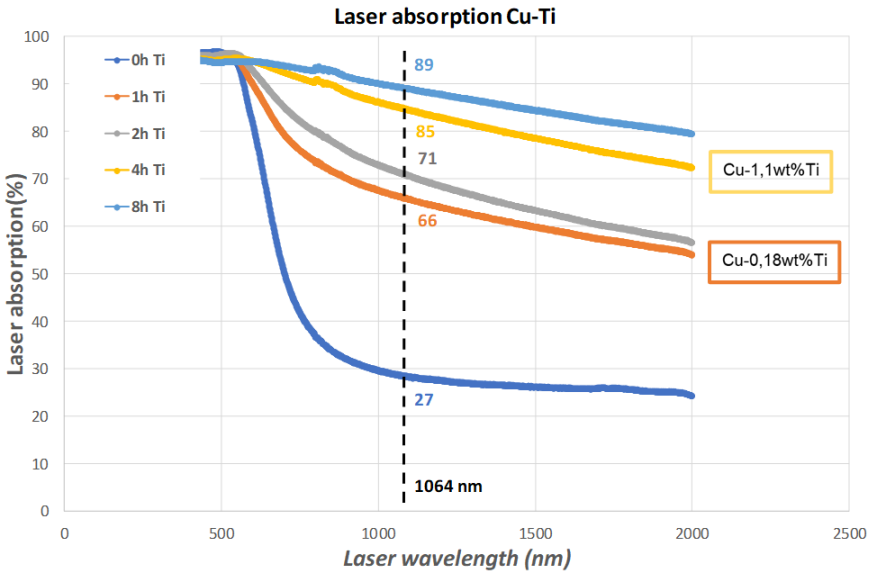

Figure 22: Laser absorption curves of coated Cu-Ti powders

Table 7: Laser absorption of the Cu powders for a fiber laser (λ = 1064 nm)

Laser absorption at λ = 1064 nm [%]	
Cu (untreated)	27%
Cu-0,18wt%Ti (coated)	66%
Cu-1,1wt%Ti (coated)	85%

Conclusions:

Powder treatment by the magnetron sputtering:

- Improvement of LASER Absorption for high reflectivity and conductivity materials
- Enhanced powder flowability for better processing and densities

and the technique is promising for:

- Protection against oxidation, water for sensitive material
- Processable composite powders

3.1.4 WP3: Manufacturing of demonstration parts / Parameter studies

3.1.4.1 Performed activities – fem

- The processability of several Cu and CuSn alloy was compared through a fast screening test using metal sheets as a substitute for powder
- Selective laser melting tests were conducted on several powders to study and understand the processability of Cu-alloys (pure Cu, CuSn6, CuSn10, oxidized Cu)
- A selection of Cu-alloys for further parameter studies was conducted based on their physical properties (CuB0,2, CuAg3, CuNi1,5Si, CuNi3Si)
- Alloys were tested using the developed fast screening test and two of them (CuNi1,5Si and CuNi3Si) were chosen
- Parameter studies with CuNi1,5Si and CuNi3Si alloy powders were conducted to optimize their processability
- The surface treated pure Cu-powders were tested with LBM (one batch of oxidized Cu, two batches of Ti-coated Cu, one batch of S-coated Cu)
- The geometry of the demonstrator (coil for electric motor) was tested and optimized with CuSn10 powder. Coils were subsequently manufactured with CuNi3Si and with Ti-coated Cu-powder
- Pre-trials for infiltration with Ag solder were conducted on pure Cu porous parts in order to improve their density and electrical conductivity

Processability of several Cu and CuSn alloy with LBM – development of a fast screening test

A study on the processability of Cu alloys and on the influence of alloying elements was conducted. Because of uneven molten tracks the additive generated Cu-parts present a high porosity. In order to correlate the processability of an alloy with its physical properties, several Cu-alloys in metal sheet form (with increasing Sn content) were processed with selective laser melting and then investigated. Three alloy variants (Cu, CuSn6 and CuSn10) were also available in powder form and were employed for the manufacturing of small test parts.

The alloy composition strongly influences the physical properties (electrical conductivity, reflectivity and melting interval) of the material to be processed. Therefore, such properties of the chosen alloys (Cu, CuSn4, CuSn5, CuSn6, CuSn8, und CuSn10) were compared. The CuSn sheets in the original state were homogenized, hot-rolled, cold-rolled, recrystallized and cold-rolled; the condition was homogeneous and according to the phase diagram. The electrical conductivity was measured with the eddy current testing (Helmut Fischer Sigmascope SMP350) on polished samples. The light reflection of the alloys was measured in the range 360 - 740 nm with a colorimeter Konica Minolta spectral photometer CM-5 on polished surfaces. A Mlab machine from Concept Laser (equipped with a 100 W Nd-YAG Laser operating at a wavelength of 1.070 nm) was used for the laser melting trials.

The different CuSn-Sheets were rolled (75% cold-deformed), blasted with corundum (grain size 120-250 µm) and subsequently mounted on the building plate; 15 squares were lasered one time with different parameter sets (Figure 23).

Figure 23: Example of a CuSn sheet after the laser test. The squares were lasered with different laser powers and speeds.

The SEM investigations were conducted with three devices: Zeiss FIB Auriga 60 with Oxford EDX-EBSD-System, Zeiss Gemini SEM 300, and Zeiss SEM Evo MA15. The documentation of the sample surface (sheets as well as produced parts) took place with SE-imaging. The investigation of the microstructure in the cross section was conducted with BSE imaging. The penetration depth of the laser and the resulting heat affected zone was evaluated by means of such BSE (back scattered electrons) pictures.

In order to confirm the insights from the proof of principle test with metal sheets, selective laser melting tests with three powders (Pure Cu, CuSn6 and CuSn10) were also conducted. The part produced is shown in Figure 24. The part features different surface orientations (vertical, horizontal, and 60° tilted) and three curved wires with different diameters. A parameter study was conducted by varying the hatch distance (0,036 to 0,027) and the laser speed (100 to 300 mm/s), while the laser power and the layer thickness were kept constant (respectively 95 W and 15µm).

The porosity in the parts was assessed by quantitative microstructural analysis on the metallographic samples (equipment: Zeiss AxioImager Z2m with Axiovision image analysis software). To that end, a mosaic including 18 single pictures with 100x optical magnification was generated, which allowed the identification of pores > 0.6 µm.

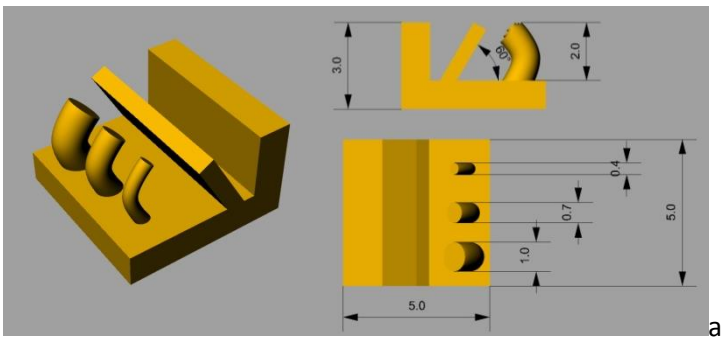

a)

b)

Figure 24: Test part a) dimensions - b) built part

The chart in Figure 25 shows the measured values of the electrical conductivity as a function of the Sn content in the alloy. The conductivity is given in % IACS: pure Cu shows by definition a value of 100%. As can be seen from the blue trend line, the conductivity strongly decreases with the increasing Sn content. Above 5% Sn and up to 10% the steepness of the red trend line is clearly lower, and therefore the reduction of the conductivity not so pronounced. In the literature [22,23] is described that from 5% Sn the δ-phase can form. Precipitations were visible in the SEM investigation of a CuSn8 sheet in cross section (Figure 26).

Concerning its light reflection, pure copper shows at 740nm a value of 86%, which sinks down to 81% in the case of CuSn10 (6% lower -Table 8). The melting intervals of the alloys are listed in Table 8: in comparison to CuSn4, the melting range of CuSn10 is by 65% widened. The values of the surface tension for CuSn alloys can be found in the literature [24], and are listed in Table 8. In comparison with pure Cu, CuSn8 presents a value which is 11% lower.

Table 8: Thermophysical properties of several alloys #- this work. Surface tension values: Cu to CuSn10 [24], CuNi3Si [25]

Material	Melting Range [°C]	Conductivity (%IACS)	Reflectivity (at 740nm) [%]	Surface tension [mN/m]
Cu	1085	100	86.4	1340
CuSn4	960 – 1060	20.7	83.9	1210
CuSn5	910 – 1040	19.0	83.5	1182
CuSn6	900 – 1030	17.2	83.1	1155
CuSn8	875 – 1025	13.8	82.1	1105
CuSn10	845 – 1010	12.1	80.8	1061
CuNi1.5Si	1050 – 1070	48.8	85.0	-
CuNi3Si	1060 – 1085	29.0	81.0	1399

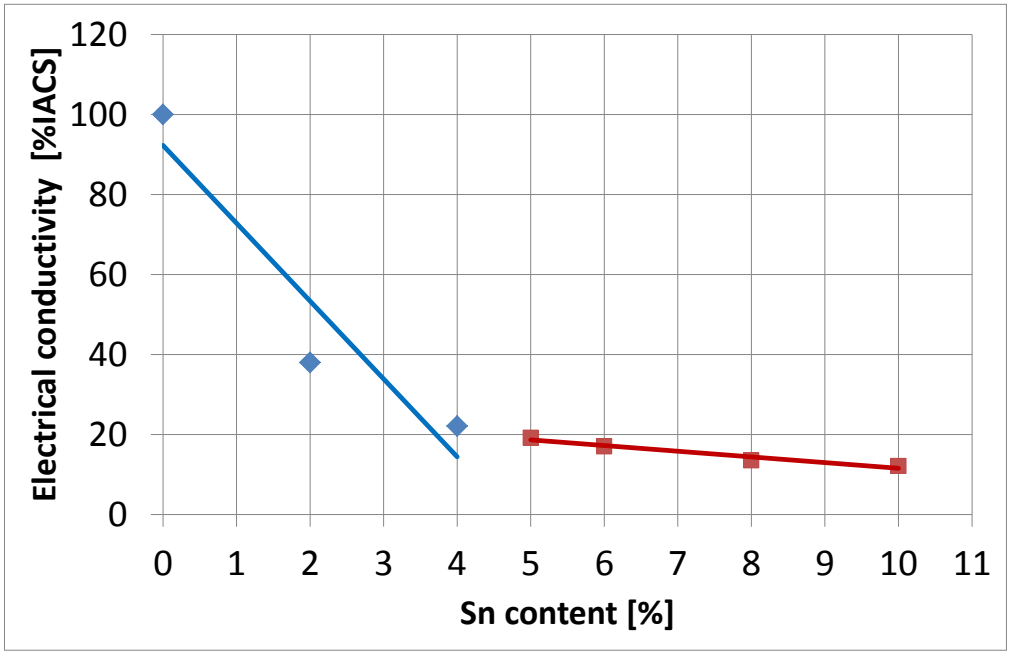

Figure 25: Electrical conductivity of CuSn-alloys as a function of the Sn content

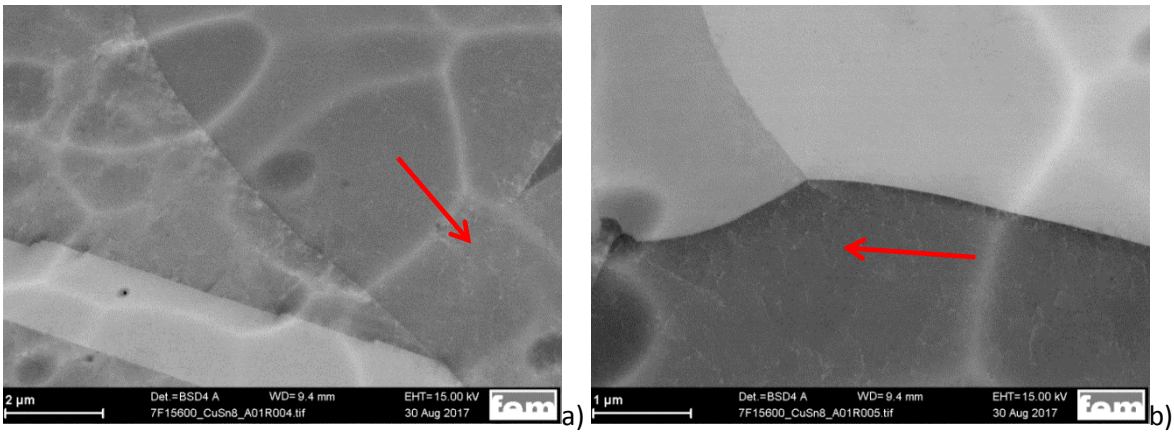

Figure 26: SEM investigation on a CuSn8 sheet in cross section (BSE imaging) – Precipitates visible in the microstructure

Because of the already mentioned high reflectivity of the material, the laser tracks were not visible in case of pure Cu. The evaluation of the results was therefore restricted to the CuSn alloys. For those the influence of the Sn content was clearly to be seen: Figure 27a and Figure 27b show a comparison between CuSn4 and CuSn8 for 95 W laser power and 100 mm/s laser speed. In case of CuSn4 the width of the molten laser tracks is not big enough, to guarantee their overlap, so that the blasted surface underneath was still visible. If the laser speed is increased von 100 mm/s to 300 mm/s the effect for CuSn4 was even more pronounced (Figure 27c). Through the higher laser speed, the linear energy is reduced by a factor of 3. Even with an increased speed, for CuSn8 an uniform melting area could still be achieved (Figure 27d). The difference between the two alloys was also evident in the cross section: while for CuSn4 there was no overlap of the laser tracks (Figure 28a), the minimal penetration depth in case of CuSn8 was ca. 12 µm (Figure 28b). Because of the overlap of the laser tracks, the laser penetration depth is substantially more homogeneous. For CuSn4 the value fluctuates between 0 µm and 8 µm, while for CuSn8 with the same parameters an almost homogeneous penetration depth (12-15µm) could be achieved.

The investigated values of the penetration depth and of the heat affected zone are displayed in Figure 29 with a 95% confidence interval for a laser power of 95 W and speed of 100 mm/s as a function of the Sn content. For lower Sn contents (up to 5% Sn) both values are low and similar: the penetration depth is about 8 µm, and the heat affected zone 10µm (Figure 30). From 5% Sn in the alloy, the penetration depth increases. In the cross section of the CuSn6 sheet the depth is 14 µm, and the heat affected zone shows more than double depth (27 µm) in comparison to CuSn5 (Figure 31). Said heat affected zone reached in case of CuSn10 a depth of 34 µm.

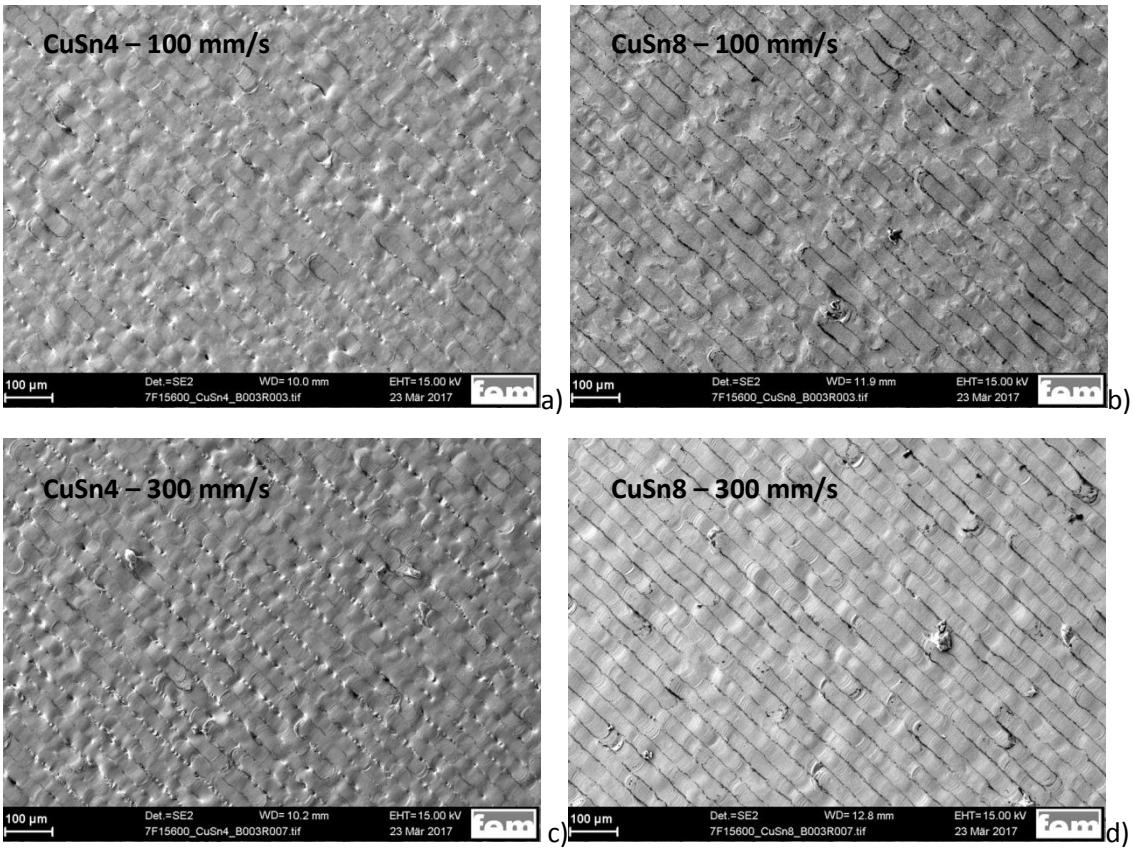

Figure 27: Laser melting trials with CuSn-sheets (95W Power) SE-imaging of the surface a) CuSn4 (100 mm/s) b) CuSn8 (100 mm/s) c) CuSn4 (300 mm/s) d) CuSn8 (300 mm/s).

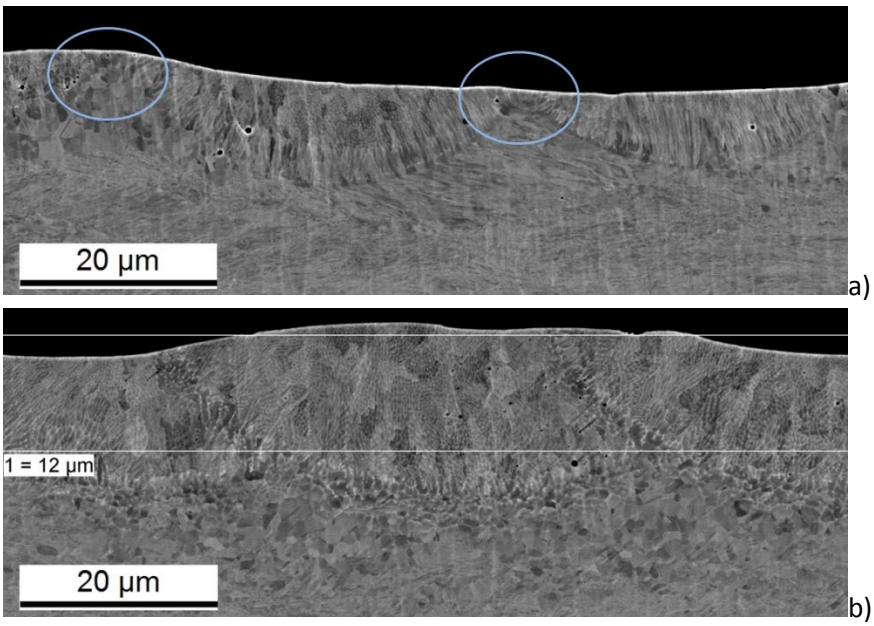

Figure 28: Investigation of the overlap of laser tracks in cross section for identical laser parameters (95W – 100mm/s) a) CuSn4: minimal penetration depth 0µm, b) CuSn8 : minimal penetration depth ~ 12µm

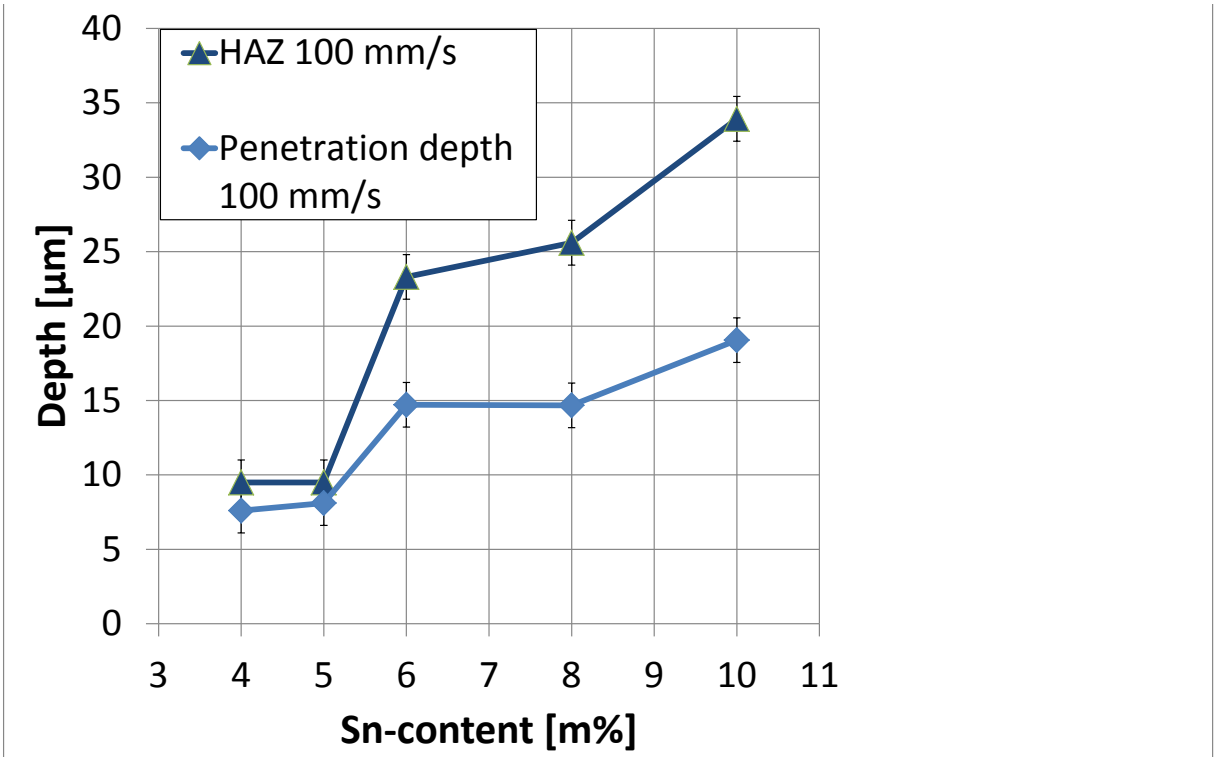

Figure 29: Laser melting trials with CuSn sheets. Evaluated heat affected zone (HAZ) and penetration depth as a function of the Sn content.

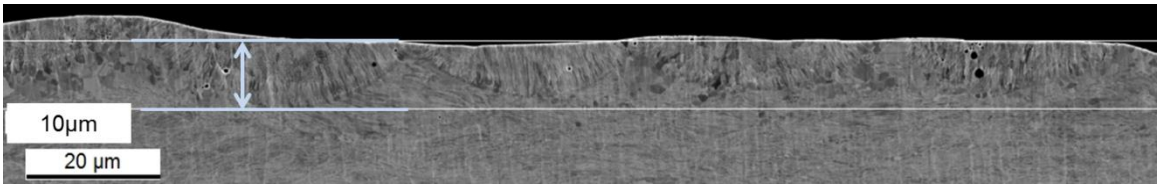

Figure 30: CuSn4-sheet after laser melting trial in cross section – Investigated depth of the heat affected zone (95W – 100mm/s)

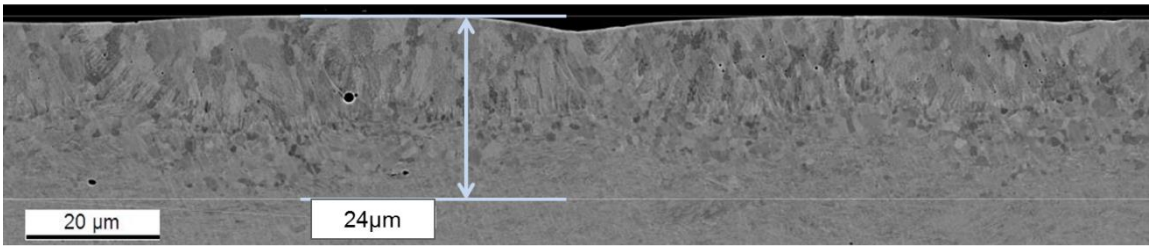

Figure 31: CuSn6-sheet after laser melting trial in cross section – Investigated depth of the heat affected zone (95W – 100mm/s)

The decreasing trend of the conductivity for an increasing Sn content can be explained with the help of the CuSn phase diagram. In Figure 32 the measured conductivity values are overlapped with the mentioned diagram. As a result it is evident that the decrease of the conductivity takes place in a single-phase section (α-solid solution), up to about 4 % Sn: with the increasing Sn content the mobility of the electrons in the Cu matrix is reduced by the foreign atoms. The atom lattice is additionally deformed, and the conductivity decreases. As soon as the solubility limit is exceeded, and with the phase formation, the conductivity reduction is not so pronounced anymore.

The conducted tests showed that the proof of principle trials with metal sheets can provide a comparison of the processability of different alloys. The results were confirmed through laser melting trials with powders (see next chapter).

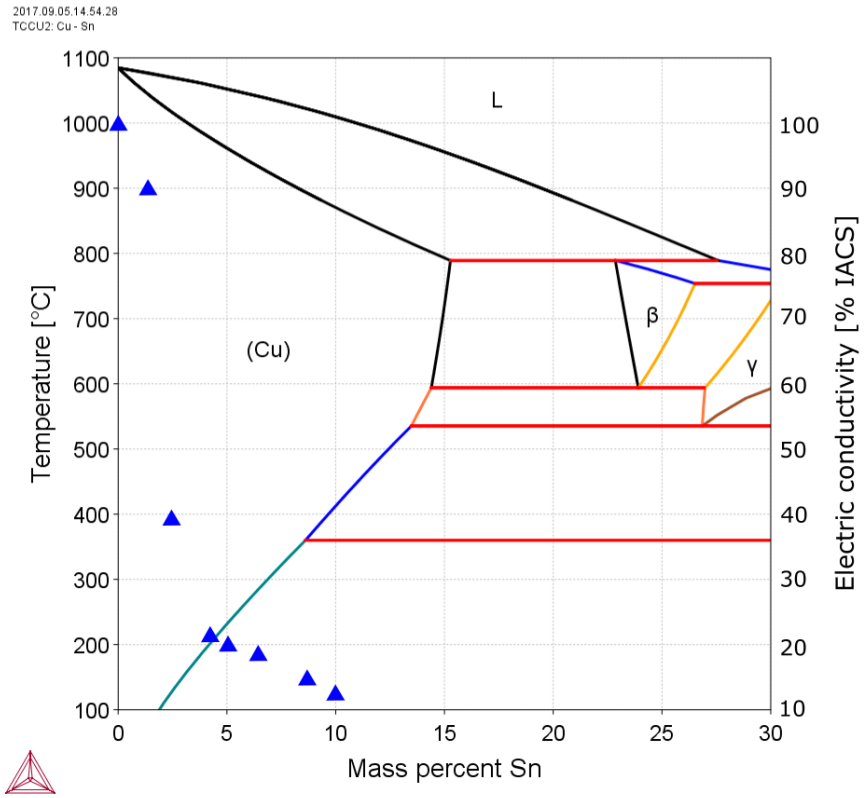

Figure 32: Overlap of the conductivity trend with a section of the CuSn phase diagram (up to 30% Sn)

LBM trials with Cu and CuSn powders

Independently from the used parameters, the Cu powder presented a bad melting behavior, which led to the expected very high porosity (23-24%) in the built parts (Figure 33a). As the SEM pictures of the upper horizontal surface (the last processed layer - Figure 33b) show, the balling effect occurs so strongly, that the molten laser tracks cannot be identified anymore. This led to the formation of agglomerates of different sizes, so that a smooth melting area by the processed layer could not be achieved, and the high porosity formed.

The use of the alloy powder CuSn6 allowed improving the melting area. The molten tracks were clearly recognizable, although also here no smooth surface could be achieved (Figure 34b). Because of the improvement, in comparison to pure Cu the porosity in the part could be reduced to 5% (Figure 34a).

The CuSn10 powder featured an even better processability. Continuous molten tracks could be achieved and the result was smooth melting area (Figure 35b). Hence the significantly lower porosity (0,38% - see Figure 35a). Both for CuSn6 and for CuSn10 parts, it was possible by EDX analysis to identify the precipitation of Sn as β-Phase (Figure 36).

The improvement of the processability through the increasing Sn content can be explained considering different effects. Solidus and liquidus temperature are reduced, and at the same time the melting range is widened. The fast cooling during the laser melting process causes a non-equilibrium solidification; under this condition alloys with higher Sn content show a smaller solid fraction at the same temperature. The metal remains longer fluid, the flowability of the molten laser tracks can be enhanced and generates a smoother melt pool for each build layer. Furthermore, the decreasing surface tension improves the wetting behavior of the alloy, so that for CuSn10 a smoother melting

area forms in comparison to CuSn6 (as observed during the laser melting trials). Therefore the porosity in the parts is reduced.

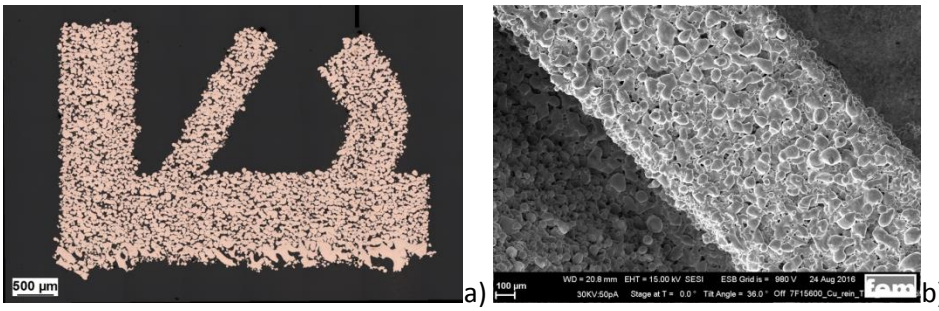

a) b)

Figure 33: Test part built in pure Cu (95W – 100mm/s) – 23,4% Porosity a) Metallographic sample b) SEM investigation of the last processed powder layer.

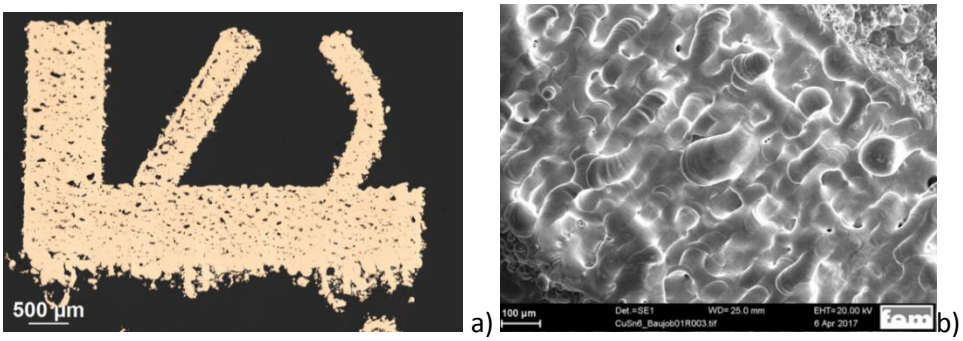

a) b)

Figure 34: Test part built in CuSn6 (95W – 150mm/s) – 5,03% Porosity a) Metallographic sample b) SEM investigation of the last processed powder layer.

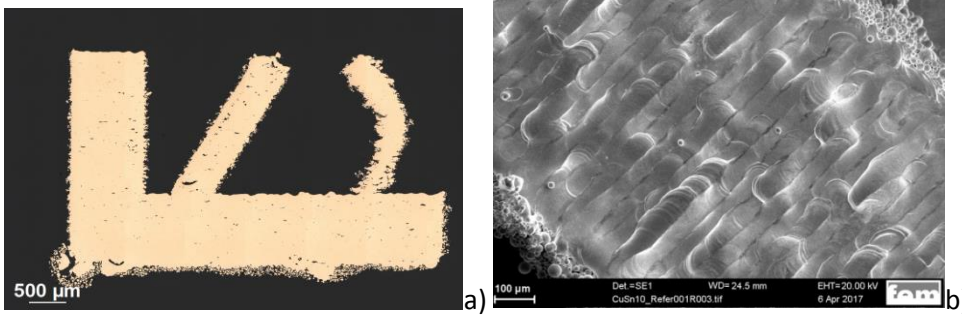

a) b)

Figure 35: Test part built in CuSn10 (95W – 150mm/s) – 0,38% Porosity a) Metallographic sample b) SEM investigation of the last processed powder layer.

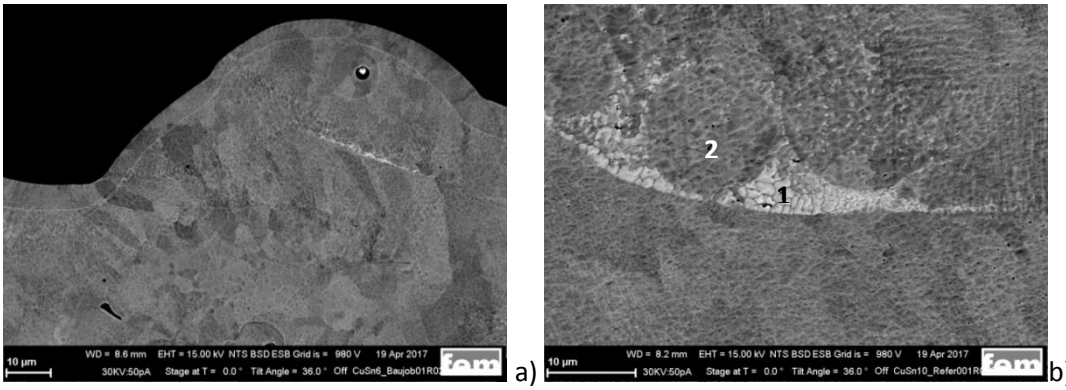

a) b)

Figure 36: Laser melting trial with CuSn6 and CuSn10 powders –Microstructure in SEM – Precipitation of Sn a) CuSn6 b) CuSn10 EDX measurement Point 1. Cu – 81,4% Sn – 18,6% (β phase) Point 2. Cu – 92,3% Sn – 7,7%

Selection of Cu-alloys for further parameter studies

Since the desired application of the alloys was the production of complex coils for electric motors, during the alloy selection particular attention was given both to the tensile strength and to the electrical conductivity. For the selection of the alloy composition several approaches were followed: the application of established Cu alloys (CuNiSi), the microalloying with B, Si and Ge (content below 1%), and the high alloying with Ag and B (content >1%). The CuNiSi alloys and the CuAg were commercially available, and their properties were known: out of those CuNi1,5Si, CuNi3Si and CuAg3 were chosen. The other alloys (micro alloyed with different contents of B, Si and Ge and high alloyed up to 2% B) were prepared at fem, melted, homogenized and their electrical conductivity was measured.

The chart in Figure 37 shows measured electrical conductivity values (both as cast and in homogenized state) for all three alloy variants: the B variant shows the highest values, which decrease significantly from 0,5% content on. Out of the three variants, and because of its high electrical conductivity (95% IACS), the variant CuB0,2 was chosen as a potential candidate for LBM trials.

The electrical conductivity and tensile strength values of several Cu alloys are also displayed in the chart in Figure 38: CuNiSi alloys offer a compromise between tensile strength and electrical conductivity (upper left corner of the chart), while CuAg alloys present a high value of conductivity, but combined with low strength (lower right corner of the chart). As already mentioned, the CuAg3 was chosen from this alloy family for further trials.

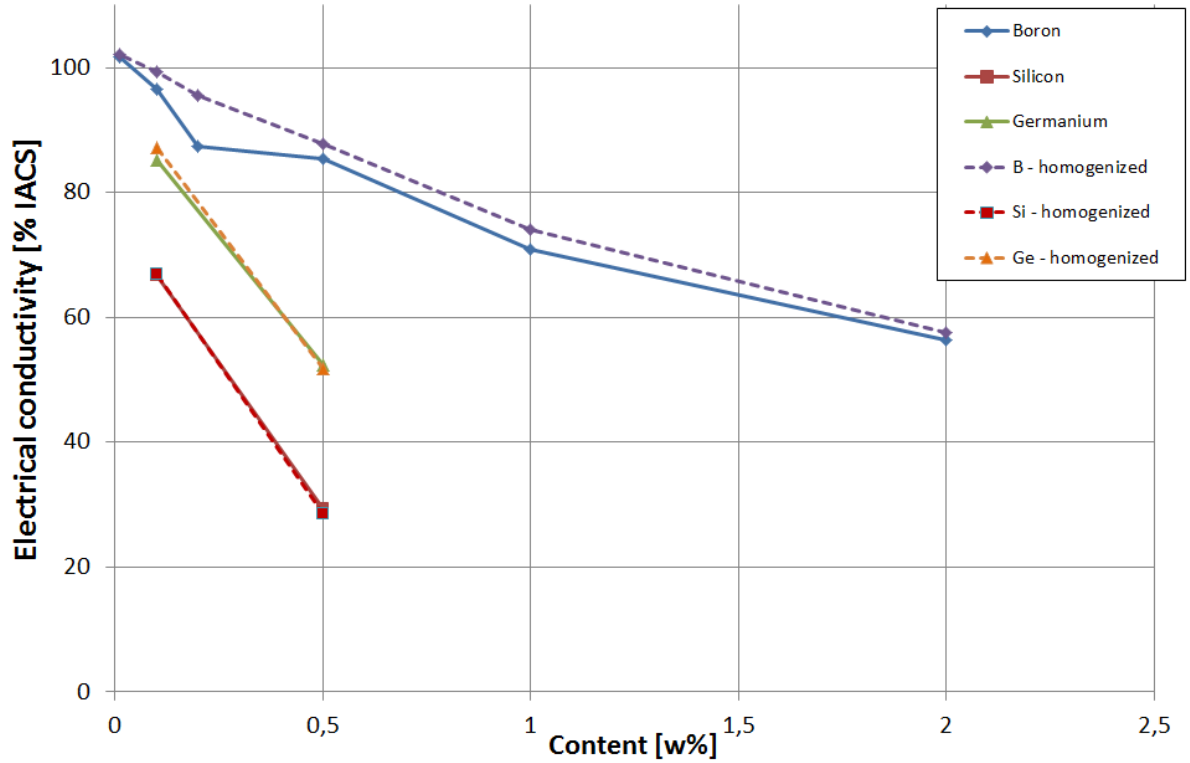

Figure 37: Measured electrical conductivity (both as cast and in homogenized state) of the at fem prepared Cu alloys with different B, Si and Ge content

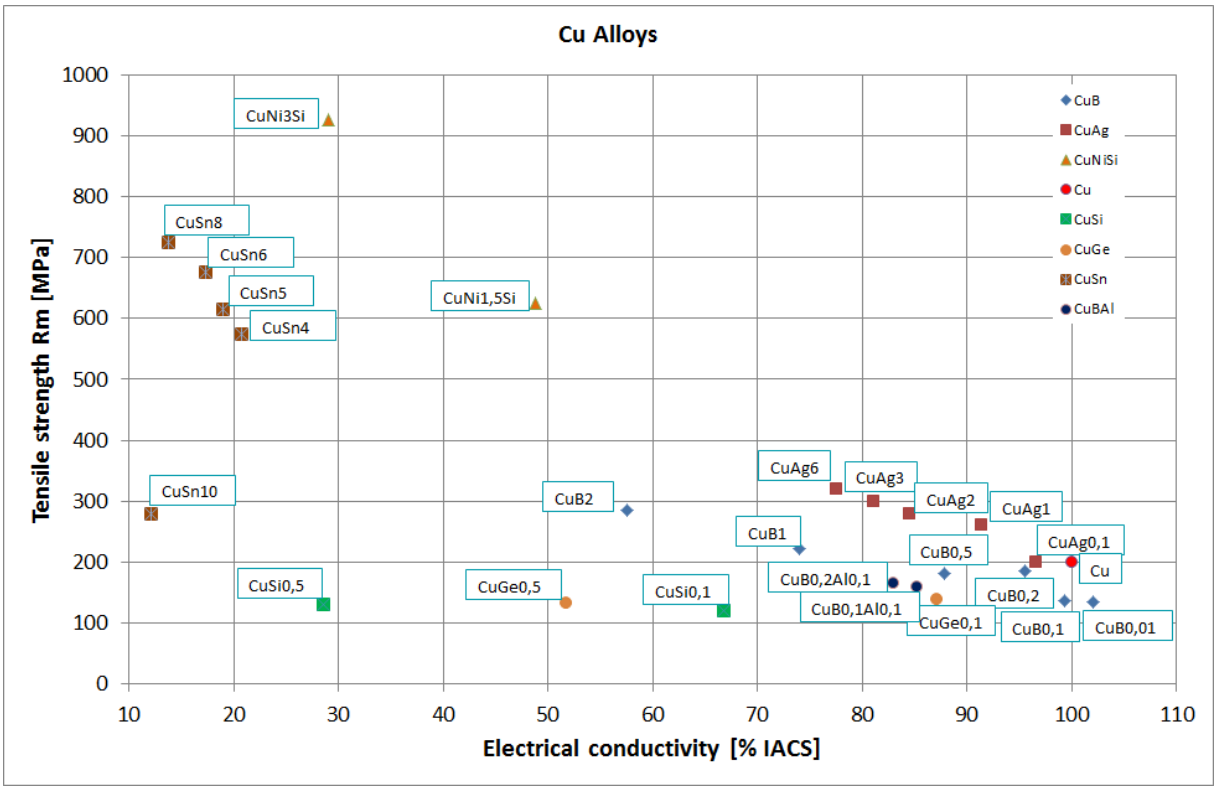

Figure 38: Comparison of the physical properties (tensile strength and electrical conductivity) of several Cu alloys

The screening methodology developed with CuSn-sheets (described above) was applied to test the processability of the selected Cu alloys (CuAg3, CuB0.2 and CuNiSi) before moving to the expensive atomization process. Metal sheets were prepared and sand blasted before being processed with selective laser melting. The results were evaluated with reference to the results obtained with CuSn sheets by using the same methodology (SEM investigation of the molten surface and measurement of the penetration depth in the metallographic sample).

In the case of the CuB0.2, the molten tracks were visible on the metal sheet, but their width was not sufficient to achieve an overlap, so that the blasted surface was still clearly recognizable in between Figure 39b), thereby proving an insight on the poor melting behavior of the alloy with the available laser power of 95 W. Said effect was much more pronounced for the CuAg3 alloy (Figure 39c): only single melting points were recognizable, instead of continuous melting tracks. The CuNi1,5Si sheet showed a much better processability, allowing to achieve a smooth melting area (Figure 39d).

The results of the investigation on the sheet in cross section confirmed the ones obtained on the surface in terms of processability: for the CuB0.2 sheet there was no visible penetration depth (Figure 40), while for the CuNi1.5Si the measured value was about 14 µm (Figure 41). Given the very poor results on its surface, the cross section of CuAg3 was not investigated.

The insights gained from the described trials led to discard the two alloys CuB0.2 and CuAg3 as candidates for atomization trials, since their processability with laser melting was too low. Therefore CuNiSi alloys (in the two variants CuNi1.5Si and CuNi3Si) were chosen for further trials with powders.

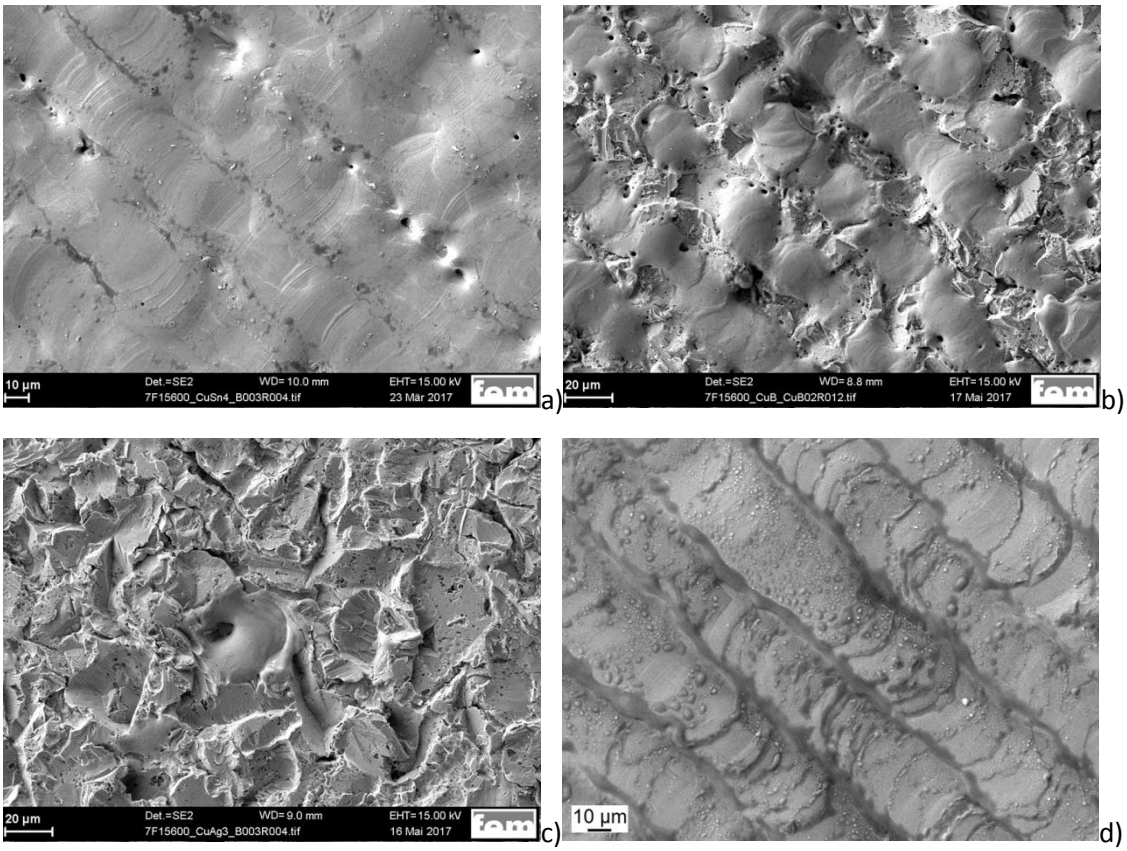

Figure 39: Comparison of the results obtained with the fast screening method on metal sheets for four alloys (95W, 100mm/s) a) CuSn4 b) CuB0.2 c) CuAg3 d) CuNi1.5Si

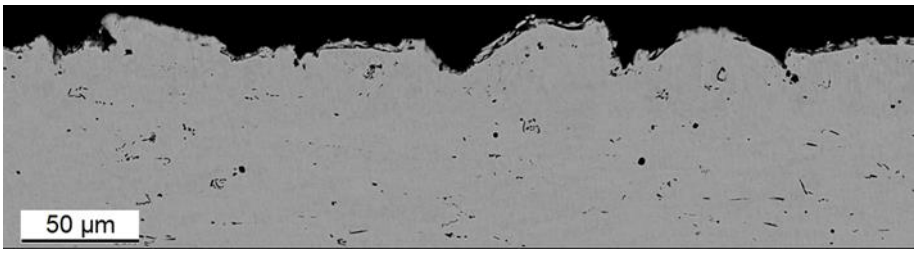

Figure 40: CuB0.2-sheet after laser melting trial in cross section – laser penetration depth is not recognizable, blasted surface not melted

Figure 41: CuNi1.5Si-sheet after laser melting trial in cross section: the measured laser penetration depth is about 14 µm

Processability of CuNiSi alloy powders

The impact of alloying elements and process parameters on the processability of Cu-alloys with selective laser melting was evaluated, by focusing especially on two of the typically used CuNiSi alloys with different Ni and Si content. The test parts were manufactured by keeping a constant laser power of 95 W while varying laser scanning speed and hatch distance (in ranges from 75 mm/s to 250 mm/s and from 9 µm to 45 µm respectively). Three layer thicknesses were selected for the building process (20 µm, 15 µm and 10 µm) and applied to the previously classified powder batches (see WP1 for details). The 10-45 µm powder could only be used for the generation of layers with 20 µm thickness, while the 10-25 µm and 5-20 µm powders allowed the manufacturing of all three said layer thicknesses. The SEM investigations were conducted with three devices: Zeiss FIB Auriga 60 with Oxford EDX-EBSD-System, Zeiss Gemini SEM 300, and Zeiss SEM Evo MA15. For the documentation of the powder morphology and of the surfaces on the built parts BSE imaging (back scattered electrons) was employed. The porosity in the parts was assessed by quantitative microstructural analysis on the metallographic samples (equipment: Zeiss AxioImager Z2m with Axiovision image analysis software). To that end, a mosaic including 18 single pictures with 100x optical magnification was generated, which allowed the identification of pores > 0.6 µm. The statistical error for these measurements can arise from two sources: an inherent porosity distribution in the sample and the manual thresholding for image segmentation. To estimate the error due to porosity distribution, the values were measured both on different positions and on different sample planes. The manual thresholding was set to extreme values to establish its influence on the measured porosity. The estimated error (1 %) deriving from these two combined sources was indicated in the different diagrams with respective error bars. The metallographic samples were accurately prepared, so that an error due to pores smearing could be excluded [26], therefore assuring the detection of the correct porosity level. The electrical conductivity was assessed on the built samples with the eddy current method (Helmut Fischer Sigmascope SMP350). The Vickers hardness using a load of 1 kg was measured on test samples with a hardness tester KB10 (KB Prüftechnik).

The comparison of the metallographic results on parts built with the same standard process parameters (10-45µm powder size and 20 µm layers) using pure Cu and the alloyed qualities (CuNiSiCr, CuNi1.5Si and CuNi3Si), shows a strong influence of the Si-content on the processability of the material and consequently on the part density (see Figure 42). The diagram in Figure 43 displays the porosity as a function of the Si-content of the powders: Cu and CuNiSiCr show a poor melting behavior and, therefore, have with values of 26 % and 14 % a high porosity, while in the case of the two CuNiSi alloys the porosity is reduced to 6.6 % and 5.5 %, respectively. The diagram in Figure 44 also shows that by decreasing the powder size and the generated layer thickness, while maintaining constant the laser scan parameters, the porosity for the two CuNiSi alloys can be reduced to values below 1.6 %. The results of the experiments with varying layer thicknesses in combination with the three specific powder size ranges are summarized in Figure 44. The porosity is decreasing by reducing the layer thickness. The 20µm layer shows the highest porosity levels (between 4 and 8 %) for all three powder sizes and high fluctuation of their values, while reducing the layer thickness to 15µm and 10µm allows to stabilize the porosity values to 3 % and 1.5 %, respectively (Figure 45). It has to be noted that thin layers could only be achieved by using the finer powder qualities (10-25 µm and 5-20 µm).

The differences in the surface structure of the parts obtained from these experiments are highlighted by the SEM investigation of the last processed layer (see Figure 46). In the case of the 20 µm layer

the molten tracks are uneven and big pores are visible between them, whereas such defects gradually disappear by reducing the layer thickness to 15 µm and to 10 µm while maintaining the hatch distance constant.

Figure 47 shows the porosity as a function of the hatch distance variation for several laser speeds and a layer thickness of 15 µm. The minimum porosity (3-4 %) is obtained here for a hatch distance range between 25 µm and 45 µm, whereas for distances below 25 µm a strong increase of the porosity values can be noted (up to 12%, as the metallography of the part shows – see Figure 48). In the mentioned hatch distance 20-45 µm range and for the 15µm layer thickness the porosity values are stable for a relatively wide laser speed window ranging from 100 mm/s to 250 mm/s (within the error margins).

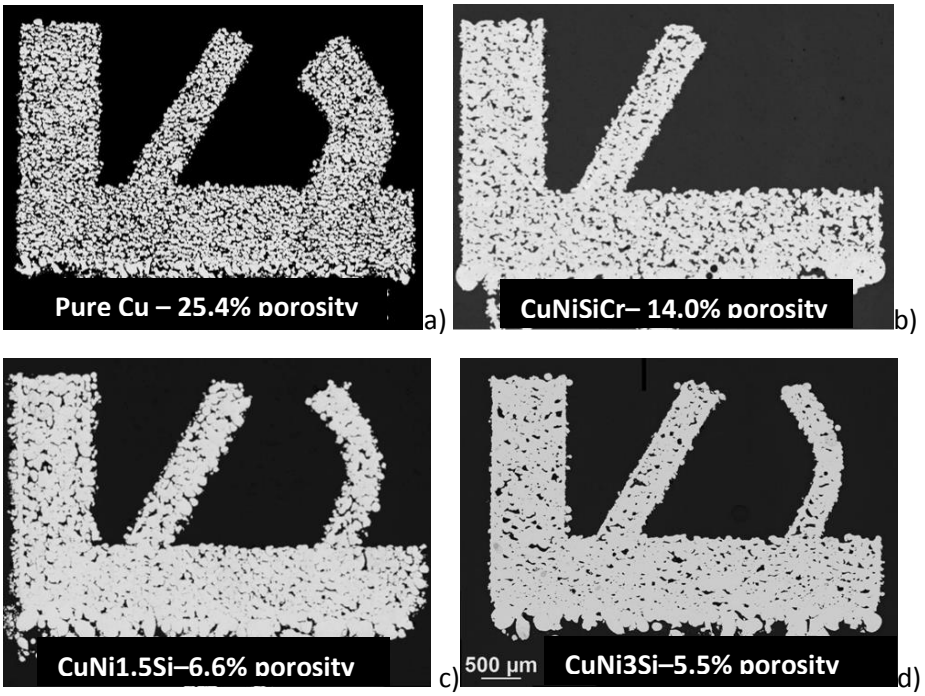

Figure 42: Metallographic cross sections of built test parts with several Cu alloys – a) Pure Cu – 25.4 % porosity b) CuNiSiCr – 14.0 % porosity c) CuNi1.5Si – 6.6 % porosity d) CuNi3Si – 5.5% porosity, layer thickness=20 µm, powder size 10-45 µm, hatch distance 36 µm, laser power 95 W, laser speed= 200 mm/s

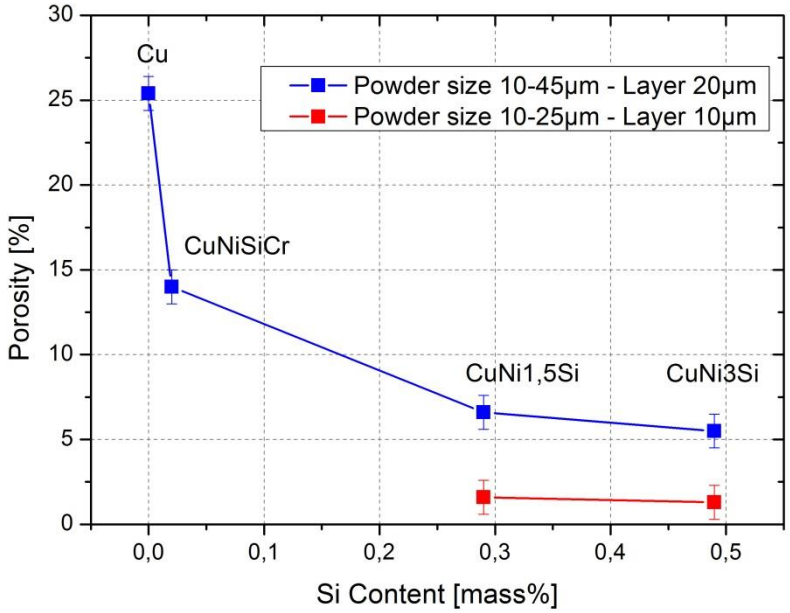

Figure 43: Effect of alloy composition in terms of the Si content and the powder size on porosity – comparison of several Cu-alloys manufactured with 95 W at 200 mm/s scanning speed

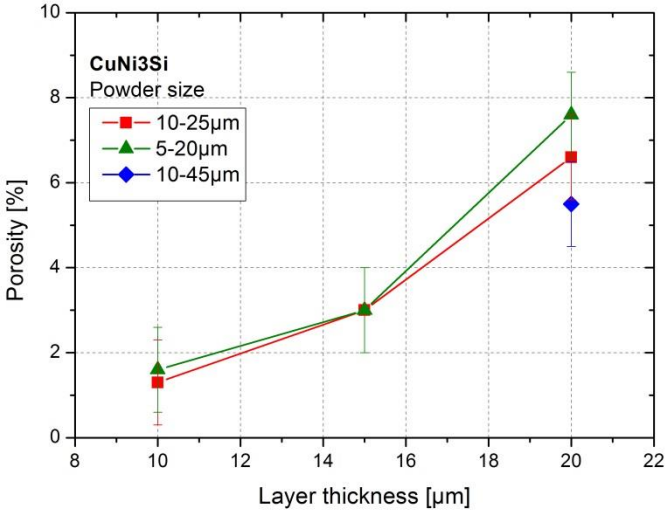

Figure 44: Effect of powder size and layer thickness on porosity for the CuNi3Si alloy

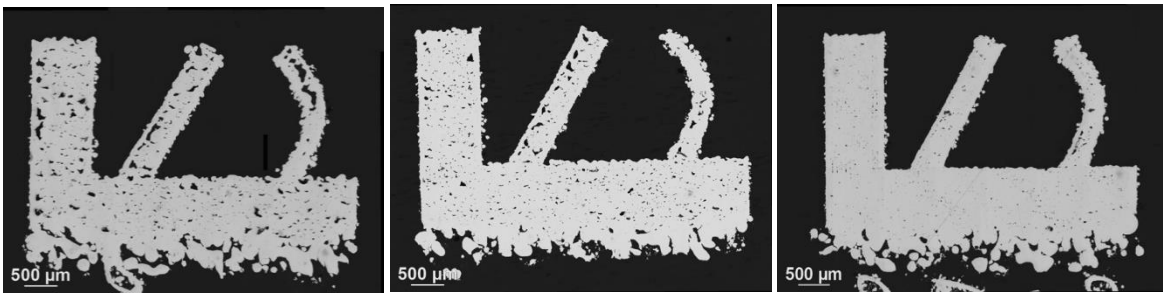

Figure 45: Metallographic cross sections of built test parts with CuNi3Si (95 W – 200 mm/s) Effect of powder layer thickness on porosity (20 µm – 15 µm – 10 µm – respectively 6.6 %, 3.0 % and 1.3 % porosity) for optimal powder size with the CuNi3Si alloy (10-25 µm)

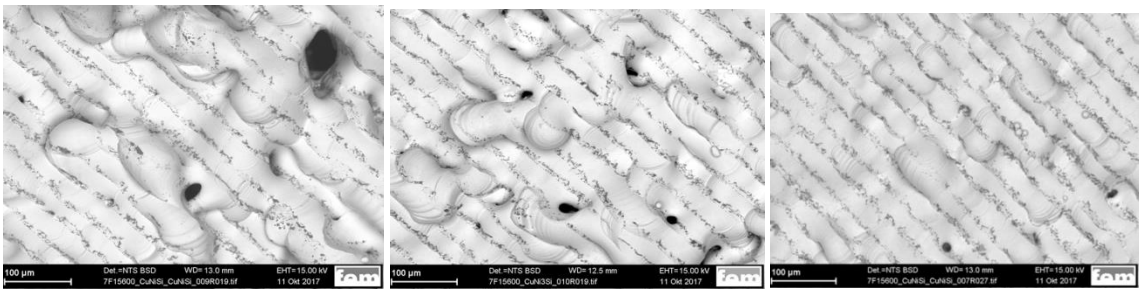

Figure 46: SEM investigation on part surface for the CuNi3Si alloys: effect of layer thickness: 20 – 15 – 10 µm (95 W – 200 mm/s)

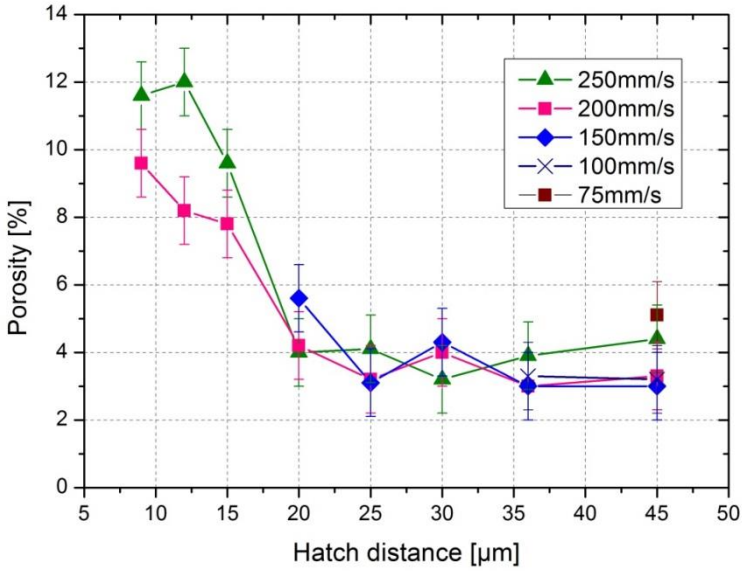

Figure 47: Effect of hatch distance and laser speed on porosity (powder size: 10-25 µm / layer thickness: 15 mm / laser power: 95 W)

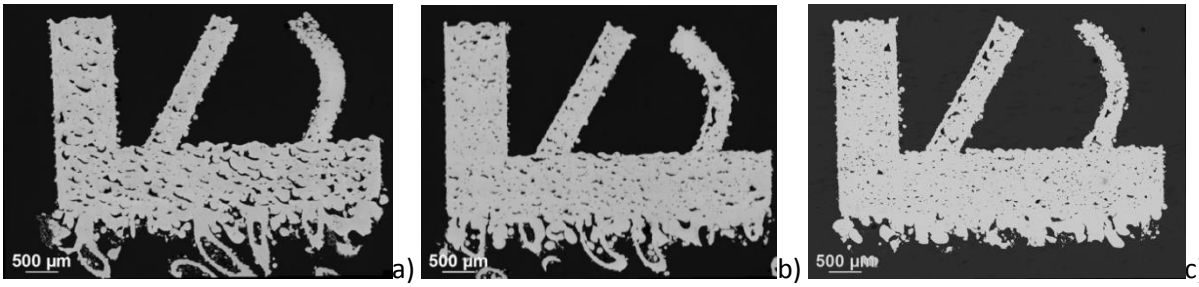

a) b) c)

Figure 48: Metallographic cross sections of built test parts with CuNi3Si (95W – 200mm/s) - Effect of laser scanning parameters (hatch distance) on porosity; from left to the right: hatch distance 9 – 20 – 36 µm, porosity values of 9.6 %, 4.2 % and 3.0 %.

The thermophysical properties of several Cu alloys are listed in Table 8. As already mentioned, the processability of the respective materials with LBM can be correlated to said properties. The difficulty in processing pure copper with selective laser melting, because of the high thermal conductivity and reflectivity of the material, has been already described in the literature [2]. The oxygen content is an important factor for the processability of the material, since it has an influence both on electrical conductivity and on surface tension. The decrease of electrical conductivity in OF-Copper has been reported by H W Bowyer to be 0.126% per 100 ppm of oxygen [27]. As described by

N. Eustathopoulos et al. [28], the surface tension of liquid Cu at 1108°C (1325 mN/m) is shown to decrease by 21% with the addition of 0,025% oxygen.

As demonstrated above in the described results, the addition of Sn to Cu improves the processability by introducing a melting range, by significantly reducing the conductivity and reflectivity, and finally by lowering the surface tension. The progressive broadening of the melting range with the increasing Sn amount, and the lowering of the solidus and liquidus temperatures allows the material to stay fluid for a longer period of time. The reduction of the conductivity is also particularly important, since it prevents heat dissipation. Additionally, the lower surface tension reduces the balling tendency of the alloy. Because of these beneficial effects, the flowability of the molten metal can be enhanced and generates a smoother melt pool for each build layer. This allows the initial porosity from 25 % in pure copper to be reduced to 0,4 % in CuSn10 [9].

CuNi3Si presents a higher conductivity and a higher surface tension than CuSn10, which are held to be responsible for the measured higher porosity levels (approx. 7 % compared to 0.4 % of CuSn10) under the standard common processing conditions (i.e. 10-45 µm powder and 20 µm layer thickness). By considering only the two CuNiSi alloys, the CuNi1.5Si alloy shows higher conductivity and reflectivity, and a smaller melting range in comparison to CuNi3Si. In combination with the lower Si content of the alloy (which results in higher surface tension), these properties can explain the higher porosity levels of the CuNi1.5Si, if compared to CuNi3Si (6.6 % against 5.5 % - see Figure 43) at standard powder size and layer thickness. The beneficial influence of the Si content is also evident when comparing the porosity obtained with the CuNiSiCr and CuNi1.5Si alloys (14 % porosity and 6.6 % porosity, respectively).

The decreasing porosity obtained by the reduction of the layer thickness and powder size (observed in Figure 43 and Figure 44) can be explained by considering that, by working with finer layers and matching powders, the energy density (in W/cm³) achieved in the material is higher. Consequently, a more effective melting and smoother processed layers can be achieved. This is also evident when observing the melt pools obtained from different layer thicknesses via SEM investigation (Figure 46). At 20µm the molten tracks are irregular and big pores can be seen on the surface Said tracks become smoother by reducing the layer thickness to 15µm and 10µm. Simultaneously, the number and size of visible pores on each layer is considerably reduced and the final density of the whole part is increased (Figure 45).

The effect of the hatch distance variation on the porosity formation during building can be attributed to the balling effect. The dynamics of this phenomenon for high laser power in combination with low laser speeds and / or small hatch distances are explained by Becker [2]. By reducing the hatch distance, and hence increasing the overlap of the scan tracks, the melting pool becomes significantly larger than the laser spot. The surrounding powder is included in the melting pool, whose width further increases. As a consequence, the pool becomes unstable and causes the processed layer to be uneven and wavy. A regular powder distribution cannot be guaranteed for the next layer and the additive process is not successful or exhibits an insufficient quality. This effect can be observed in Figure 48a for a hatch distance of 9 µm (about 10 % measured porosity), where the pores assume an elongated and semilunar shape. This effect is still partially visible up to a hatch distance value of 20 µm (see Figure 48b).

The following results could be obtained during the study on CuNiSi alloys:

- The role of alloy composition could be clearly correlated with the processability of the powders and therefore with the achieved density in the parts. Under standard processing conditions (20µm layers and 10-45µm powder size) the porosity is decreasing from 25% of pure Cu to 5.5% of CuNi3Si, because of the influence of the alloying elements on the material properties
- In particular it could be established that O and Si content play an important role for the processability of the materials, since they change the alloy properties by increasing the wetting behavior and (in the case of O) by reducing the electrical conductivity
- High energy densities are required to be able to generate stable melt pools and to reduce the porosity in the built parts. Said energy densities could be achieved for the atomised CuNiSi alloys by generating thin build layers (<15 µm) and small powder particles in a range between 5 µm and 25 µm. These processing conditions, along with a suitable laser parameter window, allowed obtaining a porosity below 2 % for the CuNi3Si alloy, even by using a relatively low laser power of 100 W. Further porosity reduction would require a higher laser power (>300 W) while maintaining the thin layer thickness and small spot size of the laser of approx. 30µm.

Processability of surface treated pure Cu-powders

Oxidized Cu-powder

The Cu powder which was thermally treated was employed for selective laser melting tests, in order to test the effect of the oxide layer on the powder particles. The treatment, however, didn't show any positive influence on the processability of the material with selective laser melting, the balling effect was still strongly present (Figure 49b), and the investigated porosity remained at the high value of 23-25% (Figure 49a)

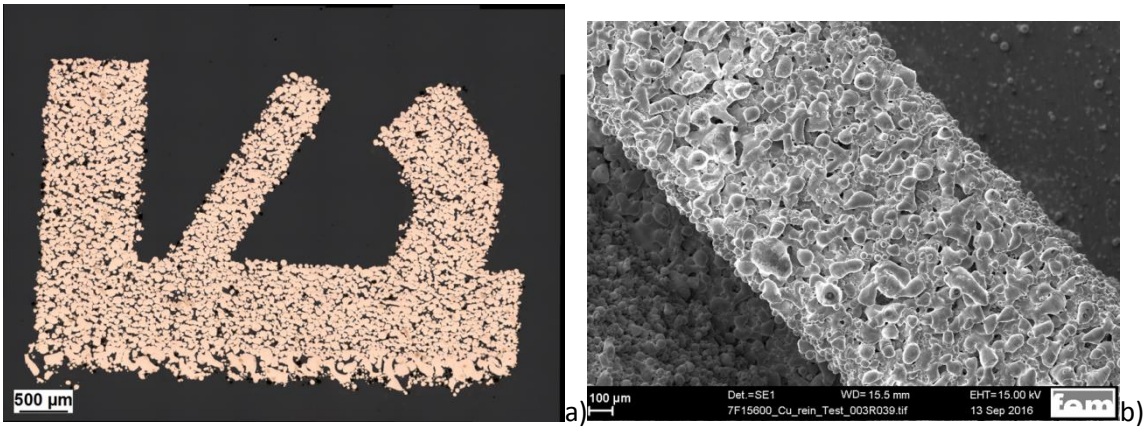

a) b)

Figure 49: Test part built with oxidized pure Cu powder (95 W – 150 mm/s) – 23,4% Porosity a) Metallographic sample b) SEM investigation of the last processed powder layer

Ti-coated Cu-powders

Both powders were employed for selective laser melting trials, and the test geometry used can be seen in Figure 45, and is the same used for the trials with CuSn and CuNiSi powders. The SEM of the last processed powder layer showed the beneficial effect of the Ti-coating on the particles. For pure copper the already mentioned balling effect was evident, and, because of the formation of large agglomerates, the molten tracks were not visibile (see Figure 52a). The first, non-optimized Ti-coating improved only slightly the melting behavior of the copper powder, and the

quality of processed layer was still poor, showing porosity (Figure 52b). With the use of the second Ti-coated batch, the molten tracks were recognizable, and the achieved overlap between them allowed to obtain a smooth melting area (Figure 52c).

The metallographic investigations on the parts showed according results: the porosity detected with image analysis decreased by increasing the Ti content in the powder and the regularity of the coating. The pure Cu part presented 23% porosity, while the parts built with the two coated powders showed respectively 18% and 3,5% porosity (Figure 53a-c).

SEM investigation, which was performed on the surface and on the cross section of parts built with the second powder batch, showed that during the LBM process Ti-oxide formed (Figure 54 and Figure 55), and the alloying of Cu and Ti took place only partially. EDX analysis on the cross section detected 0,8% Ti in the alloy. Both the Ti-oxide Ti_2O_3 and the intermetallic phase Cu_3Ti_3O could be detected through the XRD analysis on the polished sample.

The results obtained confirmed the validity of the research approach: through the applied Ti-coating, it was possible to reduce the reflectivity of the pure Cu powder, and therefore to increase the energy absorption. This resulted in an improved melting of the material and in the substantial reduction of the porosity in the part. The formation of the Ti oxide partially prevented the alloy formation between Ti and Cu: the high O content (0,25%) of the coated powder has still to be reduced in further coatings, in order to improve the achieved density by exploiting the desired widening of the alloy melting range.

Sulphur-coated Cu-powders

The test part built with the sulphur vapor deposition coated Cu-powder showed 15,8% porosity, and therefore a slightly improved density in comparison to pure copper (see Figure 53d). EDX analysis on the cross section did not reveal any sulphur traces in the part microstructure.

The coating increased the processability of the powder, and this confirmed the validity of the approach with the sulphur treatment (reduction of powder reflectivity) but further improvement of the process (in order to improve coating thickness and regularity) is still needed to achieve a higher part density as in the case of the Ti-coated powder.

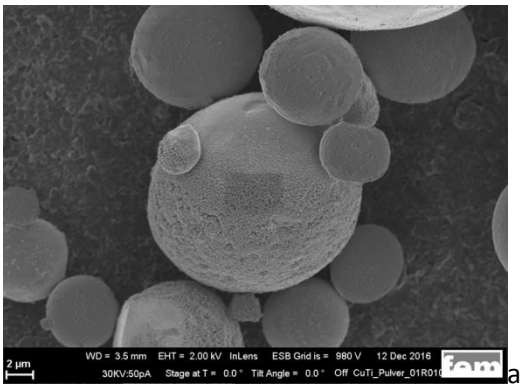

a)
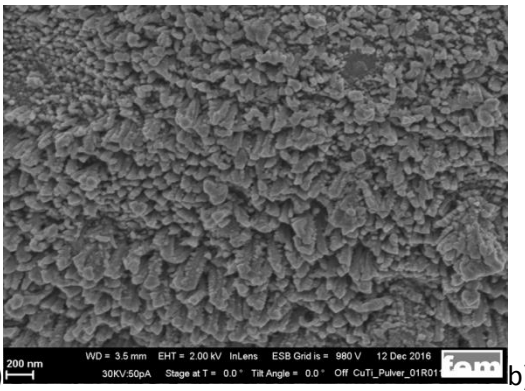

b)

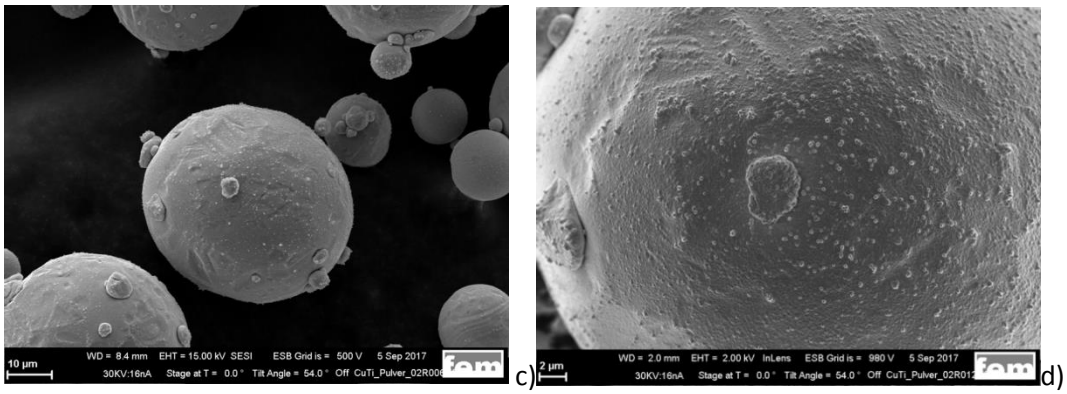

Figure 50: SEM investigation on surface of coated powder particles a) – b) first batch with irregular coating c) – d) second batch with regular coating

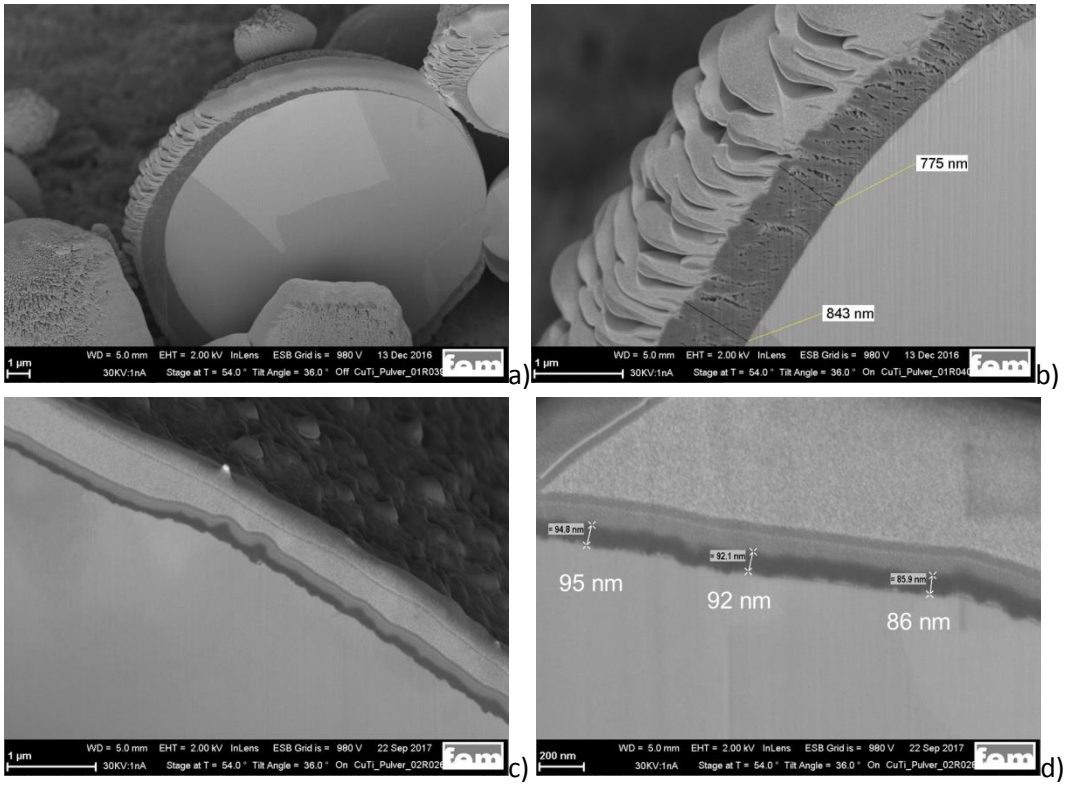

Figure 51: FIB investigation of the coating thickness (measured in the pictures) - a)-b) first coating trial with irregular coating (0-850 nm) c)-d) optimized coating with regular thickness (85 – 130 nm)

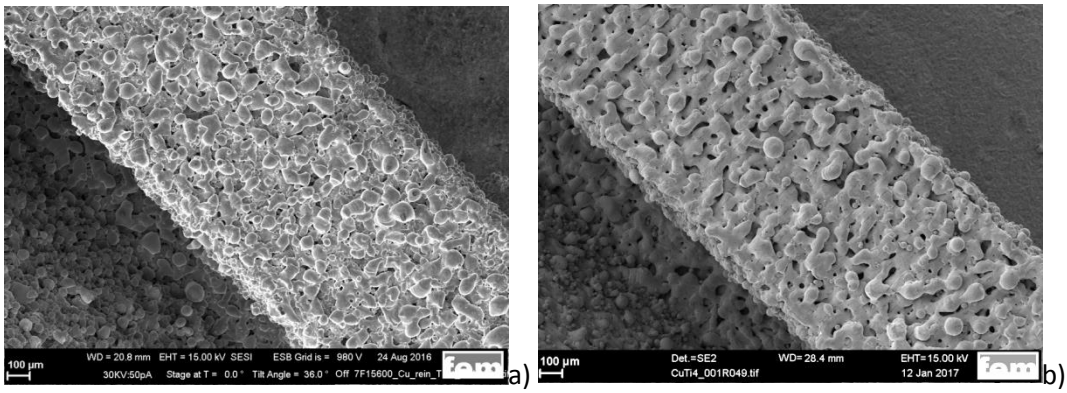

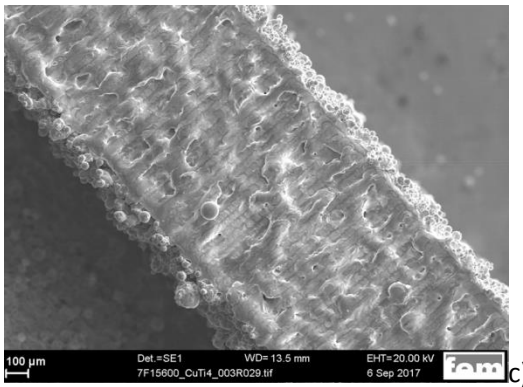

c)

Figure 52: SEM investigation of the last processed layer (95W – 300 mm/s) a) pure copper powder (b) 1st batch of Ti-coated powder (0,2 w% Ti - irregular coating) / (c) 2nd batch of Ti-coated powder (1,1 w% Ti - continuous coating)

a)

b)
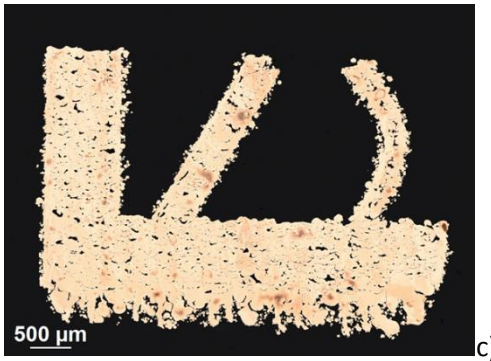

c)
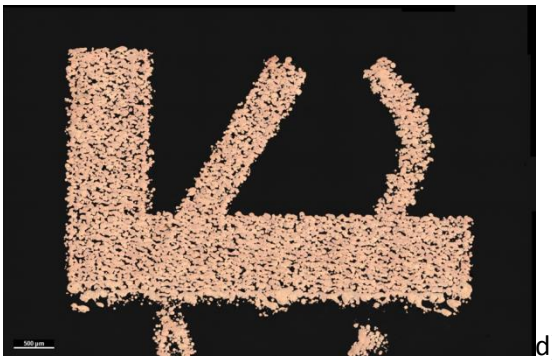
d)

Figure 53: Metallographic cross sections of built test parts (95W – 300mm/s) with different Ti-coated powder charges – a) Pure Cu powder - 23,4% porosity (b) 1st batch of Ti-coated powder (0,2 w% Ti - irregular coating – 18% porosity) / (c) 2nd batch of Ti-coated powder (1,1 w% Ti - continuous coating – 3,5% porosity) d) sulphur vapor coated Cu powder – 15,8% porosity

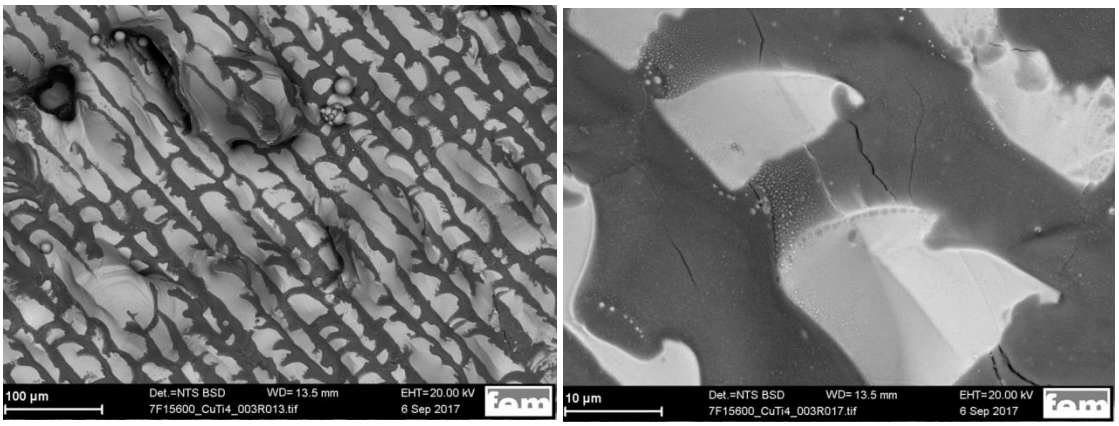

Figure 54: SEM investigation on part surface (second batch): Titanium oxide is visible between the molten laser tracks

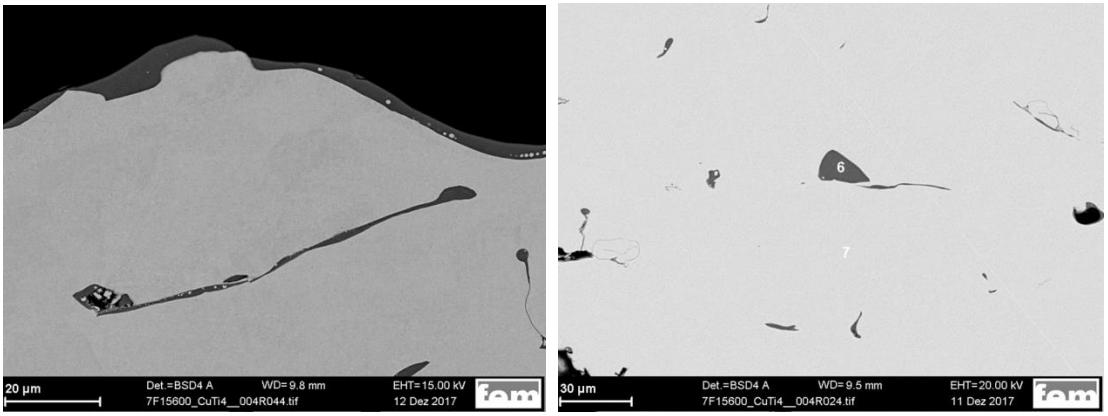

Figure 55: SEM investigation on metallographic cross section (left) Ti-oxide (Ti2O3 detected via XRD analysis) in the part and on the surface – (right) EDX measurement (point 6- 62% Ti / 3% Cu / 35 % O - point 7 - 0,4% Ti / 99% Cu / 0,6% O)

Design and optimization of the geometry of and electric motor coil for LBM

Parallel to the parameter study conducted on the CuNiSi alloys, the geometry of the coil for highly efficient electric motors (designed by the SME and industry project partner Unicorn Engineering GmbH) - Figure 56a) was optimized as a preparation for the manufacturing of the final demonstrators. CuSn10 was used for the tests: the gap between the coils was too small in the original design (0,2 mm), so that a powder sintering occurred (Figure 56b), and the necessary distance was not any longer assured. In order to solve the problem, the gap was increased to 0,4 mm (see Figure 56c-d).

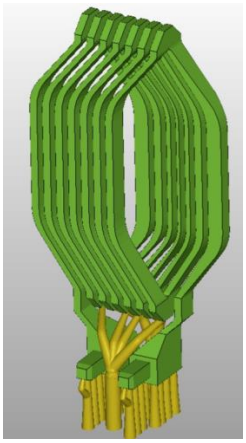
a)
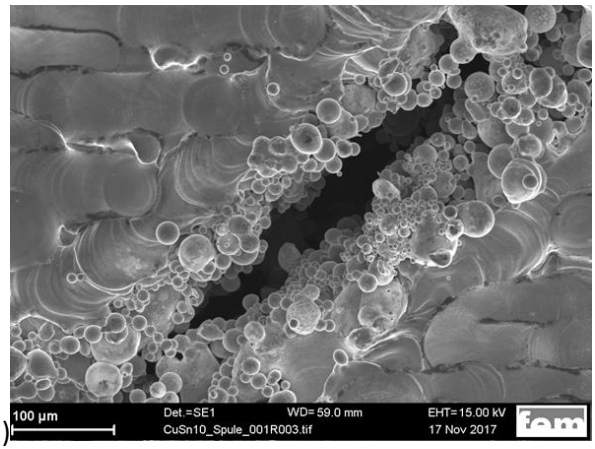

b)
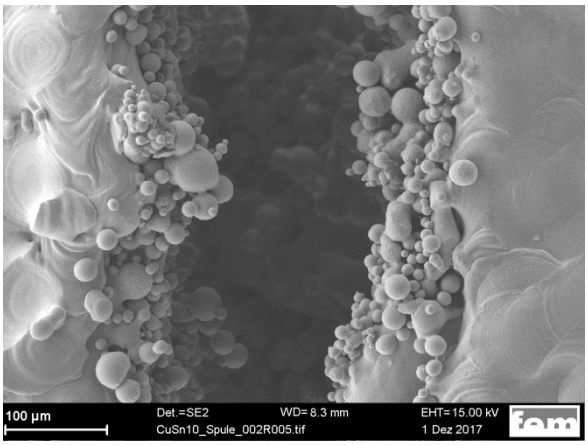

c)
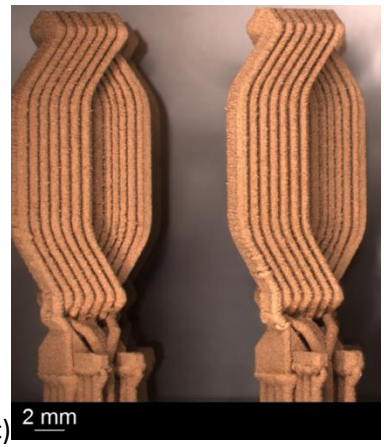

d)

Figure 56: Manufacturing of a coil for electric motor – geometry optimization (CuSn10) a) geometry with support structure b) SEM investigation of the powder adhesion between the coils in the original geometry c) SEM investigation of the increased gap between the coils in the modified geometry d) manufactured coil with optimized gap

After the optimization, the coil was built both with the CuNi3Si alloy (10-25µm powder size and 10µ layers), and with the Ti-coated Cu powder (10-45µm powder size and 20µm layers) (see Figure 57).

Figure 58a shows the investigation of the coil built with CuNi3Si in the metallographic cross section: thin sections (0,2 mm) showed higher porosity compared to thicker ones (0,5 mm) (Figure 58b-c). A wall thickness of 0,2 mm reaches the limit of process, and its optimization could reduce the porosity in certain coil sections. The porosity in the CuTi coil is higher compared to CuNiSi and uniformly distributed, and is similar to the one observed in the test part (Figure 58d).

Figure 57: Electric motor coil (design by Unicorn Engineering GmbH) built with LBM a) with CuNi3Si (10-25 µm powder size and 10 µm layers) b) with Ti coated Cu powder (10-45 µm and 20 µm layers)

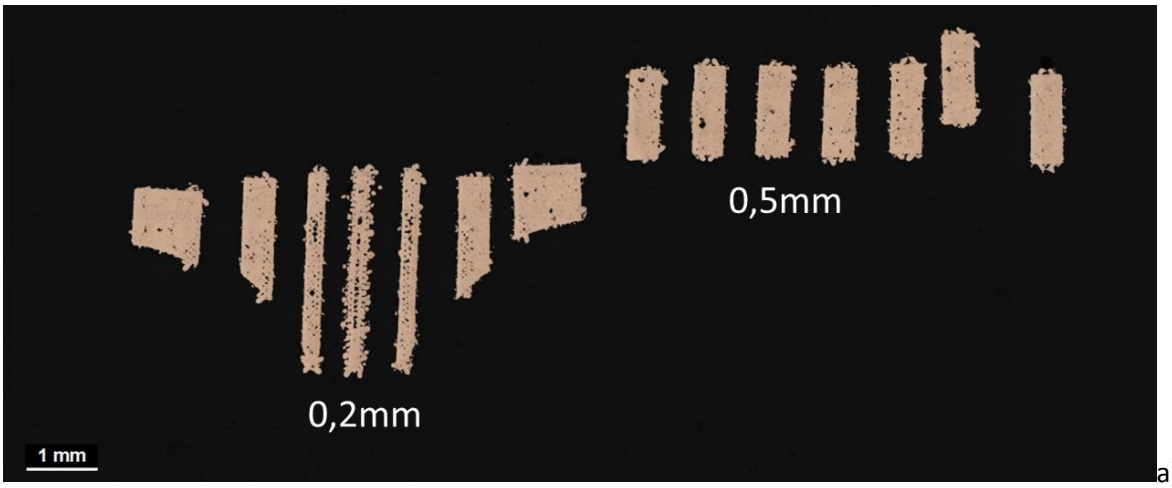

a)

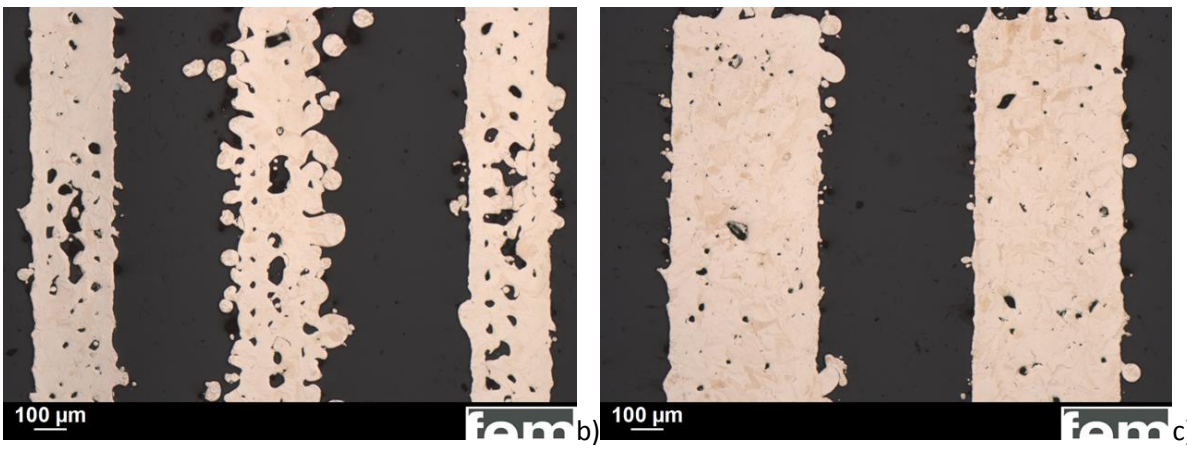

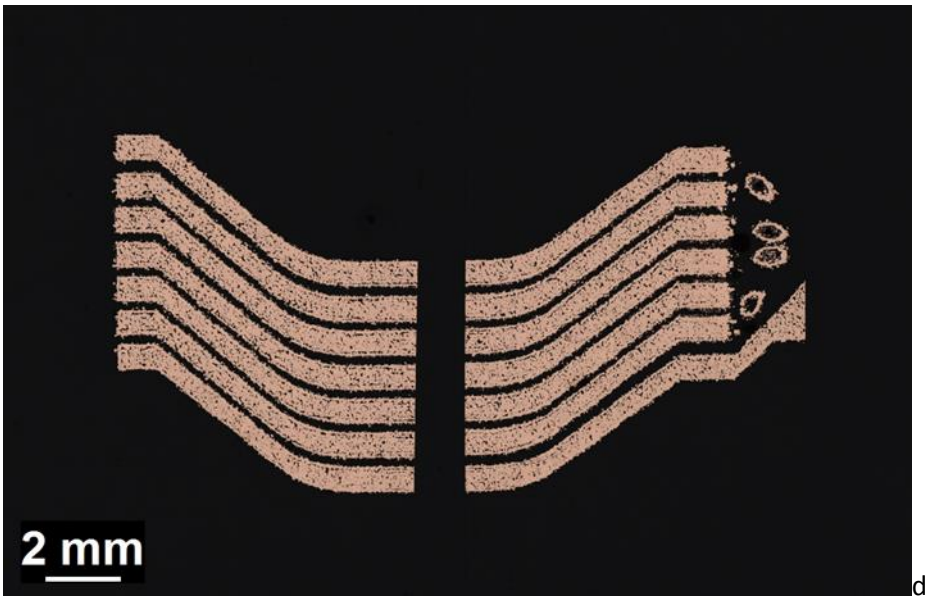

d)

Figure 58: Metallographic cross section of the manufactured coil a) CuNi3Si alloy: cross section overview with indication of the coil wall thickness b) CuNi3Si alloy: detail of 0,2 mm wall thickness c) CuNi3Si alloy: detail of 0,5 mm wall thickness d) CuTi alloy - cross section overview

Infiltration of pure Cu porous parts with Ag solders

Since the built parts in pure Cu presented a very high porosity (~25%), infiltrations tests with a silver solder were conducted on said porous parts in order to improve their density and electrical conductivity. Small plates were built in pure copper (dimensions 30 x 15 x 3 mm) and infiltrated under vacuum with three different Ag solders (whose compositions are listed in Table 9). During the test the Ag solder was placed on the Cu part and it was heated in a furnace up to 770-810 °C (depending on the melting temperature) always under vacuum, for a maximum infiltration time of about 14 minutes. Subsequently the parts were investigated with metallographic cross section (including quantitative image analysis for porosity measurement), SEM, and their properties (hardness and electrical conductivity) were measured (see Table 10). A slight deformation of part could be noted after infiltration. The metallographic investigation showed a strong increase in the part density compared to pure copper: the original porosity (23,9%) could be reduced to about 2% (Figure 59). The electrical conductivity was also increased from 25% to about 80% (depending on the trial). Through the SEM investigation on the cross section, it could be observed that diffusion of Ag in Cu takes place during the infiltration (see Figure 60).

The infiltrations tests on a porous Cu part with a Ag solder were successful, since the goal of increasing the density and electrical conductivity of porous pure copper parts were reached. The method could be an alternative route to produce Cu parts with the desired properties, if those cannot be achieved simply through the processing with selective laser melting. Additional tests would be required to find the right processing conditions (time / temperature) for a part with a more complex geometry, in order to avoid for example the mentioned occurred deformation.

Table 9: Solder compositions and melting ranges

Solder composition	Melting range [°C]
Cu 27,5% - Ag 70,5% - Zn 2%	770 - 840
Cu 28,5% - Ag 71,5%	779
Cu 15% - Ag 85%	779 - 850

Table 10 – Measured properties of the Cu plates

Plate properties	El. Conductivity [% IACS]	Porosity [%]	Hardness [HV5]
Pure Copper	25	23,9	-
Infiltrated with solder Cu 27,5% - Ag 70,5% - Zn 2%	77	1,7	69
Infiltrated with solder Cu 28,5% - Ag 71,5%	82	2,6	77
Infiltrated with solder Cu 15% - Ag 85%	85	2,4	83

Figure 59: Metallographic investigations on infiltrated Cu parts – a) Pure Cu part as built b) part infiltrated with Silver solder Ag 71,5% - Cu 28,5% c) part infiltrated with Silver solder Ag 70,5% - Cu 27,5% - Zn 2% d) part infiltrated with Silver solder Ag 85% - Cu 15%

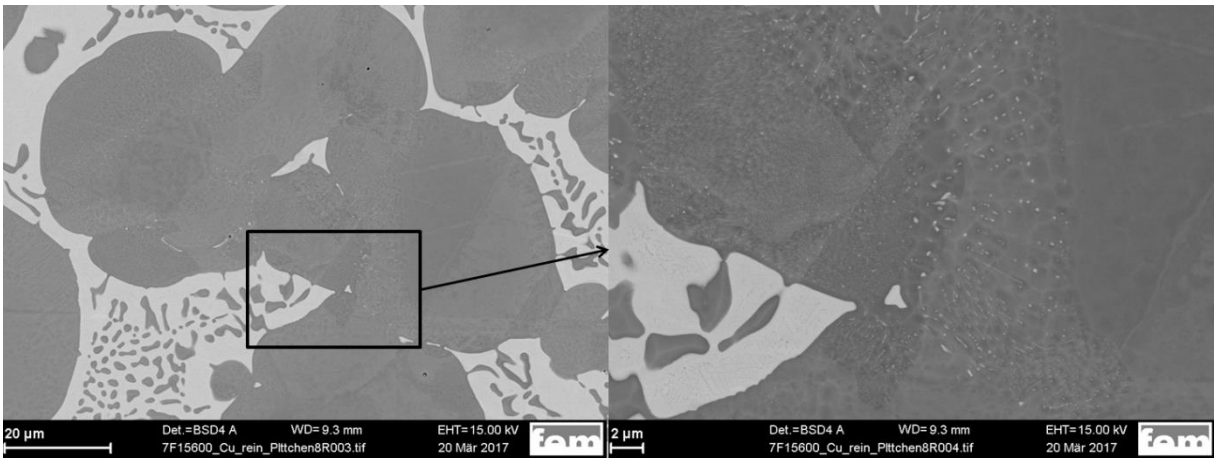

Figure 60: SEM investigation on the cross section of a Cu part infiltrated with solder Cu 28,5% - Ag 71,5%. Diffusion of Ag in Cu takes place during the infiltration

3.1.4.2 Performed activities – sirris

- Manufacturing of stainless steel and Al test parts using binder jetting/infiltration process

Printing of 316L parts

Bars of 280x10x10 mm have been printed successfully with standard parameters using 45-90 µm and 5220 powders for mechanical testing. Problems have been encountered during printing tests on 5520 powder, because of its different particle size distribution and flowability. It has been thus ruled out for the next steps. A demo part has also been printed using 45-90 µm powder (shown in Figure 61). It has dimensional, geometric and mass characteristics incompatible with LBM technology but suitable for binder jetting technology.

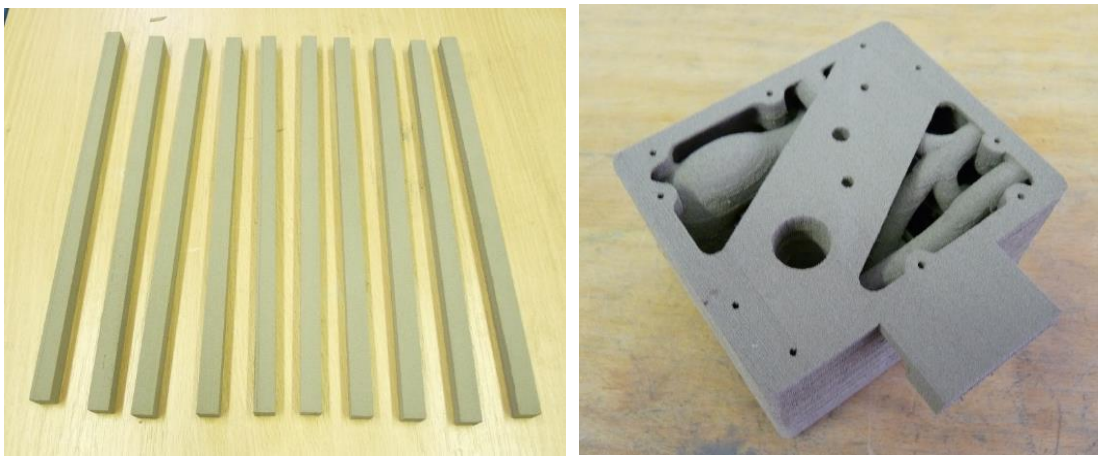

Figure 61: Bars (left) and demo part (right) printed in 316L by binder jetting.

Infiltration of 316L parts

A first test showed the feasibility of infiltration using both infiltrants BNi7 and F300 under specific conditions (temperature of 1150°C, clean argon atmosphere). But the next tests have highlighted several problems and limitations when using the traditional infiltration procedure. Infiltrant powder is put under a plate on which we place the parts to be infiltrated. All the parts are connected between them using small bars printed with the parts and linked to a main larger bar that dives into

infiltrant powder. Theoretically, during the thermal treatment, the infiltrant melts and is sucked by capillarity in the bars circuit. The process naturally stops when all the porosity is filled. It works like this using bronze. With both infiltrant BNi7 and F300, the main bar seems to melt and collapse during infiltration, cutting the infiltrant flow filling the parts porosity, as shown on Figure 62.

Figure 62: Infiltration circuit with BNi7, before (left) and after treatment (right).

This phenomenon comes from melting depressant. Silicon and phosphor are melting depressant contained in these two infiltrants. They diffuse from infiltrant to infiltrated material, reduce the melting point of the printed material and erode the main bar which ends up collapsing in molten infiltrant. This is emphasized by the high temperature that favors thermal agitation and thus diffusion, and by the high surface area of pre-sintered printed parts. Suggested solutions to avoid this problem are:

- Reduce the infiltration temperature to limit diffusion (not exceeding recommended brazing temperature)
- Reduce the length of the circuit to reduce infiltration time
- Work in recommended brazing atmosphere for debinding-infiltration (vacuum)
- Carry out a more advanced pre-sintering to reduce surface area
- Apply a protective coating on 316L powder before printing

Reducing the temperature and time of infiltration has been tested first but didn't lead to success. Melting and collapsing of the bars was still occurring. The furnace doesn't allow to work under vacuum and no partner could provide such a furnace, so this solution wasn't tested.

To reduce the infiltration path, the use of an infiltration cup was tested, which allowed to infiltrate directly the bars but led to sweating out of infiltrant excess at the lower point. In this case, the infiltrant being at the same level than the parts to be infiltrated, the physical phenomenon of infiltration by capillarity didn't stop naturally (Figure 63).

Figure 63: Infiltration cup printed in 316L used to infiltrate 2 bars with F300 infiltrant.

Another solution was to pre-sinter the parts and the circuit to consolidate them and reduce the surface area exposed to the melting depressant diffusion (Figure 64). These presintered bars were successfully infiltrated with both infiltrants. On Figure 65, however, it can be seen the infiltrant sweat out of the bars in several points. The placement of the parts at the same level than the infiltrant powder is needed to force infiltration, but is definitely not the best solution for infiltrated parts quality.

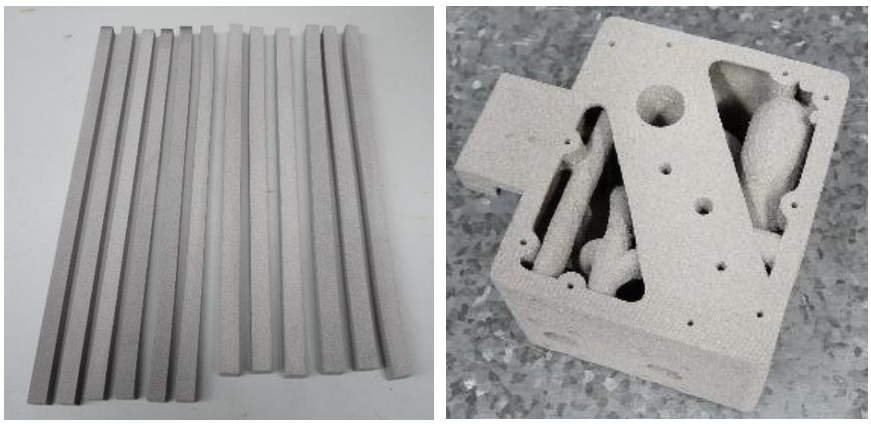

Figure 64: Bars and 3D part printed in 45-90µm 316L and sintered at 1395°C during 90 minutes under hydrogen.

Figure 65: 316L pre-sintered bars infiltrated with BNi7 (left) and with F300 (right).

A last solution that has been studied was the application of a diffusion barrier on the 316L powder. This is done in electronic to protect gold and expensive material components against interdiffusion of material in contact with these components. Material used as diffusion barrier are refractory metals such as Nb, Mo, Ta, W and Re (see Figure 66).

H																	He
Li	Be											B	C	N	O	F	Ne
Na	Mg											Al	Si	P	S	Cl	Ar
K	Ca	Sc	Ti	V	Cr	Mn	Fe	Co	Ni	Cu	Zn	Ga	Ge	As	Se	Br	Kr
Rb	Sr	Y	Zr	Nb	Mo	Tc	Ru	Rh	Pd	Ag	Cd	In	Sn	Sb	Te	I	Xe
Cs	Ba	La	Hf	Ta	W	Re	Os	Ir	Pt	Au	Hg	Tl	Pb	Bi	Po	At	Rn
Fr	Ra	Ac	Rf	Db	Sg	Bh	Hs	Mt	Ds	Rg	Cn	Nh	Fl	Mc	Lv	Ts	Og

*	Ce	Pr	Nd	Pm	Sm	Eu	Gd	Tb	Dy	Ho	Er	Tm	Yb	Lu	
**	Th	Pa	U	Np	Pu	Am	Cm	Bk	Cf	Es	Fm	Md	No	Lr	

Figure 66: Metals with a melting point higher than 2200°C in dark green and higher than 1850°C in light green

For the intended application, a metal that sinters sufficiently after debinding and before infiltration is needed (at about 800-900°C). The best candidate was chromium, present yet in 316L alloy. Partner

Materia Nova prepared a batch with a coating of Cr on 316L 45-90µm powder. This batch was used to print bars for infiltration test. Adding the refractory coating on the powder changed a little bit the thermal behavior of the powder during the printing and parameters had to be adapted. Printed bars were successfully infiltrated. As shown Figure 67, bars didn't melt but lots of molten infiltrant sweated out of the parts.

Figure 67: Bars printed with Cr coated 316L powder infiltrated with BNi7 (left) and F300 (right)

All considered solutions didn't lead to a successful infiltration procedure. Melting of the printed bars due to melting depressant in infiltrant material was avoided by playing on infiltration parameters (temperature and time) and using artefacts (pre-sintering, refractory coating). But sweating of molten infiltrant always occurred and deteriorate the part quality (post-machining needed).

Printing of 3004 Al-alloy parts

A feasibility test has been made on aluminum. Bars of 280x10x10 mm have been printed successfully after adjustment of drying parameters using 50-100 µm 3004 Al-alloy powder provided by Nanoval (Figure 68).

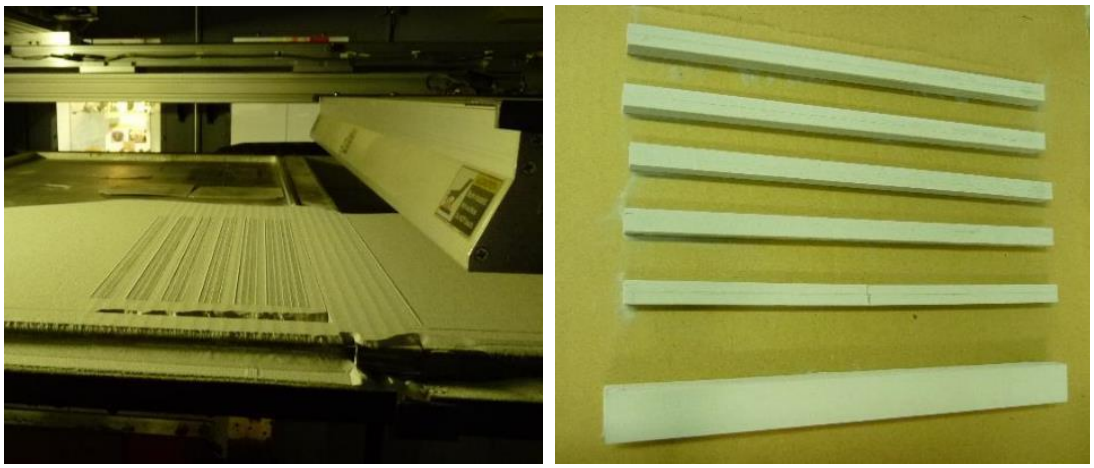

Figure 68: bars printed in 3004 aluminum alloy powder

Unfortunately, thermal treatment after printing was problematic. In fact, during printing, a water-based liquid binder is printed on powder surface. After that, the layer is partially dried by a heating element above the powder. All these steps occur in a machine chamber opened to air and not in a controlled atmosphere. After printing and before to be able to handle the parts, the glue must set

and harden. This occurs during a thermal treatment at 180°C under air. All these steps lead to an oxidation layer on the surface of Al powder which prevents sintering. Moreover, alumina has no wettability regarding molten metals and natural infiltration can't occur. Printing and curing are two steps that can't unfortunately be conducted under protective atmosphere at Sirris with existing machines.

Infiltration of aluminum parts

No infiltration test was finally conducted. But the same consideration than for 316L has been made for aluminum regarding the presence of melting depressant (Si and Mg) in infiltrant materials. A protective coating to prevent oxidation of aluminum and to stop diffusion of Si and Mg could be applied. Regarding the melting/sintering temperature, Cu could be a good candidate, but for oxidation resistance, Mn could be the best choice (melting point: 1246°C; sintering starts at ~490-500°C). Moreover, Mn is present in 3004-alloy yet. These investigations could be part of a further project.

3.1.5 WP4 Testing of demonstration parts

3.1.5.1 Performed activities – fem

- The properties of the parts produced with CuNi3Si and CuTi (hardness and electrical conductivity) were measured

The manufactured test parts from CuNi3Si were submitted to a conventional two-step heat treatment: first solution annealing at 750° C for 5 minutes and subsequent quenching in water, and then aging at 450° C for 6 hours. It has to be noted here that the parts used for the thermal treatment were not built with optimized parameters (in terms of layer thickness and powder particle size) and, thus, had a porosity of about 6%.

Figure 69 shows the hardness HV1 and electrical conductivity of the additively manufactured parts in three conditions: as-built, after solution annealing and subsequent age hardening, and after age hardening without the solution annealing step. The properties of the as-built parts are very similar to those of the solution annealed ones, while after the age hardening a pronounced increase in hardness and electrical conductivity can be determined for both treatment paths. After age hardening, the properties of the additively manufactured parts (although not produced under optimal conditions and therefore featuring 6 % porosity - see Figure 70) exceed the ones of investment cast material. In comparison to the benchmark values of the sheet material (202 HV1 and 55 % IACS), the additively manufactured parts have slightly lower hardness (180 HV1), and a noticeably lower conductivity (40 % IACS). A direct aging treatment of as-built parts leads to an even lower conductivity (33.5 % IACS), although it allows to reach the same hardness as the sheet material.

Regarding the electrical conductivity and hardness achieved in the test parts, it has to be considered that the specimens for thermal treatment were built with standard parameters, and therefore present, as already mentioned, a porosity of about 6 %. C. Vincent et al. [29] show that the thermal conductivity in sintered copper powder decreases linearly with increasing porosity (and as already mentioned the thermal conductivity is directly proportional to the electrical conductivity). The linear decrease follows a low slope in a porosity range of 0% to 6% volume; such slope becomes steeper in the 6 % to 8 % range. According to this data, it can be estimated that reducing the porosity in the parts to 1-2 % (as achieved with optimal process parameters) could increase their electrical conductivity up to 47 % IACS.

Although the electrical conductivity of these parts is still somewhat lower compared to reference of the sheet material, they are suitable to be employed for building complexly shaped parts designed for specific technical applications, such as miniature heat exchangers and electric parts.

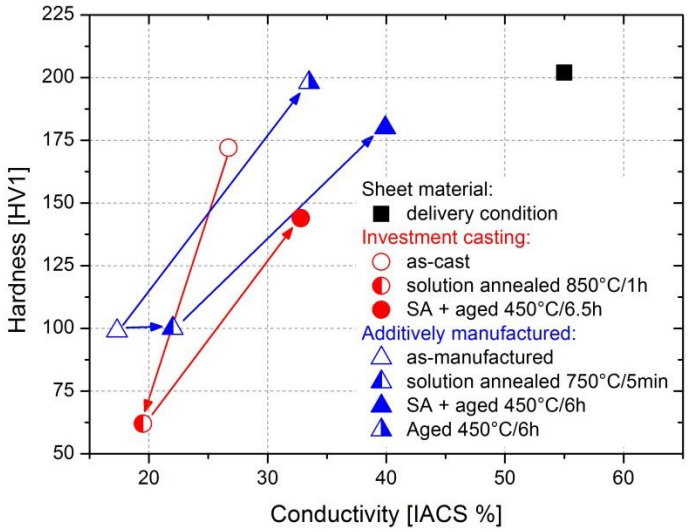

Figure 69: Hardness HV1 and electrical conductivity of the additively manufactured parts in CuNi3Si (as-built and after solution annealing and age hardening) in comparison with cast material [30] and sheet material (in delivery condition).

Figure 70: Metallographic cross sections of built test parts in CuNi3Si for thermal treatment (95 W – 200 mm/s) - Measured porosity: 6 %

The manufactured test parts from Ti coated Cu powder were also submitted to a conventional two-step heat treatment: first solution annealing at 850°C for 1 hour and subsequent quenching in water, and then aging at 415°C for 6 hours. The measured properties are listed in Table 11. While there is no noticeable increase in the hardness, the achieved el. conductivity after thermal treatment (45 % IACS) is superior to the one obtained with the CuNi3Si alloy (40 % IACS).

Table 11 – Measured physical properties on test parts built with Ti coated powder

	Vickers Hardness HV1	Electrical conductivity [%IACS]
As-built	33	33
Solution annealed – 850° 1h	-	46
Age hardened – 415° 6h	35	45

3.1.5.2 Performed activities – sirris

- Tensile tests on printed 316L bars infiltrated in the different conditions
- Metallographic investigation of infiltrated 316L printed parts

Printed 316L bars infiltrated in the different conditions have been tensile tested. Results are summarized in Table 12. Mechanical characteristics of 316L stainless steel infiltrated with bronze (measured by Exone and by Sirris) are shown for comparison.

Table 12: Results of mechanical testing on infiltrated bars

sample	Ultimate tensile Strength	Young modulus	Elongation
	MPa	GPa	%
SS316L + Bronze (Exone)	406	148	8,0
SS316L + Bronze (Sirris)	**330**	**114**	**6,3**
SS316L pre-sintered (1395°C/90')	74	46	3,8
SS316L + F300 infiltrant	**196**	**168**	**0,2**
SS316L presintered + F300 infiltrant	192	152	0,1
SS316L + Cr coating + F300 infiltrant	174	165	0,1
SS316L presintered + BNi7 infiltrant	136	128	0,2
SS316L + Cr coating + BNi7 infiltrant	169	167	0,1

Compared to bronze infiltration, 316L infiltrated with brazing steel leads to lower mechanical properties: a more brittle and fragile material, with a lower UTS. There is no real benefit of pre-sintering and chromium coating on mechanical properties. These lower mechanical properties can be due to the presence of residual porosities. In fact, optical microscopy has been done on several samples obtained in different manufacturing conditions. Figure 71 shows the 316L particles before and after infiltration, with a lot of residual porosities.

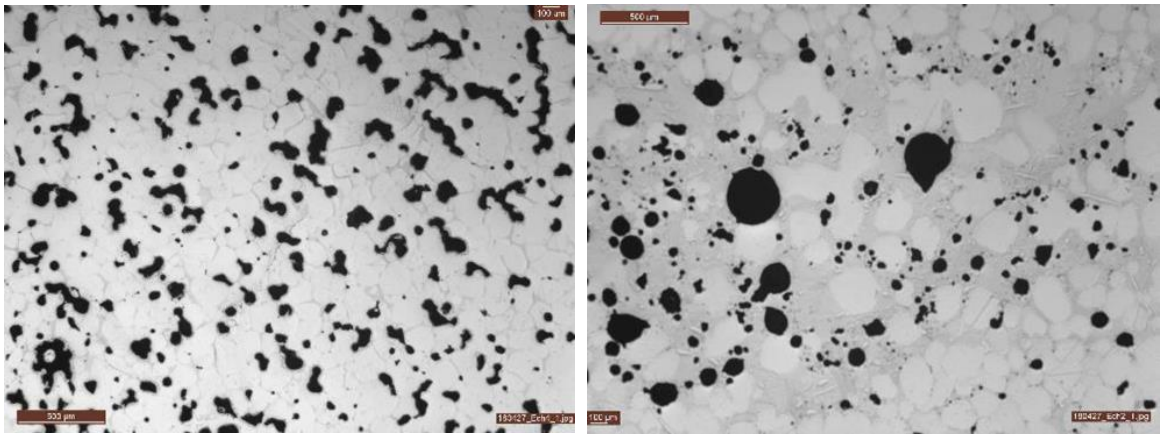

Figure 71: Optical microscopy of pre-sintered 316L powder coated with Cr and infiltrated with F300

It has been highlighted that porosities are not homogenously spread in the samples. These residual porosities are not linked to the capillarity process due to the difference in size observed. They could come from surface oxidation or residual carbon.

Finally, Figure 72 shows a local difference in density/porosity depending on the distance from the infiltration point of the part. The left picture has been taken on a cut of the bar close to the infiltration point (~4% porosity), and the right picture has been taken at the end of the bar (~13% porosity). This highlights a certain limit in length for the infiltration path using these infiltrant materials.

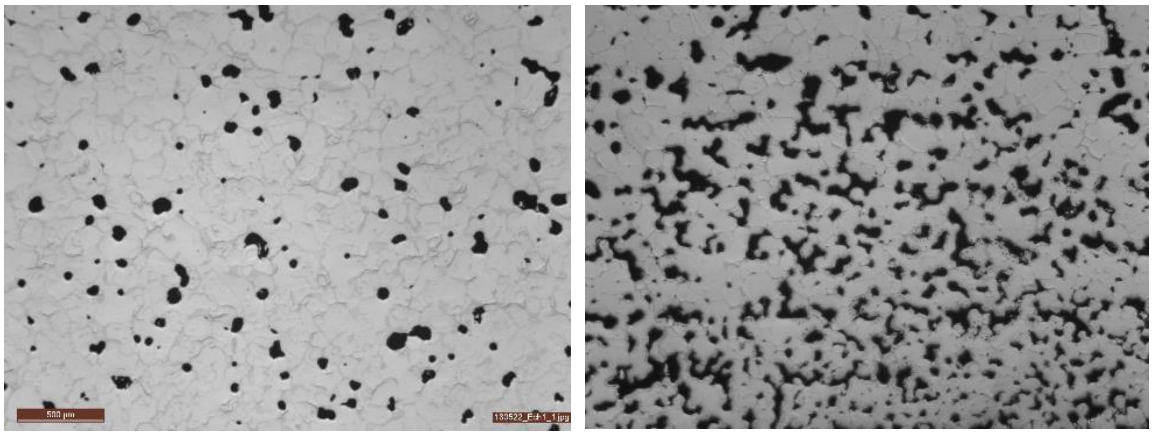

Figure 72: Optical microscopy of a 316L bar infiltrated with F300, close to (left) and far from (right) the infiltration point

3.1.6 WP5 Technical and economic assessment

3.1.6.1 Performed activities – UMSICHT

- Evaluation of materials costs

UMSICHT´s contribution in the OpP3D project is related to powder manufacturing and coatings development by using sulfur precursors for coating Cu powder. The following facts can be derived from the project results in respect to these two points and to the related materials/production costs:

1) Powder manufacturing

   Pure copper powders for additive manufacturing have to be produced via inert gas atomization (IGA) in order to keep the oxygen content low and to provide spherical particle qualities for achieving good handling properties (flowability, apparent density). Such powders are available on the powder market. Their price is mainly governed by the spot market for the raw material copper and by the demanded size fraction. The latter one is a decisive cost factor: The finer the powder and the more narrow the demanded size fraction, the more costly is the powder. This is a consequence of the production process (atomization) which commonly results in a characteristic size distribution width, typically between 2 and 2.5 (in terms of the ratio of the cumulated weight percentage of particles smaller than 84 % and the mass median at 50 %, d_{84}/d_{50}). Despite hot gas atomization experiments have not been performed at UMSICHT within this project, it is possible to make a statement for the powder costs based on previous investigations at UMSICHT:

   Figure 73 shows the typical size distribution of a copper powder in the as-atomized state from a conventional (cold) N_2 gas atomization process (IGA) under optimized conditions. If the demanded standard particle size range would be 15 µm to 45 µm, the yield from this atomization would be approx. 48 % (size limits marked by the blue dotted lines).

   The project results show that a more narrow and finer particle size range, e.g. from 10 µm to 25 µm (red dotted lines), can enhance parts qualities by considerably reducing porosities (see fem results in Figure 44). The yield of the conventional IGA process would then be only at around 18 %. Correspondingly, it can be expected that the price for such a powder will increase remarkably and hinder its industrial application. Therefore, improvements of the LBM machines and processes (green laser, higher laser power) that are currently under development, are required. This will allow the use of coarser powder, i.e. larger fractions of the atomized powder, in order to keep the powder cost low.

Hot gas atomization (HGA) provides a much more efficient atomization of the melt due to the higher gas exit velocities and increased temperatures inside the atomization zone. The achievable particle sizes decrease with increasing temperature. Simultaneously, the N_2 gas consumption is less, if compared to the cold gas alternative. The yield in the demanded size range between 10 µm to 25 µm would exceed 30 % by using the UMSICHT hot gas technique and, thus, HGA provides a still more expensive but reasonably economic powder production also for such fine and narrow particle size ranges.

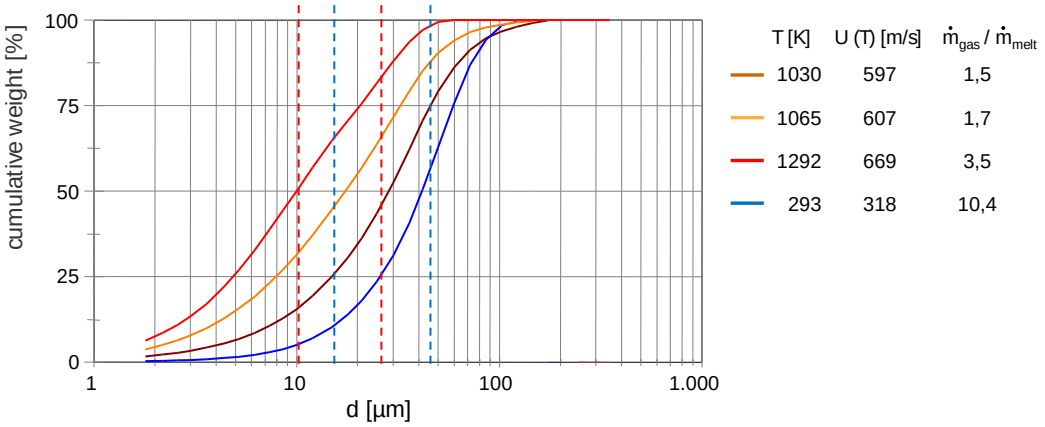

Figure 73: Particle size distributions of as-atomized (N_2) powders by using conventional cold inert gas (IGA) and N_2 hot gas atomization technique (HGA) with the gas temperature, the corresponding gas velocity at the nozzle exit and the mass flow rate ratios gas/melt (in kg/kg)

2) Cu sulfide coatings on Cu powder particles

The inferred and investigated techniques for the coating of Cu powders are basically common practice for the manufacturing of engineered powder products. The wet coating route with toluene as well as the gas and vapor based routes with a fluidized powder bed are scalable to meet industrial measures and economic procedures. However, the present results show that the achieved better absorbance of the laser light at 1060 nm through the Cu_2S coatings alone cannot provide a technical solution for the manufacturing of fully dense parts so far. It is still an open question whether the “balling effect” can be avoided, if the coatings and the LBM process parameters are further optimized and higher laser energies are applied.

3.1.6.2 Performed activities – Sirris

- Provision of process related data for use in LCA

3D-printing (binder jetting) processing costs have been determined on Sirris Exone R10 machine, using stainless steel 316L powdered material. Thermal post-treatment costs have also been analyzed (energy, consumables, equipment construction, emission and waste). Case studies have been used to determine costs for extrapolated number of parts produced. All these data have been transferred to partner Materia Nova for the life cycle assessment of the whole process, including powder production and coating.

3.1.6.3 Performed activities – Materia Nova

- Evaluation of 3DP process and material costs for use in LCA

The main contributors of the existing process can be identified by LCA with a eco-design goal. The integration of the Materia Nova process (powder treatment by sputtering magnetron) allows to measure its relative impact on the total impact of the manufacturing process in order to evaluate the balance between the gain that this new stage brings to the parts and its environmental impact.

The main results are presented here:

1) The analysis of the contribution of the various stages of the global Opp3D process for the manufacture of 316L Stainless steel parts
2) The functional unit is the manufacture of a steel part
3) The calculation is carried out with the method "ILCD 2011 midpoint +" with an adaptation of the module "water resource depletion" in "Water Use"
4) Figure 74 shows the contribution of each step for each impact category calculated by the software.

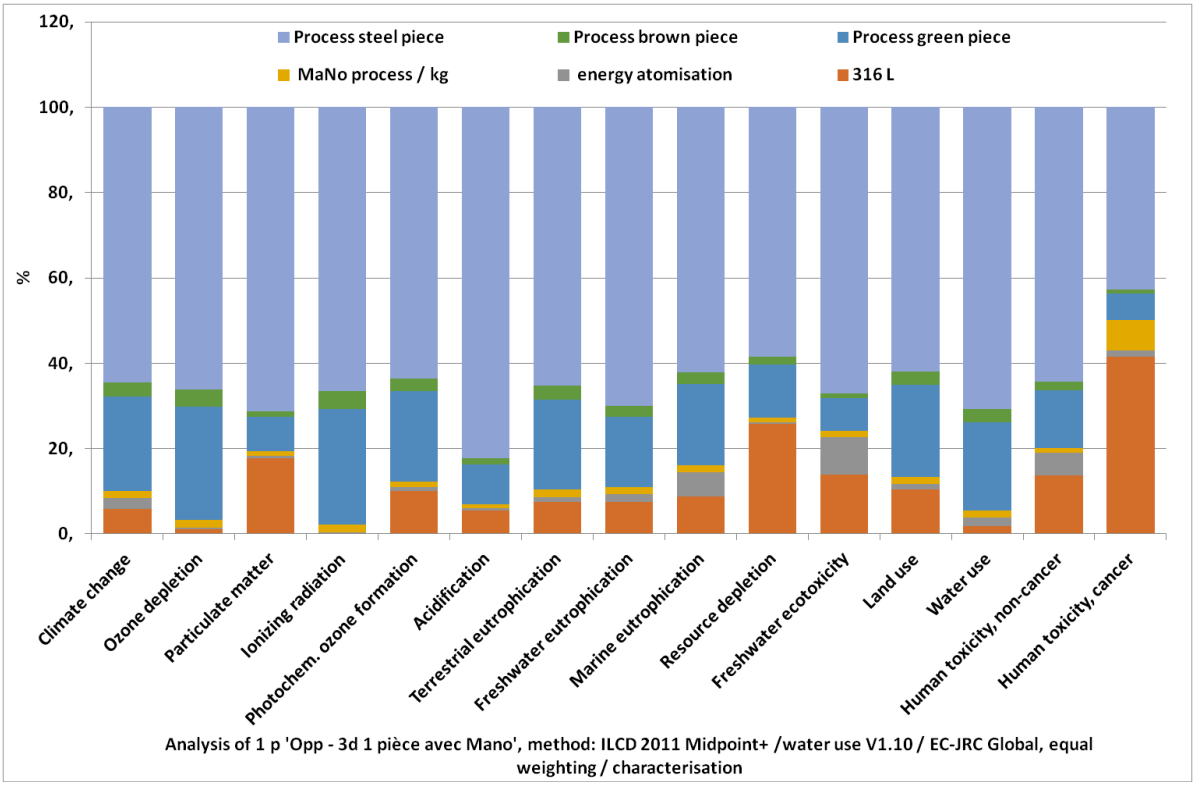

Figure 74: Contribution of each step to the manufacture of a stainless steel part

It can be seen that the main contributor is the piece steel process which consists of baking parts in the oven, with an energy input of 200 kWh. The green piece stage consists of the printing of the pieces and represents the second contributor on the majority of the impacts. For the impact of human toxicity on cancer, 316L stainless steel appears to be important. This is probably the chromium component of the material. The proportion of the plasma powder modification appears to be low on the impacts studied.

Figure 75 shows the environmental impacts of the complete process with or without the plasma modification of Materia Nova. Overall, the contribution of the MaNo process (plasma sputtering) appears to be low.

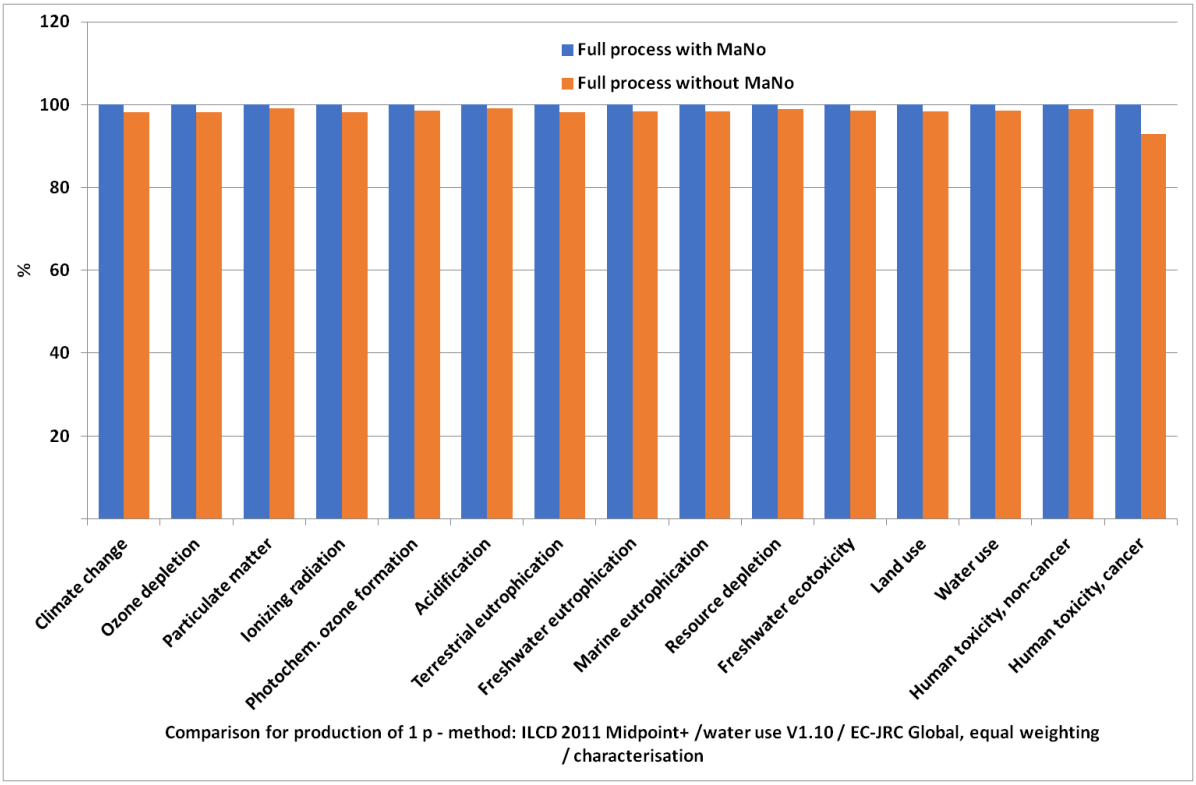

Figure 75: Impact of the MaNo process on the complete stainless steel part manufacturing process

In conclusion, the ACV study makes it possible to demonstrate that the plasma process for the treatment of powders entails little additional environmental impact compared to the complete process, so any improvement of the parts brought by this step will not lead to environmental involvement.

4 Economic importance of the research topic and of the results for small and medium-sized enterprises (SME)

See also attachment on the results estimation (Ergebniseinschätzung).

During the project a study on the processability of the Cu alloys was conducted. The difficulty in processing pure copper with LBM and the poor obtained results on standard small machines (laser power up to 200 W) are a limitation for small enterprises which aim to design and produce parts with high electrical conductivity (such as the member of the user committee Unicorn Engineering).

Alloying pure copper allows improving the results, but a careful elements selection needs to be performed in order to preserve a sufficient conductivity in the part. A tailoring of the alloy and the choice of the appropriate variants are therefore necessary, as it is always the case for the LBM process. The developed method of quick testing using metal sheets allows saving the high costs of the powder atomization when conducting material development for additive manufacturing. Two CuNiSi alloys were selected through this method, and a process parameters optimization was conducted. Through said optimization of layer thickness and powder size, it was possible to process the CuNi3Si alloy with the low laser power of 100 W (currently available on all selective laser melting machines) obtaining low porosity and (after thermal treatment) hardness and conductivity superior to those of the cast material (the reference values of the band material have not yet been reached).

The adopted research approach of coating the Cu powder with Ti proved to be successful: the reflectivity of the powder was reduced, the energy absorption was enhanced and the processability of the material with a 100 W laser was greatly increased. Smaller LBM machines equipped with a low laser power (up to 200 W) allow to use a reduced powder quantity because of their small build chamber, and their price (around 200.000 €) is normally half of the one of a bigger machine with laser power of at least 400 W (400.000 – 500.000 €), which would be required for the processing of uncoated powder.

The coating process needs additional optimization (regarding its thickness and the oxygen content in the powder) in order to further lower the porosity of the produced parts, but the results confirmed the viability of the approach. This opens new possibilities for future development: the plasma coating with low reflectivity provides great freedom in alloy design, with in-situ formation of age-hardenable alloys that cannot be processed by conventional metallurgy (e.g. immiscible systems). A follow-up CORNET project proposal was submitted with the support of the members from the current SME user committee and with the engagement of further small and medium-sized enterprises.

A coil for an iron-free electric motor was developed and designed by the UC member Unicorn Engineering GmbH and its geometry was optimized for the selective laser melting process. The part was built using two alloys, whose processing was optimized during the performed research: coated Cu and CuNi3Si. A further development of electric motors with light weight design and high efficiency for mobile applications has been planned by Unicorn Engineering, and a ZIM project proposal has already been submitted to continue the cooperation with fem.

Additionally, the conducted infiltrations trials on porous pure copper parts are also promising for companies who need dense parts with high electrical conductivity. The obtained results regarding the part properties (density and conductivity) offer input for further research in this direction (tests on more complex geometries and optimization of infiltration parameters).

5 Dissemination plan

5.1 Performed dissemination during the course of the project

Action	Goal	Place / Frame	Date(s)
Five project meetings with the SME user committee and the research partners	Progress report, input from industry, discussion and decisions	Indutherm, fem, Fraunhofer UMSICHT, SuRo Unicorn Engineering	June 1st 2016 – May 31st 2018
Project website	Short presentation of the project (goals, structure, partner)	http://www.fem-online.de/de/content/OpP3D	since June 2016
Presentation of partial results in the frame of conferences, public seminars and workshops	Discussion of specific results of the workpackages with representatives of the industry and scientific community	Kupfersymposium 2017 - Esslingen	November 8th – 9th 2017
Publication in journal, e.g.: „Metall“	Publication of results in technical journals	Scientific publication	Metall 71 (2017) 452-458
Presentation of partial results in the frame of conferences, public seminars and workshops	Public presentation of the project results in a seminar form	Final OpP3d Workshop at fem	May 8th 2018

5.2 Dissemination after the project ending

Action	Goal	Place / Frame	Date(s)
Presentation at the Friday seminar (Freitagsseminar) at fem	Report on the research project and its results, public discussion	Freitagsseminar des fem	June 22nd 2018
Public presentation	Report on the research project and its results	Summer Symposium “Technik im Zelt” at Fraunhofer UMSICHT, Sulzbach-Rosenberg	June 28th 2018
Presentation to SME network “Additive Manufacturing” of the OTH Amberg-Weiden	Report on the research project and its results, discussion of results and necessary follow-up research	Fraunhofer UMSICHT, Sulzbach-Rosenberg	July 10th 2018
Publication in journal, e.g.: „Materials Science and Technology“	Publication of results in technical journals	Scientific publication	Submitted to Materials Science and Technology in Sept.2018
Presentation of partial results in the frame of conferences, public seminars and workshops	Discussion of specific results of the workpackages with representatives of the industry and scientific community	16th Int. Conf. on Plasma Surface Eng., Garmisch-Partenkirchen	September 17th – 21st 2018
Presentation of partial results in the frame of conferences, public seminars and workshops	Discussion of specific results of the workpackages with representatives of the industry and scientific community	Kupfersymposium 2018 - Bochum	November 20th – 21st 2018

5.3 Estimation on the feasibility of the proposed and updated dissemination plan

The dissemination plan was updated and deviates very little from the planned one. The dissemination activities are realistic. The intended measures during the project course are concluded, and the ones after the project ending have been either already partially performed or they will be shortly.

6 Use of funding

6.1 Necessity and adequacy of the performed work

The performed work from the research partners matches the evaluated and approved proposal. Slight differences due to modified or revised activities were balanced through more intense investigations and activities in other working topics. All the conducted activities were necessary and appropriate to achieve the goals of the research.

6.2 Proposed and used person months

fem person months:

Monat	1	2	3	4	5	6	7	8	9	10	11	12	13	14	15	16	17	18	19	20	21	22	23	24	Summe
SOLL																									
HPA_A	0,30	0,30	0,30	0,30	0,30	0,30	0,30	0,3	0,3	0,3	0,3	0,3	0,3	0,3	0,3	0,3	0,3	0,3	0,3	0,3	0,3	0,3	0,3	0,3	7,2 MM
HPA_B	0,25	0,25	0,25	0,25	0,25	0,25	0,25	0,77	0,77	0,77	0,77	0,77	0,77	0,77	0,77	0,77	0,77	0,77	0,77	1	1	1	0,61	0,64	15,24 MM
Monat	1	2	3	4	5	6	7	8	9	10	11	12	13	14	15	16	17	18	19	20	21	22	23	24	Summe
IST																									
HPA_A	0,30	0,30	0,30	0,30	0,30	0,30	0,30	0,3	0,3	0,3	0,3	0,3	0,3	0,3	0,3	0,3	0,3	0,3	0,3	0,3	0,3	0,3	0,3	0,3	7,2 MM
HPA_B	0,25	0,25	0,25	0,25	0,25	0,25	0,25	0,77	0,77	0,77	0,77	0,77	0,77	0,77	0,77	0,77	0,77	0,77	0,77	1	1	1	0,61	0,64	15,24 MM

Fraunhofer UMSICHT person months:

Monat	1	2	3	4	5	6	7	8	9	10	11	12	13	14	15	16	17	18	19	20	21	22	23	24	Summe
SOLL																									
HPA_A	0,59	0,48	0,58	0,58	0,52	0,65	0,57	0,51	0,51	0,57	0,66	0,73	0,62	0,57	0,57	0,63	0,70	0,79	0,61	0,60	0,61	0,44	0,28	0,43	13,80 MM
HPA_B	0	0	0	0	0	0	0	0	0	0	0	0	0	0	0	0	0	0	0	0	0	0	0	0	0 MM
Monat	1	2	3	4	5	6	7	8	9	10	11	12	13	14	15	16	17	18	19	20	21	22	23	24	Summe
IST																									
HPA_A	0,23	1,06	0,37	0,55	0,66	0,58	0,62	0,63	0,62	0,46	0,06	0,22	0,19	0,08	0,31	0,77	0,90	1,23	1,03	0,83	0,85	0,77	0,80	0,78	14,60 MM
HPA_B	0	0,10	0,17	0,17	0,09	0	0	0	0	0	0	0	0	0	0	0	0,04	0,04	0,07	0,04	0,03				0,75 MM

7 Funding notes and acknowledgments

This work was funded by the public service of Wallonia and by the German Ministry for Economics and Energy based on a decision of the German Bundestag via the AiF-IGF Program, as part of transnational CORNET overall project (No 161 EN). The industrial project partners are acknowledged in particular for their support: Indutherm Gießtechnologie GmbH for conducting atomization trials, Wieland-Werke AG for providing materials (CuSn sheets), Unicorn Engineering GmbH for providing designs and, Arnd Sauter GmbH, HMW Hauner GmbH & Co. KG, New Materials Development GmbH and 3D Laser GbR for their advice and input on the project activities.

8 References

[1] European Commission, Additive Manufacturing in FP7 and Horizon 2020, Report from the EC Workshop on Additive Manufacturing held on 18 June 2014
[2] Becker, D., 2014. Selektives Laserschmelzen von Kupfer und Kupferlegierungen, Dissertation, first ed. Apprimus Verlag, RWTH Aachen, pp. 7-9., pp. 39.
[3] Ikeshoji, T.-T., Nakamura, K., Yonehara, M., Imai, K., Kyogoku, H., 2018. Selective Laser Melting of Pure Copper. JOM 70 (3), 396-400.
[4] Becker, D., Wissenbach, K., 2017. Additive manufacturing of copper components. https://www.ilt.fraunhofer.de/content/dam/ilt/en/documents/annual_reports/JB09/s83.pdf (08.01.2018)
[5] Poltz, I., Jürgens, P., Blüm, M., Weber, S., 2016. Additive Fertigung von CuSn11 Werkstoffen mit selektivem Laserschmelzen (SLM). Metall 70, 438-442.
[6] Khan, M. and P. Dickens, "Selective Laser Melting (SLM) of pure gold", Gold Bulletin, 432, (2010): pp. 114-121
[7] Hötter, J-St., Fateri M., Gebhardt A. „Prozessoptimierung des SLM-Prozesses mit hochreflektiven und thermisch sehr gut leitenden Materialien durch systematische Parameterfindung und begleitende Simulationen am Beispiel von Silber“, RTejournal - Ausgabe 9 (2012) - https://www.rtejournal.de/ausgabe9/3363
[8] Guschlbauer, R., Osmanlic, F., Körner, C., 2017. Herausforderungen bei der Additiven Fertigung von Reinkupfer mit dem selektiven Elektronenstrahlschmelzen. Metall 71, 459-462.
[9] Tiberto D.,Klotz U., Held F. „Einfluss der thermophysikalischen Eigenschaften auf die Verarbeitbarkeit von CuSn-Legierungen durch das selektive Laserschmelzen“ Metall 71 (2017) - VERLAGSGRUPPE HUTHIG - 452
[10] Brush Wellmann GmbH: Technische Daten Brush-Legierung 25, CuBe 2. Datenblatt, (2010)
[11] Deutsches Kupferinstitut, 08.01.2018. https://www.kupferinstitut.de/de/werkstoffe/eigenschaften/niedriglegierte-kupferwerkstoffe.html
[12] Zhao, D. M., Dong, Q. M., 2003. Structure and strength of the age hardened Cu–Ni–Si alloy. Materials Chemistry and Physics 79(1), 81-86.
[13] http://www.pgmdatabase.com
[14] W.M. Rohsenow and H. Choi, Heat Mass and Momentum Transfer, Prentice Hall, New York, (1961)
[15] Godlinski, D.; Petzoldt, F.; Morvan, S. : Tailored Functional Gradients by 3D-Printing using Metal Powder and Nano-particulate Inks (2004)
[16] D. Gravet, NMP-2007-3.4-1 - Grant No. 213477 - Rapid manufacturing concepts for small series industrial production – COMPOLIGHT – 2011/10/30
[17] FOURNEE Vincent, KENZARI Samuel. Procédé d’élaboration de pièces en alliage d’aluminium. Patent WO 2009/144405 A1. 3 décembre 2009
[18] X.F. Zheng and all, Renewable and sustainable Energy Reviews 32 (2014) 486-503
[19] N. Showaiter and all, Materials and Design 29 (2008) 752–762
[20] O. Kylián and all, Thin Solid Films, Volume 548, 2 December 2013, Pages 1-17

[21] Ghribi, F., Alyamani, A., Ben Ayada, Z., K. Djessas, EL Mir, L.: „Study of CuS thin films for solar cell applications sputtered from nanoparticles synthesis by hydrothermal route, Energy Procedia 84 (2015), 109-203.
[22] Radomila Konečná and Stanislava Fintová (2012). Copper and Copper Alloys: Casting, Classification and Characteristic Microstructures, Copper Alloys - Early Applications and Current Performance – Enhancing Processes, Dr. Luca Collini (Ed.), ISBN: 978-953-51-0160-4, InTech, Available from: http://www.intechopen.com/books/copper-alloys-early-applications-and-current-performance-enhancingprocesses/copper-and-copper-alloys-casting-classification-and-characteristics
[23] Liliana Gianni „Corrosion behavior of bronze alloys exposed to urban and marine environment: an innovative approach to corrosion process understanding and to graphical results presentation", Joint Ph.D, Ghent University - Sapienza University of Rome (2011), https://biblio.ugent.be/publication/1997096 /file/1997145.pdf
[24] Amore, S., Ricci, E., Lanata., T., Novakovic, R., 2008. Surface tension and wetting behaviour of molten Cu-Sn alloys. Journal of Alloys and Compounds 452, 161-166.
[25] Ricci, E., Battezzati, L., Brooks, R., Chapman, L.A., 2009. Thermophysical properties of Cu-based industrial alloys in the liquid phase. High Temperatures-High Pressures, Volume 38, 43-61.
[26] Klotz, U.E., Tiberto, D., Held, F., 2016. Additive manufacturing of 18-karat yellow-gold alloys. Proceedings of the 30th Santa Fe Symposium, Albuquerque, New Mexico, pp. 260.
[27] Bowyer, W. H., 1999. The Effects of Impurities on the Properties of OFP Copper Specified for the Copper Iron Canister. Swedish Nuclear Power Inspectorate (SKI) Report 99:44 - SKI Project Number 99099 -, pp. 11.
[28] Eustathopoulos, N., Nicholas, M.G., Drevet, B., 1999. Wettability at High Temperatures, Volume 3, Pergamon, pp. 154.
[29] Vincent, C., Silvain, J.F., Heintz, J.M., Chandra, N., 2012. Effect of porosity on the thermal conductivity of copper processed by powder metallurgy. Journal of Physics and Chemistry of Solids 73, 499-504.
[30] Kött S., 2018, personal communication, Pforzheim University.